In Search of Opioid Sensitive GABA afferents to Midbrain Dopamine neurons

By

Aya Matsui

A DISSERTATION

Presented to the Neuroscience Graduate Program

and the Oregon Health & Science University

School of Medicine

in partial fulfillment of the requirements for the degree of

Doctor of Philosophy

October 2012

School of Medicine

Oregon Health & Science University

CERTIFICATE OF APPROVAL

This is to certify that the Ph.D. dissertation of

Aya Matsui

has been approved

Mentor/Advisor

Member

Member

Member

Member

Table of Contents

List of Figures

List of Abbreviations

AAV; adeno-associated virus

ACSF; artificial cerebrospinal fluid

AMPA; a-amino-3-hydroxy-5-methyl-4-isoxazolepropionic acid

ANOVA; analysis of variance

AHP; afterhyperpolarization

BAPTA; 1,2-Bis(2-aminophenoxy)ethane-N,N,N',N'-tetraacetic acid

β-CNA; β-chlornaltrexamine

BNST; bed nucleus of the stria terminalis

ChR2; channelrhodopsin-2

CIN; cholinergic interneurons

CTX; cholera toxin B

CV; the coefficient of variation

DAMGO; [D-Ala^2, N-Me-Phe^4, Gly^5-ol]enkephalin

DPDPE; [D-Pen^{2,5}]enkephalin

DR; dorsal raphe nucleus

DREADD; the Designer Receptors Exclusively Activated by Designer Drugs

EGTA; ethylene glycol tetraacetic acid

EM-1; endomorphin-1

GABA; gamma-aminobutyric acid

GAD; glutamate acid decarboxylase

GIRK; G-protein coupled inwardly rectifying potassium channel

GPCR; G-protein coupled receptors

GTP; guanosine 5'-triphosphate

IPSC; inhibitory postsynaptic current

IPSP; inhibitory postsynaptic potential

ISI; interspike interval

K_{IR}; inward rectifying channel

$K_{IR}3$; G-protein-coupled, inwardly rectifying, potassium channel

KOR; κ-opioid receptor

LC; locus coeruleus

LDTg; laterodorsal tegmental

LHb; lateral habenula

ME; [Met^5]enkephalin

MOR; μ-opioid receptor

MSN; medium spiny neurons

NAc; nucleus accumbens

NBQX; 1,2,3,4-Tetrahydro-6-nitro-2,3-dioxo-benzo[f]quinoxaline-7-sulfonamide

NMDA; N-methyl-D-aspartic acid

PFC; prefrontal cortex

PPT; pedunculopontine tegmental

PBS; phosphate buffered saline

RMTg; rostromedial tegmental nucleus

SK; Small conductance calcium-activated potassium channels

SN; substantia nigra

SOP; slow oscillatory potential

TH; tyrosine hydroxylase

TTX; tetrodotoxin

tVTA; tail of VTA

U69593; (+)-(5α,7α,8β)-N-Methyl-N-[7-(1-pyrrolidinyl)-1-oxaspiro[4.5]dec-8-yl]-benzeneacetamide

VTA; ventral tegmental area

Acknowledgments

Many people have been helpful to make my graduate career memorable. Without their help, I could not have achieved everything I have. First of all, I have been extremely lucky to work with my mentor, Dr. John T. Williams. I cannot say enough to convey his patience, his hands-on mentorship, and the scientific and personal advice that I received throughout my graduate career. His guidance and enthusiasm for science motivate me to pursue my scientific career, and work hard to achieve my goal. Like many other alumni, I hope to keep this relationship after my graduation.

I would also want to give many thanks to the current members of the Williams lab: Erica, Will, Seksiri, Stephanie, Paul, and Jim, and former lab members: Chris, Shane, and Nidia for support during my graduate schools. They helped throughout my graduate career with lots of insightful comments, technical advice, and good times in both at work and outside work.

My thesis advisory committee, Drs. Craig Jahr, Larry Trussell, Steven Johnson, and Susan Ingram, have guided me with constructive ideas for my thesis work. I am grateful for their support and guidance. Many thanks also extended to the neuroscience graduate program and my classmates who started with me in the fall of 2007.

I am also greatly indebted to my family especially my parents, Susumu and Michiko Matsui, for their tremendous love, support, and encouragement throughout my life. Without their understanding, I wouldn't be living outside the country in order to pursue a scientific career. Thank you everyone.

Abstract

Dopamine neurons in ventral tegmental area (VTA) and substantia nigra play a key role in motivation and reward learning. The activation of the mesolimbic dopamine system is the key neuronal circuit that develops adaptive synaptic modification leading to drug addiction. Opioids increase dopamine neuron activity in the mesolimbic system by inhibiting presynaptic GABA terminals. This opioid disinhibition of dopamine neurons is a key first step to result in long-term synaptic adaptations. Therefore, characterizing how opioids increase dopamine neuron activity is crucial for elucidating mechanisms of opioid addiction.

There are several GABA inputs in VTA that can be inhibited by opioids. Historically, interneurons in VTA are thought to be a main source of opioid disinhibition of dopamine neurons. Strong GABA inputs also arise from striatum although it is still not clear whether those inputs terminate on dopamine or non-dopamine neurons in VTA. μ-opioid receptors are expressed in striatum and nucleus accumbens neurons. Moreover, the newly characterized structure, rostromedial tegmental nucleus (RMTg) or the tail of the VTA, sends dense GABA inputs to dopamine neurons, some of which express μ-opioid receptors. Thus, it is possible that those inputs mediate disinhibition.

The focus of the dissertation is to examine GABA inputs projecting to dopamine or non-dopamine neurons in the midbrain and determine where the opioid sensitive GABA inputs originate. Whole-cell recordings were made from

dopamine and GABA neurons in VTA and SN. Using expression of channelrhodopsin-2 (ChR2), RMTg, VTA, and NAc neurons were individually activated by light stimuli to evoke GABA-A IPSCs. Opioid sensitivity of GABA inputs from each of these areas were examined.

Activation of interneurons in VTA, RMTg and NAc neurons with light stimuli evoked GABA-A IPSCs in dopamine neurons. Repetitive light stimuli also evoked GABA-B IPSCs only from the inputs from RMTg and NAc neurons. Opioid inhibition of GABA inputs from VTA interneurons was surprisingly low. However, RMTg inputs to dopamine neurons were strongly inhibited by μ-opioid receptor agonists. NAc inputs were also moderately inhibited by μ-opioid receptor agonists. Most of the striatal inputs to the midbrain project to GABA neurons in SNr and VTA. The sensitivity of striatal inputs to opioid was mixed; some were inhibited by μ- opioid receptor agonists and others were inhibited by κ-opioid receptor agonists. Altogether the RMTg sends a dense opioid sensitive GABA inputs to VTA and that plays an important role in activity of dopamine neurons.

Chapter 1: Introduction

Dopamine neurons in the ventral tegmental area and substantia nigra pars compacta (VTA/SNc) are essential for the endogenous mesolimbic pathway that encodes for reward learning motivational value. Dopamine neurons exhibit single spike rhythmic action potentials that are dependent on intrinsic mechanisms, whereas synaptic inputs generate high frequency bursting of action potentials. During the phasic burst firing, the dopamine level in the brain increases, which contributes to long-term synaptic plasticity. Following opioid consumption, the dopamine level in the brain also increases. Opioids are endogenous and exogenous compounds that bind to opioid receptors in the central and peripheral nervous systems. The most common use of exogenous opioids is for analgesia; however, opioids produce euphoria by activating the mesolimbic dopamine system. The accepted view of how opioids increase dopamine release is that activation of μ-opioid receptors (MORs) hyperpolarizes GABA interneurons in the VTA to disinhibit dopamine neurons. Additionally, the repeated use of opioids can alter the synaptic plasticity in mesocorticolimbic system and eventually leads to drug addiction. Long-term regulation of the reward system depends on dopamine neuron activity, so it is important to elucidate the mechanisms by which opioids modulate dopamine neuron activity. This dissertation focuses on opioid inhibition of three main GABA inputs to dopamine neurons, i.e. rostromedial tegmental nucleus (RMTg), nucleus accumbens (NAc), and VTA interneurons. This chapter will describe the anatomical circuits in the

midbrain, the intrinsic and extrinsic regulation of dopamine neurons, and current knowledge concerning opioid regulation of dopamine neurons.

The afferents to dopamine neurons

Dopamine neurons in VTA/SNc spontaneously generate action potentials without receiving any synaptic inputs, and dynamic synaptic interactions govern the activity and function of mesolimbic dopamine system. The burst firing of dopamine neurons is implicated in reward-base associated learning by elevating dopamine levels in the NAc (Grace et al., 2007; Tsai et al., 2009; Yawata et al., 2012). The excitatory inputs are particularly important to trigger burst firing. Excitation is elicited by activation of glutamate (AMPA, NMDA, and kainate) and acetylcholine (nicotinic and muscarinic) receptors. However, the majority of synaptic inputs on dopamine neurons are GABAergic. GABA inputs set an inhibitory tone to prevent burst firing of dopamine neurons. Additionally, numerous neuromodulators can act on presynaptic terminals to control the release of excitatory and inhibitory transmitters as well as alter the excitability of dopamine neurons postsynaptically. This section discusses the anatomy of the afferent pathways to dopamine neurons.

Glutamate and acetylcholine

Previous studies suggested that dopamine neurons receive excitatory inputs from the medial prefrontal cortex (PFC), the pedunculopontine tegmental

(PPTg) and laterodorsal tegmental (LDTg) nuclei, the bed nucleus of the stria terminalis (BNST), the subthalamic nucleus, and the superior colliculus (Kita and Kitai, 1987; Tong et al., 1996a; Georges and Aston-Jones, 2001; 2002; Floresco et al., 2003; Dommett et al., 2005; Lodge and Grace, 2006; Figure 1.1). The majority of glutamate inputs originate from PFC and activity of PFC can alter dopamine levels in the striatum (Karreman and Moghaddam, 1996; Geisler et al., 2007; Moorman and Aston-Jones, 2010). PFC neurons modulate reward-seeking behavior and control the activity of dopamine neurons (Phillips et al., 2008). Electrical stimulation of PFC *in vivo* has shown that a single stimulus was sufficient to induce burst firing of dopamine neurons (Tong et al., 1996a; Moorman and Aston-Jones, 2010). Thus, PFC activation is sufficient to modulate dopamine neuron excitability. However, other brain regions also modify dopamine neuron activity. The PPTg and LDTg release both glutamate and acetylcholine in VTA and SNc. Acetylcholine increases dopamine neuron activity by activating nicotinic and muscarinic M1 receptors (Lacey et al., 1990; Gronier and Rasmussen, 1998; Mameli-Engvall et al., 2006). Activation of PPTg enhanced burst firing of dopamine neurons *in vivo*; however, activation of LDTg neurons promotes an increase in spontaneous activity of dopamine neurons, yet failed to induce burst firing (Floresco et al., 2003; Lodge and Grace, 2006). Inactivation of PPTg and LDTg eliminated the burst firing indicating that tonic activity of PPTg and LDTg increases the basal activity of dopamine neurons and gates burst firing. Moreover, inactivation of LDTg alone is sufficient to decrease the percentage of burst firing (Lodge and Grace, 2006). Since PPTg stimulation

in vivo produced the burst firing of dopamine neurons, LDTg neurons must be tonically activated. Therefore, inactivation of LDTg prevents burst firing and activation of LDTg may play a role in the coincident detection to generate burst firing.

In addition to previously known excitatory inputs, the lateral hypothalamic area, preoptic areas, pariaqueductal gray, amygdala and the dorsal raphe were also found to send glutamate inputs to the midbrain (Geisler et al., 2007). The lateral hypothalamic neurons projecting to VTA also contain orexin/hypocretin. Since glutamate and orexin transmission in the VTA are required for cue-induced reinstatement of cocaine seeking (James et al., 2011; Mahler et al., 2012), lateral hypothalamus input is probably important for the reward-base dopamine signals. However, it is still undetermined whether those glutamate projections synapse on dopamine or non-dopamine neurons.

Because dopamine neurons in brain slice preparations do not generate burst firing due to deafferention of excitatory inputs, it was difficult to determine which excitatory inputs play a key role in generating burst firing of dopamine neurons. Simultaneous excitatory AMPA inputs are required to remove Mg^{++} block from NMDA receptor to successfully elicit burst firing in dopamine neurons (Overton and Clark, 1992). Interestingly, PFC neurons project to BNST and LDTg that both send glutamate input to the VTA. Additionally, neurons in the BNST project to the PPTg and amygdala that also send glutamate input to the VTA. It

remains to be determined the mechanisms by which dopamine neurons generate burst firing.

GABA

Dopamine neurons receive inhibitory inputs from nucleus accumbens (NAc)/striatum, and the ventral pallidum/external globus pallidus from the rostral brain (Zahm, 1989; Smith and Bolam, 1990; Kalivas et al., 1993; Figure 1.1). A recent trans-synaptic study suggested that dorsal and ventral striatal and ventral pallidum synapse directly on dopamine neurons (Watabe-Uchida et al., 2012). Specifically, medium spiny neurons (MSNs) in the patch compartment of striatum and NAc project to dopamine neurons, and MSNs in the matrix compartment project to GABA neurons in VTA and substantia nigra pars reticulata (SNr). However, using an optogenetic approach where channelrhodopsin-2 (ChR2) was expressed in MSNs, GABA inputs from NAc and striatum mainly projected to non-dopamine neurons (Chuhma et al., 2011; Xia et al., 2011). Another inhibitory input to dopamine neurons originates locally from interneurons in the VTA and SNr (Johnson and North, 1992a; Tepper et al., 1995). Inhibition of interneurons in the VTA were traditionally believed to be the main source to regulate dopamine neuron activity (Johnson and North, 1992a). However, recent studies conducted by two separate groups identified and characterized a strong GABA afferent from a nucleus named the rostromedial tegmental nucleus (RMTg), also known as tail of the VTA (Kaufling et al., 2009;

Jhou et al., 2009b). The discovery of the RMTg raised questions of whether RMTg neurons directly project to dopamine neurons. The following section describes the characteristics of RMTg neurons.

An unrealized GABA input; Discovery of the RMTg

RMTg neurons, located slightly caudal to VTA and dorsal to interpeduncular nucleus, were found using the activity of early response genes, cFos or ΔFosB, after the administration of psychostimulants (Hope et al., 1994; Scammell et al., 2000). Based on expressed mRNA for GAD67, the enzyme required for GABA synthesis, RMTg neurons were determined to be GABAergic. Strong μ-opioid receptor immunoreactivity was also detected in RMTg neurons. RMTg neurons received input predominantly from lateral habenula (LHb), and send a dense efferent projection to SNc and VTA (Kaufling et al., 2009; Jhou et al., 2009b). Aversive stimuli increase the activity of LHb neurons followed by decreased tonic firing of dopamine neurons. Since LHb neurons are glutamatergic, there had to be GABAergic inhibitory neuron that resulted in the inhibition of dopamine neurons. Based on tracing and immunolabeling studies, neurons in the RMTg and a small population of VTA interneurons have been shown to be the relay neurons to inhibit dopamine neurons (Balcita-Pedicino et al., 2011; Li et al., 2011; Maroteaux and Mameli, 2012). Thus, the afferent connections from LHb to RMTg and possibly LHb to VTA interneurons have a huge impact on dopamine neuron firing. Interestingly, RMTg lesions reduced

passive fear response (i.e. freezing, open-arm bar avoidance) (Jhou et al., 2009a). That behavior is dependent on the activity of neurons in the amygdala, periaqueductal gray, and septum, all of which project to the RMTg. Animals self-administer the MOR agonist, endomorphin-1 (EM1), into RMTg and conditioned place preference was observed in the animals infused with EM1 into the RMTg (Jhou et al., 2012). Since RMTg neurons are not yet well characterized, it is critical to examine the synaptic connection between neurons in the RMTg and dopamine neurons, the sensitivity of that connection to opioids, and finally to compare the strength of opioid modulation of this pathway to other major GABA inputs.

Neuromodulators

Catecholamine (norepinephrine, serotonin, and dopamine) and opioids peptide neuromodulators are released in VTA and SN and modulate dopamine neurons activity. Influence of neuromodulator inputs to dopamine neurons are briefly described.

Norepinephrine inputs originate from locus coeruleus neurons, A1, A2, and A5 areas (Mejías-Aponte et al., 2009). Norepinephrine produces both excitatory and inhibitory effects in dopamine neurons. Excitatory effects are mediated by activation of α1 adrenergic receptors causing direct depolarization of dopamine neurons. Activation of α1 adrenergic receptors also inhibits mGluR-IPSCs in dopamine neurons (Paladini et al., 2001). However, the activation of α1

adrenergic receptors also directly hyperpolarize dopamine neurons by activating SK channels (Paladini and Williams, 2004). The application of norepinephrine causes a brief excitation followed by long inhibition in dopamine neurons *in vivo* (Grenhoff et al., 1993).

Serotonin is released from terminals arising from neurons in the median and dorsal raphe. A subset of dopamine and GABA neurons in VTA is hyperpolarized by serotonin (Cameron et al., 1997). Serotonin inhibits GABA transmitter release by a presynaptic mechanism. This inhibition of GABA release was only observed in GABA-B mediated slow IPSCs, but not in GABA-A IPSCs in dopamine neurons (Johnson et al., 1992; Sugita et al., 1992a; Cameron and Williams, 1994). Serotonin also inhibits the EPSCs in dopamine neurons (Jones and Kauer, 1999). Thus, serotonin action is taking place at both postsynaptic sites and presynaptic terminals.

Dopamine is released from somatodendritic sites of dopamine neurons for autoinhibition (Beckstead et al., 2004). A release of dopamine causes a pause of spontaneous firing of dopamine neurons. Afferents to dopamine neurons express both D1- and D2-receptors to modulate transmitter release. Activation of D1-receptors facilitate GABA release in dopamine neurons in VTA and GABA neurons in SNr (Cameron and Williams, 1993; Radnikow and Misgeld, 1998). On the contrary, D2-receptor activation decreases glutamate transmitter release (Koga and Momiyama, 2000). Dopamine is the most abundant neuromodulator in VTA/SN and controls dopamine neuron activity by both pre- and postsynaptic mechanisms.

Endogenous opioid peptides are released from the interpeduncular nucleus, periventricular hypothalamus, and the lateral septum. Dynorphin and enkephalin is released from striatal projection (Kalivas et al., 1993; Greenwell et al., 2002). Although endogenous opioid release has not been detected *in vivo* or *in vitro*, exogenous application of opioids modulates dopamine neuron activity. The details of opioid regulation are discussed further below.

Altogether, neuromodulators control a state of neuronal excitability whereas excitatory and inhibitory synaptic transmissions regulate the activity of dopamine neurons. The present work focuses on identifying the GABAergic synaptic input to dopamine neurons that are modulated by opioids.

The regulation of dopamine neurons

Dopamine neurons are located in the ventral tegmental area (VTA, A10) the substantia nigra pars compacta (SNc, A9), and the retrorubral field (A8) in the midbrain. There is growing evidence showing that dopamine neurons are heterogeneous. The firing pattern, tyrosine hydroxylase expression level, the projection areas, and expression of many ion channels vary considerably (Wolfart et al., 2001; Neuhoff et al., 2002; Ford et al., 2006; Lammel et al., 2008; 2011; Figure 1.2). Although individual neuronal channel properties differ, all dopamine neurons exhibit both single rhythmic tonic firing and high frequency phasic firing. This section describes how the firing rate and pattern of activity are shaped by intrinsic and extrinsic mechanisms.

Intrinsic Dopamine Neuron Activity

Without any synaptic input, VTA and SNc dopamine neurons exhibit autonomous pacemaker firing at 1-5 Hz (Johnson and North, 1992b; Cameron et al., 1997; Neuhoff et al., 2002; Korotkova et al., 2003; Ford et al., 2006). The action potential during the tonic firing has a low coefficient of variation (CV) of the interspike interval (ISI) indicating that dopamine neurons exhibit rhythmic action potentials (Li et al., 2012). However, VTA and SNc neurons differ in terms of ion channel composition. The hyperpolarization-activated current (Ih) is more prominent in SNc than VTA neurons. Inhibition of Ih in SNc dopamine neurons decreases the firing rate (Neuhoff et al., 2002; Khaliq and Bean, 2010). ATP-sensitive potassium (K-ATP) channels also control burst firing of dopamine neurons. Elimination of K-ATP channels robustly decreases the burst firing rate in medial SNc but not in lateral SNc or VTA (Schiemann et al., 2012). Blocking calcium channels decreases or stops pacemaking firing of dopamine neurons in SNc but increases the firing rate in VTA (Khaliq and Bean, 2010). Since VTA and SNc dopamine neurons use different mechanisms for the pacemaking action potential, the intrinsic action potential mechanisms are discussed separately.

In acutely dissociated SNc dopamine neurons, the upstroke of action potentials is carried by the opening of a sodium conductance followed by a slow calcium conductance to produce a broad action potential in SNc dopamine neurons. Potassium channels bring the membrane potential back to resting potential. During the interspike interval, subthreshold persistent sodium and calcium currents are involved in sustained depolarization to generate tonic firing

(Puopolo et al., 2007). In fact, in the presence of the sodium channel blocker tetrodotoxin (TTX), some SNc dopamine neurons reveal calcium channel dependent action potentials or a slow oscillatory potential (SOP). Inhibition of L-type and P/Q-type calcium channels slows spontaneous firing of dopamine neurons. Moreover, activation of L-type calcium channel is required for generating the SOP (Puopolo et al., 2007; Putzier et al., 2009). During the SOP, intracellular calcium concentration oscillates in phase with the action potential and plays a key role in basal second messenger signaling in dopamine neurons. Calcium influx activates a SK conductance presumably coupled to T-type calcium channel to create a prominent afterhyperpolarization (AHP) (Wilson and Callaway, 2000; Wolfart and Roeper, 2002). Interestingly, application of the SK channel blocker apamin increases firing rates of SNc dopamine neurons and increases the CV of ISI (Shepard and Bunney, 1988). These results suggest that single-spike spontaneous action potentials are mediated by sodium, calcium, SK and other potassium channel activation in SNc dopamine neurons.

VTA dopamine neurons have different electrophysiological characteristics. Application of TTX completely eliminated the SOP, unlike in the SNc (Chan et al., 2007; Khaliq and Bean, 2008). Moreover, inhibition of Ih using Cs^+ did not decrease firing rate of VTA dopamine neurons as was observed in SNc (Khaliq and Bean, 2008). This observation was not due to lack of Ih conductance in VTA. VTA dopamine neurons exhibit Ih current, although it is smaller than SNc neurons (Neuhoff et al., 2002; Ford et al., 2006). Blocking calcium channels also did not slow or stop the spontaneous firing of dopamine neurons in the VTA (Liss

and Roeper, 2008; Khaliq and Bean, 2010). Thus, dopamine neurons in SNc and VTA are clearly distinct. Nevertheless, similar to SNc dopamine neurons, VTA dopamine neurons fire spontaneously at a slightly higher frequency. VTA dopamine neurons utilize a TTX-insensitive persistent sodium conductance to depolarize the membrane potential until activating TTX-sensitive sodium conductance to trigger the action potential (Khaliq and Bean, 2010). During the depolarizing phase of the ISI, a subthreshold A-type potassium conductance is activated to slow the spontaneous firing of VTA dopamine neurons (Koyama and Appel, 2006; Khaliq and Bean, 2008). Thus, those intrinsic characteristics of VTA dopamine neurons differentially generate slow rhythmic firing pattern.

The Synaptic Regulation of Dopamine Neurons

Glutamate transmission: The phasic burst firing pattern of dopamine neurons in VTA and SN encodes reward and motivational values. Although burst firing can be generated by inhibition of SK channel to decrease the AHP, depolarizing currents were required to mimic burst firing (Shepard and Bunney, 1991) suggesting that synaptic inputs are necessary for burst firing. Application of N-methyl-D-aspartic acid (NMDA) receptor agonists successfully generate burst firing in dopamine neurons (Seutin et al., 1993; Paladini et al., 1999b; Johnson and Wu, 2004). Previous *in vivo* studies revealed that glutamate inputs from the PFC, PPTg, subthalamic nucleus triggered burst firing in dopamine neurons (Smith and Grace, 1992; Murase et al., 1993; Lokwan et al., 1999; Floresco et al.,

2003). The burst firing of dopamine neurons could be stimulated by activation of NMDA receptors, but not AMPA receptors (Overton and Clark, 1992; Christoffersen and Meltzer, 1995; Tong et al., 1996b). Some of the behavioral consequences were facilitated by burst firing and were eliminated when NMDA receptors on dopamine neurons were selectively deleted (Zweifel et al., 2008; 2009). The activity patterns of excitatory inputs are crucial to general burst firing. For example, PPTg neurons are tonically active neurons releasing both glutamate and acetylcholine. Thus, dopamine neurons constantly receive excitatory inputs without exhibiting continuous burst firing. Because NMDA receptor activation is required for burst firing, dopamine neurons must be depolarized in order to remove Mg^{++} block from NMDA receptors. It is of interest to determine which excitatory inputs from multiple brain area contribute to the generation of burst activity.

In addition to fast synaptic transmission, glutamate release also activates metabotropic glutamate receptors (mGluR) in dopamine neurons (Fiorillo and Williams, 1998). mGluRs are Gq-protein coupled receptors which activate phosphoinositide hydrolysis and induce calcium release from intracellular store. The release of calcium activates SK channel conductance to hyperpolarize the cell. Therefore, glutamate release triggers burst firing of dopamine neurons followed by inhibition of firing.

GABA transmission: Over 70% of synaptic inputs to dopamine neurons are GABAergic. The firing rate of dopamine neurons was strongly controlled by multiple GABA inputs. It appears that tonic GABA input sufficiently suppresses

the burst firing of dopamine neurons (Lobb et al., 2010; Jalabert et al., 2011). Conversely, the removal of GABA input triggers burst firing of dopamine neurons although excitatory inputs are also necessary (Jalabert et al., 2011). The disinhibition of dopamine neurons was thought to originate primarily from a decrease in GABA input from VTA interneurons. However, the recent discovery of the nucleus called RMTg has changed that interpretation. The RMTg sends a strong GABA input to dopamine neurons synapsing on proximal dendrites (Kaufling et al., 2009; Jhou et al., 2009b; Balcita-Pedicino et al., 2011). The proximity of the RMTg, VTA, and SN made it difficult to determine the role of the GABA interneurons in the VTA. However, when animals were trained to self-administrate endomorphine-1 (EM1) directly into the RMTg or VTA, self-administration was facilitated with injections into the RMTg (Jhou et al., 2012). Thus, it is critical to differentiate these GABA inputs to investigate which GABA inputs modulate the burst firing of dopamine neurons.

Additionally there is a strong GABA input from medium spiny neurons (MSNs) in the striatum. The striatal medium spiny output neurons are traditionally divided into two classes that make up the direct and indirect pathways. The direct pathway, expresses κ-opioid receptor (KOR) and D1-like receptors and project to GABA neurons in SNr. The indirect pathway, expresses MOR and D2-like receptors and project directly to the external globus pallidus which then inhibit GABA neurons in SNr (Alexander and Crutcher, 1990). Since SNr neurons project to dopamine neurons in SNc, the direct pathway from striatum can be another input that indirectly modulates dopamine neurons (Lobb

et al., 2011). In addition, a small percentage of neurons expressed both D1- and D2-like receptors as well as dynorphin and enkephalin (Bertran-Gonzalez et al., 2008; Valjent et al., 2009). Thus, there are a more dynamic interactions taking place between the striatal inputs and midbrain. ChannelRhodopsin-2 (ChR2) expression in NAc and Striatum showed that GABA inputs were activated GABA-A receptors on GABA neurons in VTA and SNc (Chuhma et al., 2011; Xia et al., 2011). However, a recent trans-synaptic retrograde study suggested that dopamine neurons in VTA and SNc also receive direct inputs from NAc and DS (Watabe-Uchida et al., 2012). Moreover, striatal inputs to dopamine neurons were thought to activate a GABA-B slow inhibitory potential (Sugita et al., 1992a). Thus, more studies are required to determine specific projections from the striatal GABA afferents and how those inputs are modulated.

Altogether, in order to generate burst firing, excitatory and inhibitory inputs orchestrate the dopamine neuron activity. Given multiple inputs that terminate in midbrain, the pathways involved in modulating dopamine neuron firing have not been elucidated. Additionally, there are multiple neuromodulators, i.e. opioids and dopamine, can alter the synaptic activity in dopamine neurons. My thesis work focused on characterizing GABA inputs from RMTg, VTA interneurons, and NAc, and how those inputs are modulated by opioids.

Opioid regulation of Midbrain

Many drug of abuse elevate dopamine release in the mesocorticolimbic system by several mechanisms (Lüscher and Malenka, 2011). In the case of opioids, tonic GABA input to dopamine neurons is removed by activation of MORs on GABA afferents so that dopamine neurons are disinhibited (Gysling and Wang, 1983; Johnson and North, 1992a). This disinhibition model was not the only evidence of the opioid disinhibition of primary neurons. Originally the opioid disinhibition mechanism was proposed based upon the observations that opioids inhibited GABAergic input to pyramidal cell in hippocampus, mitral cells in olfactory bulb, and in spinal cord (Nicoll et al., 1980). The classical model for disinhibition of dopamine neurons was from inhibition of local interneurons in the VTA (Johnson and North, 1992a). Application of the MOR agonist DAMGO increased the firing of dopamine neurons. Moreover, an excitation was also observed with the treatment of slice with the GABA-A antagonist bicuculline. Based on the observation that opioids hyperpolarized interneurons in the VTA, it was suggested that the opioid inhibition of interneurons increased the activity of dopamine neurons (Johnson and North, 1992a). The recent finding that RMTg neurons send a dense GABA input to dopamine neurons and express MORs has changed the original interpretation (Kaufling et al., 2009; Jhou et al., 2009a; 2009b). In addition, dopamine neurons also received GABA inputs from other nuclei including substantia nigra pars reticulata (SNr), nucleus accumbens (NAc), globus pallidus, ventral pallidum, and diagonal band of Broca (Tepper et al., 1995; Watabe-Uchida et al., 2012). It remains to be determined whether those

GABA inputs terminate on dopamine neurons and the sensitivity of those inputs to opioids.

Opioid receptors are also expressed postsynaptically on dopamine neurons. MORs are expressed only a small subset of VTA dopamine neurons projecting to basolateral amygdala. Those VTA neurons were hyperpolarized by MOR agonists (Ford et al., 2006). This result contradicts the idea that the rewarding effect of MOR agonists is due to the release of dopamine. However, the activation of MORs increases the dopamine release in NAc to elicit reward effects (Bals-Kubik et al., 1993). In addition, KORs are expressed in VTA and SNc dopamine neurons (Margolis et al., 2003; Ford et al., 2007). Application of the KOR agonist, U69593, induced GIRK mediated outward current, and reduced somatodendritic dopamine release in VTA and SNc. The suppression of dopamine neuron activity by KORs is consistent with the behavioral observation that KORs in the VTA elicit a conditioned place aversion (Bals-Kubik et al., 1993). Thus, opioid modulation of dopamine neurons takes place in both pre- and postsynaptic sites and is more dynamic than previously mentioned.

General Aims

This thesis focused on the major GABA inputs that might modulate dopamine neuron firing. GABA afferents from interneurons in the VTA, neurons in the RMTg and the NAc to dopamine neurons were examined. Additionally, the reciprocal connection from VTA to NAc was investigated. The opioid sensitivity of

those inputs was tested to determine which GABA afferent was the major opioid sensitive input. The results provide the mechanism by which opioid disinhibit dopamine neuron activity. Repeated administration of opioids causes the circuit level modifications in synaptic plasticity that may underlie the development of opioid addiction. The implications of this work will help to find the target nucleus that may be aimed to develop the new therapeutic strategies to prevent opioid addiction.

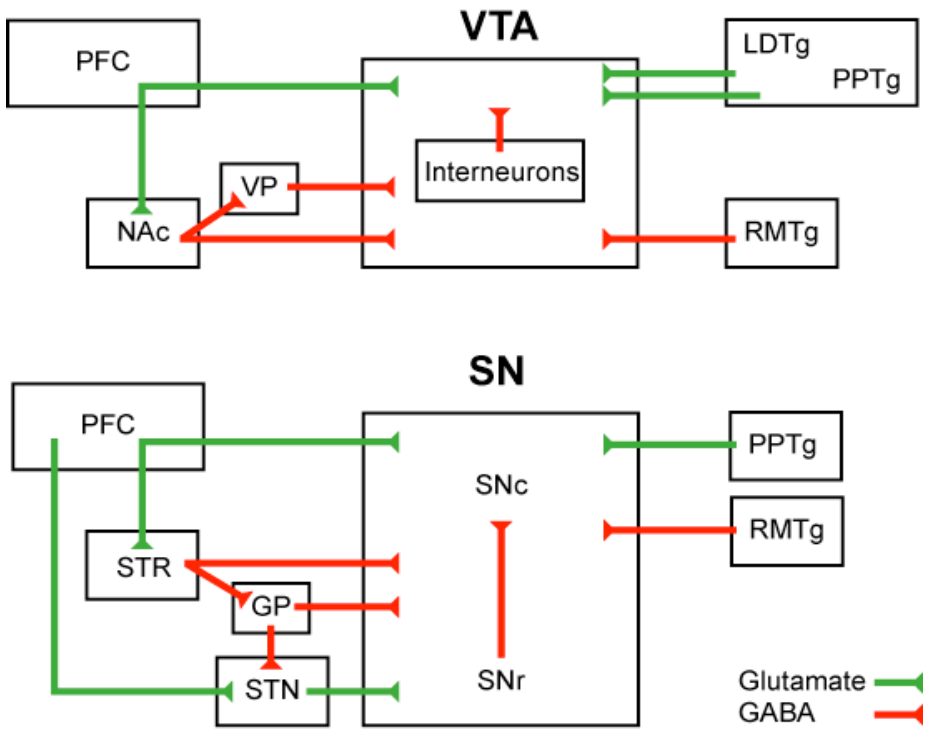

Figure 1.1: Summary of the major afferents to VTA and SN

Schematic illustrations showed glutamate (green) and GABA (red) inputs to VTA and SN. LTDg and PPTg also release acetylcholine. GP, globus pallidus; LDTg, laterodorsal tegmental nucleus; NAc, nucleus accumbens; PFC, prefrontal cortex; PPTg, pedunculopontine tegmental nucleus; RMTg, rostromedial tegmental nucleus; SNc, substantia nigra pars compacta; SNr, substantia nigra pars reticulata; STN; subthalamic nucleus; STR, striatum; VP, ventral pallidum; VTA, ventral tegmental area.

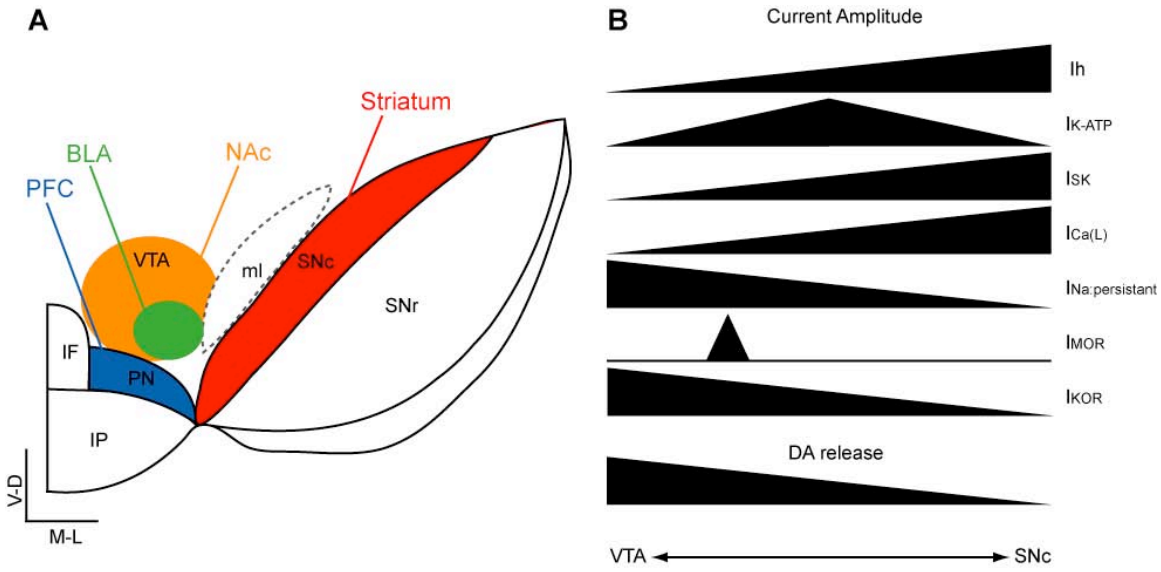

Figure 1.2: Location-specific efferents and intrinsic properties of VTA and SNc dopamine neurons

A. Anatomical illustration of midbrain dopamine neuron in coronal plane. Different colors represent different axonal projection to striatum (red), NAc (orange), BLA (green), and PFC (blue). BLA projecting dopamine neurons locates rostral to NAc projecting dopamine neurons. B. Comparison of current amplitudes of various ion channels and dopamine release between VTA and SNc dopamine neurons. IK-ATP was prominent in medial SNc dopamine neurons. Only dopamine neurons projecting to BLA express MORs.

Chapter 2: Manuscript 1

Opioid-sensitive GABA inputs from Rostromedial Tegmental Nucleus synapse onto midbrain dopamine neurons

Aya Matsui and John T. Williams

Vollum Institute, Oregon Health and Science University, Portland, OR, USA

Corresponding author:
John T. Williams
Vollum Institute,
Oregon Health & Science University,
Portland, Oregon 97239,
williamj@ohsu.edu

Acknowledgements: This work was supported by NIH grants, DA08163 and DA04523 JTW

[This manuscript is presented as published in Journal of Neuroscience, Nov 30, 2011, 31(48):17729-35.]

Abstract

Opioids increase dopamine release in the brain through inhibition of GABA-A IPSCs onto dopamine cells. Immuno-labeling indicates that GABA neurons in the rostromedial tegmental nucleus (RMTg), also known as the tail of the ventral tegmental area, send a dense projection to midbrain dopamine neurons stain for μ-opioid receptors. There is however, little functional evidence that these neurons play a role in the opioid-dependent increase in dopamine neuron activity. The present study used retrograde tracers injected into the ventral tegmental area and substantia nigra (VTA/SN) to identify RMTg neurons that project to the VTA/SN. Whole-cell current clamp and cell-attached recordings from labeled RMTg neurons were carried out in sagittal slices from rat. The rhythmic spontaneous firing rate of RMTg neurons was decreased and the membrane potential was hyperpolarized in response to application of μ-opioid agonist DAMGO. Agonists that act at kappa and delta opioid receptors (U69593 and DPDPE) failed to hyperpolarize RMTg neurons. Whole-cell recordings made in dopamine neurons revealed rhythmic, large amplitude spontaneous IPSCs that had a similar frequency, pattern and opioid sensitivity to the firing of RMTg neurons. In addition, electrical and channelrhodopsin2 stimulation within the RMTg evoked GABA-A IPSCs in dopamine neurons that were inhibited by μ-opioid agonists DAMGO, but not kappa and delta opioid agonists. Thus, this study demonstrates functional connection from the RMTg to the VTA/SN mediated by a dense, opioid sensitive GABA innervation, and that the RMTg is a key structure in the μ-opioid receptor dependent regulation of dopamine neurons.

Introduction

Many drugs of abuse, including opioids, increase the activity of dopamine neurons resulting in increased dopamine release in the mesocorticolimbic system. Dopamine release specifically in the nucleus accumbens is thought to be essential for reward learning and goal-oriented behavior (Di Chiara and Imperato, 1988; Nicola and Malenka, 1997; Thomas et al., 2001). Thus, the synaptic regulation of dopamine neurons is a key initial step in reward circuits leading to drug addiction (Wise, 1996; Di Chiara et al., 2004). Drugs of abuse also induce adaptive changes that alter the synaptic strength of inputs to dopamine neurons. For example, the probability of GABA release was increased during withdrawal in slices from animals treated chronically with morphine (Bonci and Williams, 1997). In addition, glutamate synaptic transmission was enhanced following treatment of animals with many drugs of abuse, including opioids (Saal et al., 2003). Characterizing the synaptic mechanisms by which opioids alter the excitability of dopamine neurons is a necessary first step in understanding the resulting adaptive changes.

It is well known that μ-opioid agonists inhibit GABA input onto dopamine neurons (Johnson and North, 1992a; Shoji et al., 1999; Ford et al., 2006; Madhavan et al., 2010). The dis-inhibition results in increased firing of dopamine neurons. The opioid sensitive cells that underlie this dis-inhibition were thought to be GABA-interneurons within the ventral tegmental area and substantia nigra (VTA/SN; Johnson and North, 1992a). There is, however, no direct evidence of a functional connection between GABA interneurons and dopamine neurons.

Recently, the rostromedial tegmental nucleus (RMTg), also known as tail of VTA, has been recognized as the major GABA afferent to dopamine neurons (Kaufling et al., 2009; Jhou et al., 2009b). The RMTg was originally defined as an area that was caudal and medial to the VTA that was marked by a robust increase in early response genes such as cFOS and Δ-FOS expression following an injection of cocaine or amphetamine (Perrotti et al., 2005; Geisler et al., 2008; Kaufling et al., 2010a; 2010b). Antero- and retro-grade tracing studies revealed that RMTg neurons receive a strong glutamate input from lateral habenula and send a dense GABA projection to dopamine neurons in the VTA/SN (Kaufling et al., 2009; Jhou et al., 2009b; Balcita-Pedicino et al., 2011). Stimulation within the lateral habenula in vivo inhibited dopamine neurons, an action that was mediated by GABA-A receptors (Ji and Shepard, 2007). Aversive stimuli increased the activity of lateral habenula neurons and decreased the activity of dopamine neurons. Finally, the observation that neurons in the medial RMTg were immunopositive for μ-opioid receptors suggested that this GABAergic pathway could be another opioid sensitive pathway that mediates the dis-inhibition of dopamine cell activity. This study indicates that the RMTg is another opioid sensitive inhibitory relay to dopamine neurons.

Materials and methods

All procedures were performed in accordance with the guidelines of the Oregon Health & Science University and the Animal Care and Use Committees approved all of the experimental procedures.

Intracerebral microinjections

Male and female Sprague-Dawley rats (p20-23, Charles River Laboratories) were used in all experiments. Rats were anesthetized with isoflurane and immobilized in a Stereotaxic Alignment System (Kopf Instruments). A solution of fluorescent microspheres (100 nl; 0.04 μm diameter; EX/EM=488/560; Invitrogen) or cholera toxin subunit B conjugated to Alexa Fluor 488 (200 nl of 0.1% in PBS; Invitrogen) was injected bilaterally over 5-10 minutes into VTA [from bregma (in mm); -4.35 anteroposterior, ±0.8 lateral, -7.5 ventral]. 30 among 66 injected rats were used to record from RMTg. Channelrhodopsin-2 (ChR2) was expressed using adeno-associated virus constructs prepared by the Vollum Institute Viral Core (Portland, OR). The vector AAV-CAG-ChR2-Venus (100 nl; 5 x 10^{12} genomes/ml) was injected bilaterally using a nanoject II (Drummond Scientific Company) into RMTg [from bregma (in mm); -5.7 anteroposterior, ±0.8 lateral, -7.25 ventral]. 21 among 29 injected rats were used for ChR2 stimulation experiments. After 7-10 days acute brain slices were prepared. Animals were excluded from the study if injections missed the target.

Slice preparation and recording

Adult rats (150-300 g) were anesthetized with isoflurane and killed. Brains were quickly removed and placed in a vibratome (Leica). In addition to intracerebral microinjected animals, 36 rats were used for spontaneous IPSCs and electrical stimulation experiments. Midbrain sagittal slices (220 μm) were prepared in ice-cold physiological solution containing the following (in mM): 126 NaCl, 2.5 KCl, 1.2 $MgCl_2$, 2.4 $CaCl_2$, 1.4 NaH_2PO_4, 25 $NaHCO_3$, 11 D-glucose, and 0.005 MK-801. Slices were incubated in warm (35 °C) 95%O_2/5%CO_2 oxygenated saline containing MK-801 (10 μM) for at least 30 min. Slices containing midbrain were then transferred to the recording chamber that was constantly perfused with 35°C 95%O_2/5%CO_2 oxygenated saline solution at the rate of 1.5-2 ml/min.

RMTg and midbrain dopamine neurons were visualized with a 40 x water-immersion objective on an upright fluorescent microscope (BX51WI, Olympus USA) equipped with gradient contrast infrared optics. Wide field activation of ChR2 was achieved with collimated light from an LED (470 nm; Thorlabs). A 100-200 μm diameter focal laser spot (473 nm laser, IkeCool) was used to activate a ChR2 within RMTg nucleus using 4x objective. Physiological identification of dopamine neurons was based on the presence of D2 receptor mediated GIRK currents and the rate of spontaneous action potential activity (1-5 Hz) with spike widths ≥1.2 ms (Ungless et al., 2004; Ford et al., 2006; Chieng et al., 2011).

Whole-cell and cell-attached recordings were made from RMTg or dopamine neurons using an Axopatch-1D amplifier (Molecular Devices). All recording were

digitized at 10 kHz and filtered at 5 kHz. GABA-A IPSCs were recorded with patch pipettes (2-2.5 MΩ) filled with an internal solution containing the following (in mM): 115 KCl, 20 NaCl, 1.5 $MgCl_2$, 5 HEPES (K), 10 BAPTA, 2 ATP, 0.2 GTP, and 10 phosphocreatine, pH 7.4, 280 mOsM. Cells were voltage clamped at -60 mV. For the recordings from RMTg, KCl was replaced with K-methylsulfate. Series resistance was monitored throughout the experiment (range; 3-15 MΩ), and compensated by 80%. A monopolar saline-filled glass electrode (3-6 MΩ) was used to evoke synaptic release. GABA-A IPSCs were evoked with electric stimulation or presynaptic depolarization induced by ChR2 activation (2 stimuli at 20 Hz; every 20 s). GABA-A IPSCs were pharmacologically isolated with 6,7-dinitroquinoxaline-2,3 (1*H*,4*H*)-dione (DNQX; 10 μM).

Immunohistochemistry

Identification of the RMTg was based on the stimulation of cFOS activity using *d*-amphetamine (4 mg/kg, subcutaneous) 2 hours prior to killing the animals and removing the brain (10 animals including saline control). Brains were post-fixed in 2% paraformaldehyde in PBS overnight at 4 °C. Sagittal brain sections (100 μm) that included the RMTg, VTA/SN were cut in PBS. Free-floating sections were washed three times for 20 min in PBS and blocked with 0.3% Triton-X with 5% normal goat serum for 4 hours. Sections were incubated with rabbit anti-cFOS (1:2000; Santa Cruz Biotechnology) and mouse anti-TH (1:1000; IncStar) overnight. Sections were washed three times in PBS (20 min each) and incubated in Alexa-647 anti-rabbit and Alexa-555 anti-mouse secondary antibody (1:1000;

Invitrogen) for 2 hours. Sections were washed with PBS and mounted with anti-fade gel mount (Biomeda), and visualized with a laser scanning confocal microscope (LSM710, Zeiss).

Data Analysis

Data was collected on a Macintosh computer using AxoGraphX (Axograph Scientific), and stored for offline analysis. Statistical significance was assessed with Student's *t* tests or one-way ANOVA (Bonferonni's *post hoc* analysis) to determine significance; $*p < 0.05$, $***p < 0.001$. Data are presented as mean ± SEM.

Materials

Drugs were applied by bath pefusion. The solution containing [Met^5]enkephalin (ME) included the peptidase inhibitors, bestatin hydrochloride (10 μM) and thiorphan (1 mM). [D-Pen^{2,5}]enkephalin (DPDPE) was obtained from Bachem. ME, [D-Ala^2, N-Me-Phe^4, Gly^5-ol]enkephalin (DAMGO), (+)-(5α,7α,8β)-N-Methyl-N-[7-(1-pyrrolidinyl)-1-oxaspiro[4.5]dec-8-yl]-benzeneacetamide (U69593), naloxone, picrotoxin, and tetrodotoxin (TTX) were obtained from Sigma.

Results

Identification of retrograde labeled neurons within the RMTg in sagittal slices

The RMTg was located as previously reported using the increase in cFOS expression following an injection of *d*-amphetamine (Jhou, 2005; Perrotti et al., 2005; Kaufling et al., 2009). A dense cluster of cFOS immuno-positive cells was found in an area 1-1.5 mm caudal to VTA, 0.5-0.8 mm lateral from midline and 0.1 mm ventral to the decussation of the superior cerebellar peduncle (Figure 2.1A). The retrograde tracer, cholera toxin B (CTX), injected into VTA resulted in the co-localization with cFOS positive neurons (Figure 2.1A inset). Because VTA and substantia nigra are in close proximity, retrograde tracers included both areas. Although not all cFOS neurons co-localized with retrograde tracer, approximately 80% of retrogradely labeled neurons were cFOS positive within RMTg nucleus where dense cFOS immunoreactivity was found. Thus neurons in the RMTg that projected to the VTA/SN could be identified for whole-cell and cell-attached electrophysiological recordings in living slices.

Opioids hyperpolarize RMTg neurons

Retrograde transport of fluorescent microspheres was used to identify neurons in the RMTg that projected to the VTA/SN. This method was preferred over the use of CTX because the microspheres were bright and less susceptible to photobleaching as was found with CTX. Whole-cell current clamp recordings

were made from retrogradely labeled neurons to measure membrane potential and firing rate. Application of [Met^5]enkephalin (ME; 1-10 μM) resulted in hyperpolarization and a decrease in the firing rate (Figure 2.1B). Only cells that were responsive to ME and recovered to baseline following washout were considered to be opioid sensitive (36%; 42/118 neurons). Application of ME (1 μM) and the μ-opioid selective agonist, DAMGO (1 μM) significantly hyperpolarized the retrograde tracer positive neurons (-6.3±0.67 mV; n=8; t_7=9.4; p<0.001, and -5.5±1.67 mV; n=6; t_5=3.3; p<0.05, respectively; student's t test single group comparison to 0 mV), whereas the kappa-opioid agonist, U69593 (1 μM) and the delta-opioid agonist, DPDPE (1 μM) had no significant effect (-0.3±0.30 mV; n=4; t_3=1.1; p=0.36, and -0.9±0.42 mV; n=4; t_3=2.1; p=0.12, respectively, Figure 2.1C).

Opioids inhibit spontaneous activity of RMTg neurons

Cell-attached recordings were made to monitor the spontaneous firing of retrogradely labeled neurons in the RMTg (Figure 2.2A). Approximately half of these neurons fired spontaneously in a rhythmic pattern at 6.7±0.49 Hz (12/26 neurons; Figure 2.2B). The rate of firing was slower than that found in vivo (20.2 Hz, 17.8 Hz, 18.2 Hz, and 15.5 Hz; Jhou et al., 2009a;Hong et al., 2011; Jalabert et al., 2011; Lecca et al,. 2011), but slightly higher than reported with the use of whole-cell current-clamp recording (4.7 Hz; Lecca et al., 2011). The firing rate of RMTg neurons was decreased to 1.7±0.55 Hz by ME (1 μM) and DAMGO (1 μM)

within a few minutes (Figure 2.2B; n=12; $F_{(2,33)}$=33.1; p<0.001 one-way ANOVA Bonferroni). In some cases, opioids completely inhibited the firing of RMTg neurons within 1-2 minutes (n=4). Following the washout of ME or superfusion with naloxone (1 μM) the firing rate gradually returned to the baseline frequency at 6.9±0.52 Hz within 5 minutes (Figure 2.2B). Thus, the spontaneous activity of retrogradely labeled RMTg neurons was sensitive to μ-opioid agonists.

In whole-cell voltage clamp mode, current-voltage plots constructed before and after ME or DAMGO revealed an inwardly rectifying current indicating the activation of an inwardly rectifying potassium channel (GIRK) conductance (data not shown). DAMGO (1 μM) only induced a small outward current (18.0±5.3 pA; n=6), but this was enough to decrease spontaneous firing of the RMTg neurons because of the high input resistance (552±84.6 MΩ). Therefore, the mechanism by which μ-opioid agonists decreased the spontaneous firing of RMTg neurons was from a hyperpolarization through the activation of GIRK.

Opioids inhibit spontaneous GABA-A IPSCs in DA neurons

Whole-cell voltage clamp recordings were made from dopamine neurons in VTA/SN and spontaneous GABA-A IPSCs (sIPSCs) were examined. A high chloride internal was used such that the reversal potential of GABA-A IPSC was 0 mV. Large rhythmic sIPSCs were occasionally observed in recordings from dopamine neurons located in the caudal portion of the VTA/SN (n=7; Figure 2.2C). The average frequency of the rhythmic sIPSCs was 7.1±0.69 Hz and

amplitude of 248±44.1 pA. These sIPSCs were eliminated by bath application of tetrodotoxin (TTX; 300 nM) indicating the dependence on action potentials and the presence of cell body and axonal projection in the brain slice. ME (1 μM) and DAMGO (1 μM) decreased the frequency of the sIPSCs (1.7±0.70 Hz; $F_{(2,18)}$=14.0; p<0.001 one-way ANOVA Bonferroni). The reduction in sIPSC frequency was selective for μ-opioid receptors because the kappa- and delta-opioid agonists U69593 (1 μM) and DPDPE (1 μM) did not significantly affect the sIPSC frequency (87±14.4%; n=9; $F_{(2,24)}$=0.50; p=0.61, and 81±8.5%; n=4; $F_{(2,9)}$=0.20; p=0.83, respectively, one-way ANOVA Bonferroni). The amplitude of the sIPSC was also not changed by the kappa- and delta-opioid agonists (95±10.3%; n=9; $F_{(2,24)}$=0.80; p=0.46 and 95±10.6%; n=4; $F_{(2,9)}$=0.70; p=0.52, respectively, one-way ANOVA Bonferroni). The frequency and opioid sensitivity of sIPSCs on dopamine neurons was remarkably similar to spontaneous firing of RMTg neurons. Stimulation within the RMTg was next used to determine if the pathway from RMTg to the dopamine cells was intact.

Presynaptic GABA transmission from RMTg to dopamine neurons

Electrical stimulation

Electrical stimulation with electrodes placed within RMTg evoked GABA-A IPSCs (eIPSCs) in dopamine neurons (Figure 2.3A). Stimulating electrodes were placed approximately 0.3-1 mm away from the dopamine cells (Figure 2.3B). Successful activation of eIPSCs was only possible in certain 'hot' spots, a small region (50-

100 μm) in the pathway between VTA/SN to RMTg where electrical stimulation successfully activate IPSCs on DA neurons. If the stimulating pipette was moved ±100 μm away from that spot, the same stimulus failed to evoke IPSCs. The delay from the stimulus to the onset of the eIPSC was between 2.2-10.7 ms (5.3±0.32 ms) depending on the distance between the stimulating pipette and the dopamine neuron. The GABA projection from RMTg to the VTA is mainly unmyelinated (Balcita-Pedicino JJ. et al. 2011), therefore, the long latencies of eIPSC following stimulation within the RMTg was due to the slow conductance velocity of unmyelinated axons. Application of the μ-opioid receptor agonist, DAMGO (1 μM) decreased eIPSCs amplitude to 31±3.6% of control (n=40; t_{39}=-19.5; p<0.0001) and superfusion of the opioid antagonist naloxone (1 μM) reversed this inhibition (96±5.5%, n=40; t_{39}=-0.65; p=0.52; student's t test single group comparison to 100% control; Figure 2.3C). However kappa- and delta-opioid agonists (U69653 1 μM, and DPDPE 1 μM) did not decrease eIPSC amplitude significantly (85±7.5%, n=20; t_{19}=-2.1; p=0.053 and 95±3.3%, n=10, t_{9}=-1.6; p=0.13 respectively; Figure 2.3C).

ChR2 stimulation

The expression of ChR2 in the RMTg allowed selective stimulation of cell bodies within the RMTg and terminals from the RMTg that projected to the VTA/SN. Bilateral injections of AAV-ChR2-Venus constructs into the RMTg were used to express ChR2. Light stimulation was used to activate ChR2 expressed on the terminals of RMTg neurons and resulted in the release of GABA on to dopamine

cells (Figure 2.4A). The first experiment was to use wide field stimulation in the VTA/SN. Fluorescent fibers extended from the RMTg toward VTA/SN (Figure 2.4B). Whole-cell voltage clamp recordings (V_m = -60 mV) were made from dopamine neurons in VTA/SN and flashes of light (0.3 ms) were applied at the dopamine cell body (latency 2.8±0.12 ms). A paired light flash (50 ms separation) evoked GABA-A IPSCs (fIPSCs) in most of the caudal portion of VTA/SN. Light stimuli did not induce a direct current in the dopamine neurons indicating that ChR2 was not expressed in the cell that was being recorded (data not shown). The amplitude of fIPSCs varied between 2 nA and 50 pA depending upon the expression level of ChR2, the area that was illuminated and a duration of the light flash. The fIPSCs were completely blocked by TTX (300 nM; 4.6±2.6% of control, n=5) confirming that the GABA release was action potential dependent. In addition, the GABA-A receptor antagonist picrotoxin (100 μM) blocked fIPSC (3.5±0.5% of control, n=12).

To investigate the action of opioids, stimulation was adjusted to evoke ~600 pA GABA-A IPSC (627±75.9 pA, n=34 neurons). Application of ME or DAMGO inhibited the amplitude of fIPSC in all cells tested and the inhibition was graded and reversed by naloxone (1 μM; Figure 2.4A). The inhibition by DAMGO was concentration dependent having an EC50 of 64±10 nM (Figure 2.4C). The paired pulse ratio (PPR, fIPSC2/fIPSC1) was significantly increased from 0.79±0.08 in control to 1.91±0.52 after ME application (1 μM; n=13; t_{24}=-2.1; p=0.04). The PPR was also increased from 0.83±0.05 in control to 1.26±0.15 after application of μ-opioid specific agonist DAMGO (300 nM or 1 μM; n=16; t_{30}=-2.7; p=0.01;

student's t tests unpaired data). The increase PPR suggested that opioid inhibition of fIPSCs was mediated by a presynaptic mechanism. Thus, in addition to reducing the firing rate of RMTg neurons, μ-opioid agonists acted directly at presynaptic terminals to inhibit GABA release onto dopamine neurons.

Light stimulation within the RMTg in slices expressing ChR2 was used to demonstrate the connection between the RMTg and dopamine neurons. For these experiments a focal laser flash (100-200 μm diameter) was applied approximately 0.6-2 mm away from the dopamine neuron in the area of the RMTg (Figure 2.5B). This focal stimulation evoked GABA-A IPSCs with an average amplitude of 338±109 pA (Figure 2.5A). When the focal laser stimulation was moved by ±100 μm the flash failed to evoke an IPSC. The latency between the flash and the initial rise of the GABA-A IPSC was 5.4±0.50 ms, similar to that found with electrical stimulation in the RMTg. Both ME (1 μM) and DAMGO (1 μM) significantly inhibited the IPSC amplitude to 27±5.7% (n=13; t_{12}=-12.8; p<0.001) and 17±5.1% of control (n=10; t_9=-16.3; p<0.001), respectively (Figure 2.5C). This inhibition reversed upon washout of ME or application of naloxone (96±4.0%; n=13; t_{12}=-1.1; p=0.29, and 97±6.7%; n=10; t_9=-0.47; p=0.65, of control, respectively, student's t tests single group comparison to 100% control). Thus, electrical and ChR2 stimulation within RMTg ev0ked GABA-A IPSCs in VTA/SN that were sensitive to inhibition by μ-opioid receptors.

Discussion

This study shows that the dense GABA afferent connection from RMTg to the dopamine neurons is another GABAergic pathway that is sensitive to inhibition by μ-opioid agonists. Application of μ-opioid agonists inhibited the spontaneous firing of RMTg neurons and spontaneous GABA-A IPSCs recorded in dopamine neurons. Electric stimulation in the RMTg triggered GABA-A IPSCs that were blocked by μ-opioid agonists. Expression of ChR2 in the RMTg resulted in light sensitive terminals in the VTA/SN that upon stimulation resulted in GABA-A IPSCs on dopamine neurons. These GABA-A IPSCs were potently inhibited by μ-opioid agonists. Finally, in slices where ChR2 was expressed in the RMTg, focal light stimulation within the RMTg resulted in opioid sensitive GABA-A IPSCs on dopamine neurons. The results indicate that the neurons in the RMTg synapse onto dopamine neurons in VTA/SN and the strength of that connection is reduced upon μ-opioid receptor activation.

GABA interneurons in the VTA/SN are believed to play a major role in opioid dis-inhibition on dopamine neurons (Johnson and North, 1992a). This hypothesis was based on the observation that spontaneous opioid sensitive GABA-A IPSPs were present in horizontal brain slices. The fact that that these spontaneous IPSCs were sensitive to TTX indicated that the cell bodies were located within the slice. There have also been multiple publications demonstrating that non-dopamine neurons in the VTA/SN are sensitive to inhibition by opioids (Johnson and North, 1992a; 1992b; Cameron et al., 1997; Chieng et al., 2011). There is, however, no direct functional evidence that the non-dopamine neurons synapse

onto dopamine neurons in VTA/SN. It may be that interneurons and RMTg neurons both synaptically regulate dopamine neurons. Previous reports indicated that 35-50% of VTA and 20% of substantia nigra neurons are GABA neurons (Margolis et al., 2006; Nair-Roberts et al., 2008; Balcita-Pedicino et al., 2011; Chieng et al., 2011) although the density of synapses onto a dopamine neuron arising from interneurons is not known. In addition, VTA/SN neurons receive GABA inputs from striatum, nucleus accumbens, external globus pallidus. However, the relative role of opioid action on those pathways is not known. With non-selective electrical stimulation within the VTA/SN, opioids inhibited GABA-A IPSCs by a maximum that varied between 40 and 75% (Johnson and North, 1992a; Ford et al., 2006; Madhavan et al., 2010). With selective stimulation of the RMTg used in this study DAMGO (1 μM) inhibited the amplitude of IPSCs by an average of 69% using electrical stimulation and 83% using ChR2 stimulation. In 5 of 10 experiments using ChR2 stimulation in the RMTg, the amplitude of the IPSC was decreased by more than 90%. This observation indicates that the IPSCs from the RMTg are more sensitive to inhibition by opioids than when non-selective stimulation is used to evoke IPSCs. Whole-cell recording from RMTg neurons showed that not all RMTg neurons were inhibited by opioids. Yet, stimulation in the RMTg resulted in GABA-A IPSCs that were always sensitive to opioids. This observation suggests that there may be a heterogeneous population of RMTg neurons but that most neurons that project to the VTA/SN were sensitive to opioids. Given the density of GABA innervation from the RMTg to dopamine neurons, it is possible that this pathway is another major contributor

in the opioid sensitive GABA input onto dopamine neurons (Kaufling et al., 2009; Jhou et al., 2009b; Balcita-Pedicino et al., 2011; Lecca et al., 2011). This suggestion is supported by a recent study *in vivo* demonstrating that morphine acts in the RMTg to increase the firing of dopamine neurons (Jalabert et al., 2011).

Electrophysiological characteristics of RMTg/tVTA

Neurons in the RMTg receive a strong glutamate input from lateral habenula (Hong et al., 2011) and fire action potentials at approximately 10-20 Hz *in vivo* (Jhou et al., 2009a; Hong et al., 2011; Jalabert et al., 2011; Lecca et al., 2011). The spontaneous activity of RMTg neurons in the present study and previous publications using brain slices was 4.7-10.5 Hz. This activity was considered to be intrinsic because the glutamate pathway from the lateral habenula was severed (Lecca et al., 2011). Thus, the difference in frequency between *in vivo* and *in vitro* preparations most likely results from the removal of afferent excitatory drive in brain slices.

The frequency and sensitivity to opioids of sIPSCs recorded in dopamine neurons was also similar to the firing rate of RMTg neurons. The all-or-none waveform and rhythmic pattern of sIPSCs probably originates from the firing of a single neuron. As previously reported, opioids gradually decreased the frequency of sIPSC without affecting the amplitude (Johnson and North, 1992b). This all-or-none inhibition suggests that the spontaneously firing of presynaptic GABA

neurons in the slice was decreased by opioids. The potential mechanism for the inhibition of sIPSCs is mainly through a hyperpolarization of the presynaptic membrane potential as was observed in the RMTg.

Opioid agonists also inhibit transmitter release through an inhibition of voltage dependent calcium channels as well as a direct action of βγ-subunits on the release machinery SNAP-25 (Blackmer et al., 2005; Gerachshenko et al., 2005). Unlike the all-or-none inhibition of sIPSCs by opioids, a graded inhibition of IPSCs by opioids was observed in experiments where axons and terminals within the VTA/SN were activated using ChR2 (Figure 2.4). This observation suggests that there are multiple opioid sensitive release sites that synapse on a single dopamine neuron that arise from the RMTg. This also suggests that the underlying mechanism for the inhibition of GABA release from terminals may differ from the activation of GIRK conductance measured in RMTg somata.

The activity of lateral habenula neuron is increased following the absence of an expected reward or an aversive stimulus. This increased activity preceded a pause in dopamine cell firing (Matsumoto and Hikosaka, 2007; Hong et al., 2011). Although the RMTg might receive inputs from reward related brain regions other than lateral habenula, some RMTg neurons were activated in response to a negative reward cue and this activation was followed by an inhibition of dopamine neurons (Hong et al., 2011). Thus, RMTg neurons are an inhibitory relay structure to dopamine neurons.

The relative role of RMTg in opioid actions within the VTA/SN is not known. FOS expression in the RMTg increased during acute withdrawal from several psychostimulants, however, morphine applied acutely did not elevate FOS expression (Kaufling et al., 2010b). The lack of FOS expression might be due to the inhibition of RMTg neurons by opioid. During the withdrawal from a 1-week exposure to morphine, the probability of GABA release was increased in the VTA and substantia nigra (Bonci and Williams, 1996; 1997). This may suggest that during withdrawal from morphine the firing of dopamine neurons is suppressed through an increased GABA input from the RMTg. The role of the RMTg in this observation remains to be determined given that there are multiple GABA inputs onto dopamine neurons.

In conclusion, the GABA neurons in the RMTg send a dense projection to dopamine neurons in the VTA/SN. This GABA input is potently inhibited by the activation of mu-, but not kappa-or delta- opioid receptors. Given the density of the GABA innervation and the potency of the opioid inhibition of GABA release from these cells it appears that the neurons of the RMTg are a key site of opioid action in the mesolimbic reward pathway.

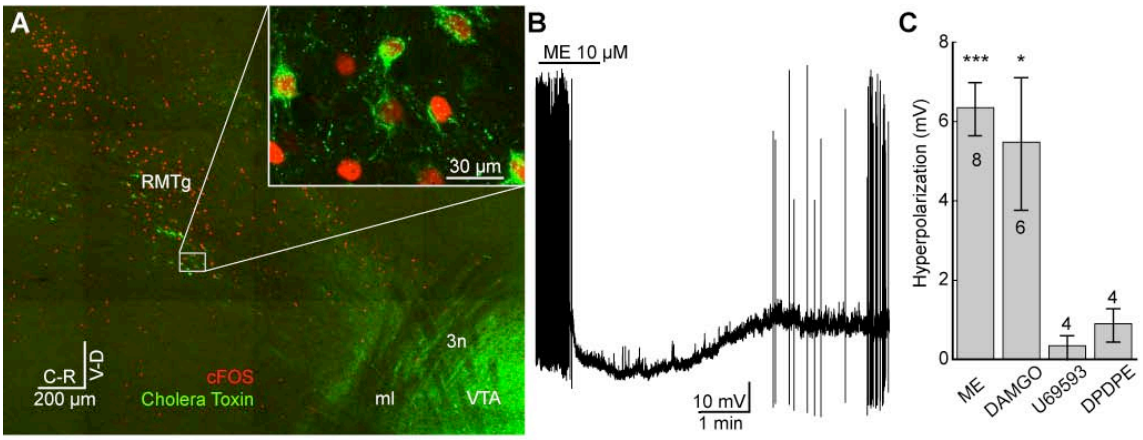

Figure 2.1: Hyperpolarization of identified RMTg neurons mediated by μ-opioid agonists

A. Confocal mosaic image of a sagittal slice containing VTA/substantia nigra and RMTg. RMTg neurons were identified with elevated cFOS (red) activity two hours after an injection of amphetamine. The retrograde tracer, Cholera Toxin Subunit B (Green), was injected into VTA. cFOS positive neurons frequently co-localized with retrograde tracer (Inset). VTA, ventral tegmental area; RMTg, rostromedial tegmental nucleus/the tail of the ventral tegmental area; ml, medial lemniscus; 3n, oculomotor nerve. B. Whole-cell current clamp recording from retrograde tracer positive neuron. ME (10 μM) caused hyperpolarization and decreased spontaneous firing. C. Retrogradely labeled neurons in the RMTg were hyperpolarized through an activation of μ-opioid receptors DAMGO. Application of ME and DAMGO but not kappa- or delta-opioid agonists (U69593 or DPDPE) significantly induced a hyperpolarization of the membrane potential from the baseline potentials. Number of cells indicated in or above the bars. Error bars indicate SEM. *p<0.05, ***p<0.001

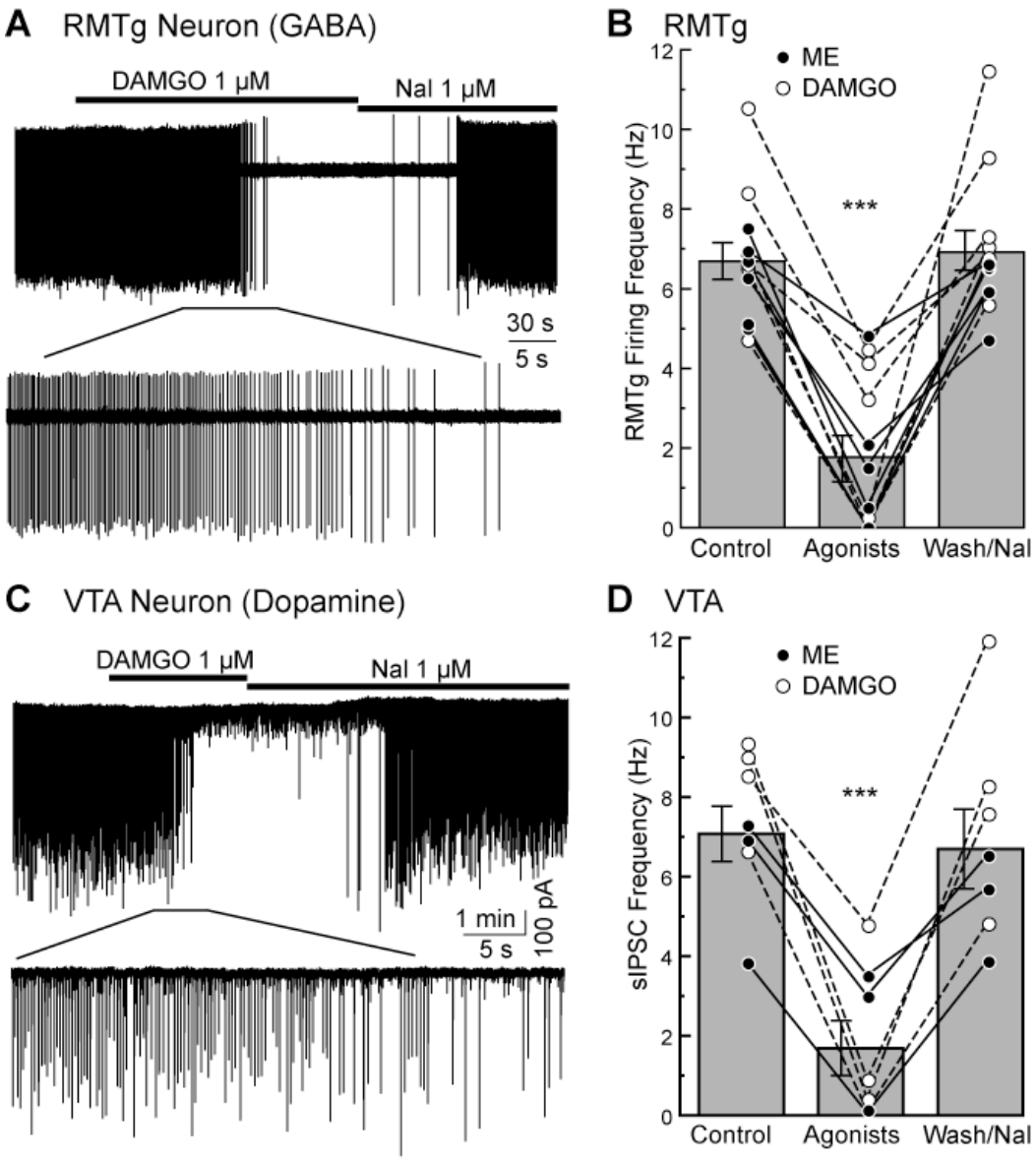
A RMTg Neuron (GABA)
DAMGO 1 μM
Nal 1 μM
30 s
5 s
B RMTg
ME
DAMGO
RMTg Firing Frequency (Hz)
***
Control
Agonists
Wash/Nal
C VTA Neuron (Dopamine)
DAMGO 1 μM
Nal 1 μM
1 min
5 s
100 pA
D VTA
ME
DAMGO
sIPSC Frequency (Hz)
***
Control
Agonists
Wash/Nal

Figure 2.2: The firing rate of retrogradely labeled RMTg neurons and rate of spontaneous GABA-A IPSCs were inhibited by μ-opioid agonists

A. Cell-attached recording from RMTg neuron. Application of μ-opioid agonist DAMGO (1 μM) gradually inhibited the firing of the neuron. This inhibition was reversed by application of opioid antagonist naloxone (1 μM). B. Summary plot of the firing rate of RMTg neurons in control, during application of ME (filled circle; 1 μM) or DAMGO (open circle; 1 μM), and washout ME or superfusion of naloxone after DAMGO (n=12). Application of ME or DAMGO significantly reduced frequency of spontaneous firing from control and washout. Bar graphs represent the average firing frequency of shown data. C. Whole-cell voltage clamp recording from a VTA/SN dopamine neuron. Rhythmic spontaneous GABA-A IPSCs were examined. The μ-opioid agonist DAMGO (1 μM) decreased large amplitude sIPSCs, but not miniature IPSCs and the inhibition was reversed by naloxone (1 μM). D. Summary plot of the frequency of the large amplitude sIPSCs in control, during ME (filled circle; 1 μM) or DAMGO (open circle; 1 μM), and washout of ME or superfusion of naloxone after DAMGO. Application of ME or DAMGO significantly reduced frequency of sIPSC from control and washout. Bar graphs represent the average sIPSC frequency of shown values. In B and D, lines connecting circles indicate recordings made from the same cell. Error bars indicate SEM. *** $p<0.001$

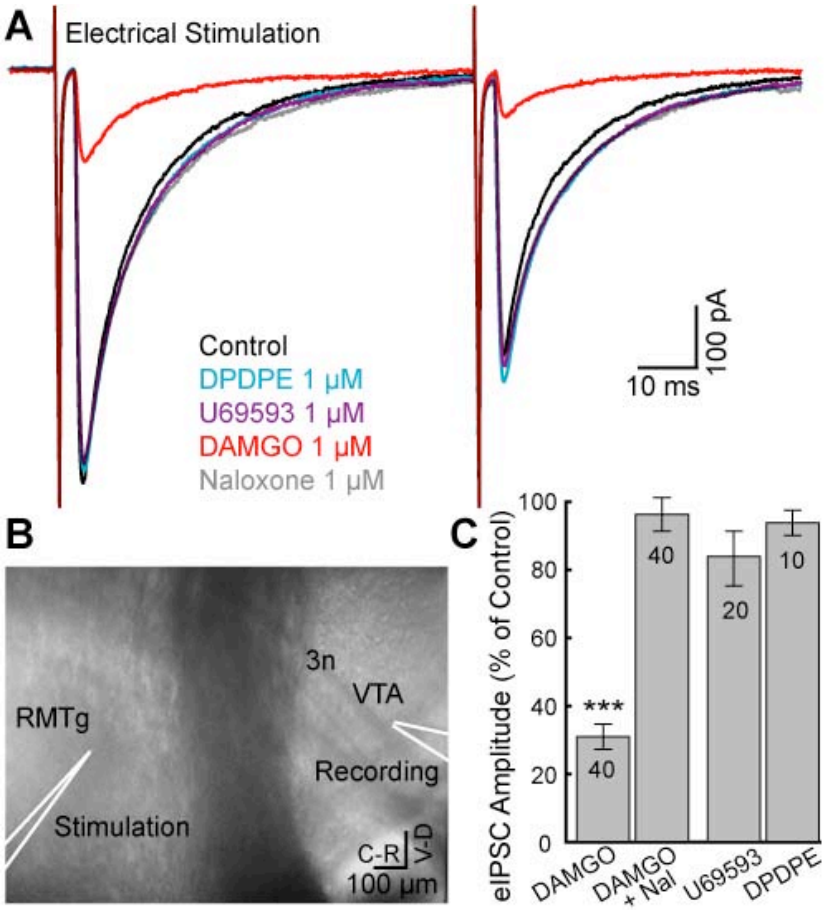

Figure 2.3: Electrical stimulation in the RMTg evoked µ-opioid sensitive IPSCs in dopamine neurons

A. Superimposed traces of evoked IPSCs in a dopamine neuron (Vm=-60 mV, average of 10). Application of DAMGO, but not U69593 or DPDPE, decreased the amplitude of eIPSCs. B. Representative image indicating the location of an electrical stimulation and site of recording in the sagittal plane. C. Summary graph of eIPSC amplitude (% of control) during µ-opioid agonist (DAMGO), reversal by opioid antagonist (Naloxone), and during kappa-, or delta-opioid agonists (U69563, or DPDPE). DAMGO significantly reduced eIPSC amplitude compared to 100% control. Number of cells indicated in bars. Error bars indicate SEM. ***p<0.001

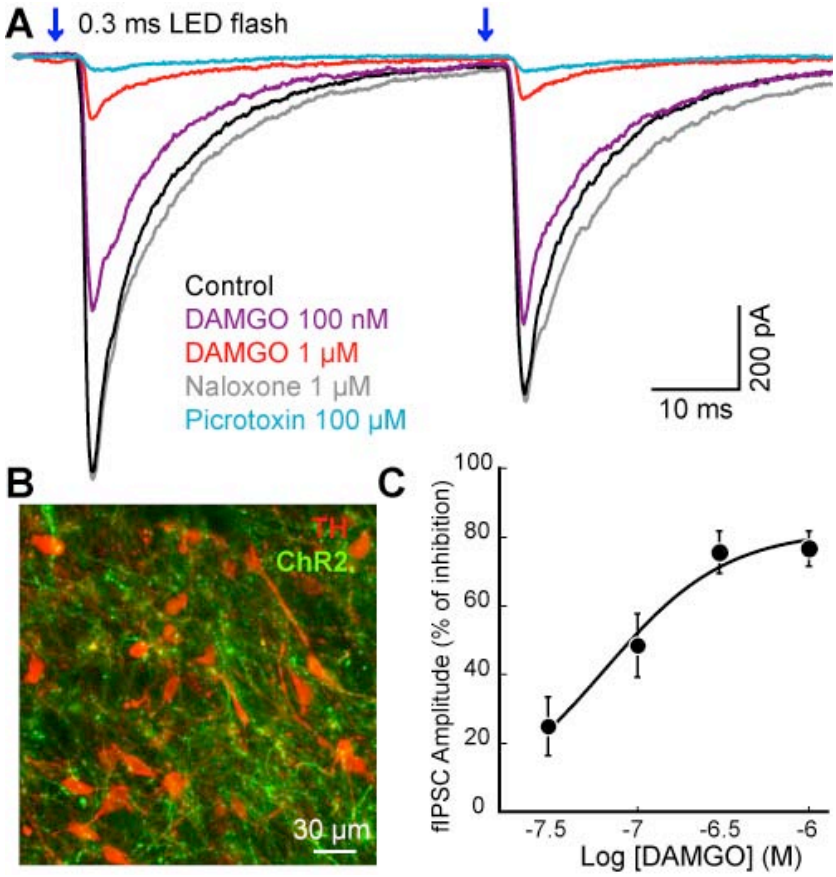

Figure 2.4: DAMGO inhibited ChR2 evoked IPSCs on dopamine neurons

A. Superimposed traces of flash evoked fIPSCs (0.3 ms; 470 nm) in a dopamine neuron (Vm=-60 mV, average of 10). DAMGO decreased the amplitude of fIPSCs in a concentration-dependent manner. The GABA-A receptor antagonist picrotoxin (100 µM) blocked fIPSCs. B. Confocal image stained for tyrosine hydroxylase (TH; red) and ChR2 conjugated with Venus (green) in VTA. ChR2 expressing axons were densely innervated in the VTA/SN 7 days after AAV viral expression of ChR2 in the RMTg. C. Concentration-response curve of the inhibition of fIPSC by DAMGO. Error bars indicate SEM.

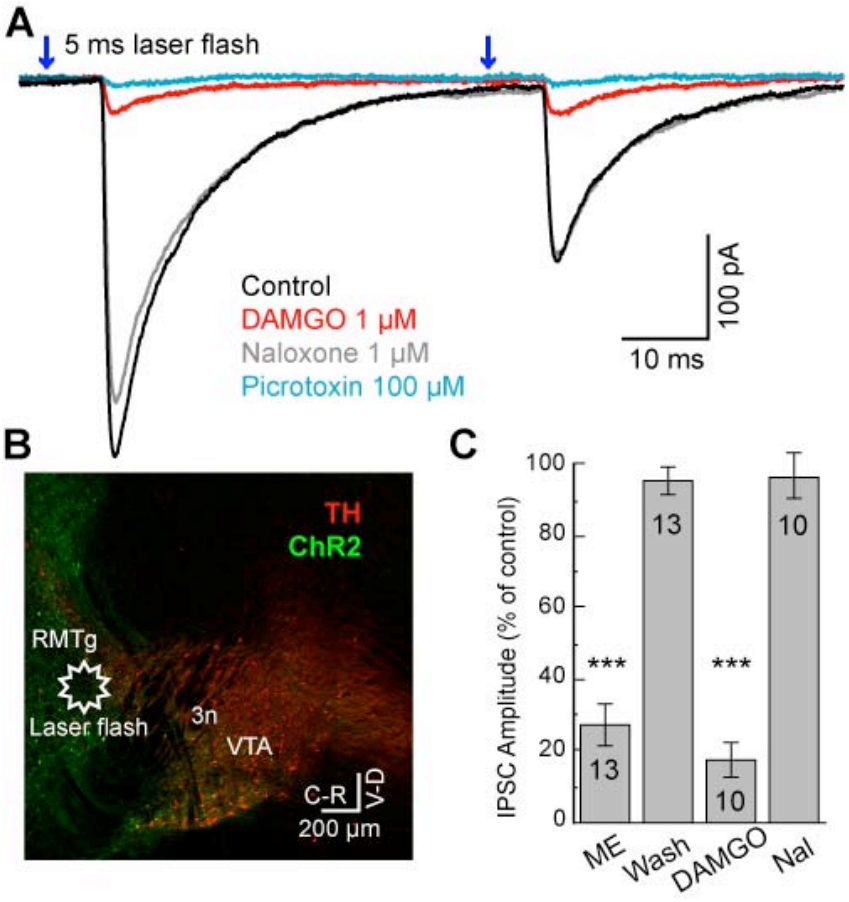

Figure 2.5: Activation of ChR2 in the RMTg evoked IPSCs in dopamine neurons that were inhibited by µ-opioid agonists

A. Superimposed traces of IPSCs in a dopamine neuron evoked by laser flashes (5 ms; 473 nm, average of 5) in the RMTg. DAMGO (1 µM) and picrotoxin (100 µM) inhibited amplitude of IPSCs. Notice the latency between laser stimulation and the onset of the IPSC (5.4±0.5 ms). B. Wide-field mosaic confocal image stained for tyrosine hydroxylase (TH; red) and ChR2 conjugated with Venus (green) in sagittal plane. The star indicates the location of laser stimulation in RMTg. C. Summary graph of flash evoked IPSC amplitude. ME (1 µM) and DAMGO (1 µM) significantly decreased IPSC amplitude compared to 100% control. The inhibitions were reversed by washout of ME or by naloxone (1 µM) after DAMGO that were not significantly different than 100% control. Number of cells indicated in the bars. Error bars indicate SEM. ***p<0.001

Chapter 3: Manuscript 2

Opioid Mediated Inhibition of GABA Inputs to Dopamine Neurons Occurs Primarily on Inputs Arising from Outside the VTA

Aya Matsui,[1] Brooke C Jarvie,[2] Shane T Hentges,[2] and John T. Williams[1]

[1]Vollum Institute, Oregon Health and Science University, Portland, OR, 97239, USA, and [2]Department of Biomedical Sciences, Colorado State University, Fort Collins, CO, 80523, USA

Corresponding author:
John T. Williams
Vollum Institute,
Oregon Health & Science University,
Portland, Oregon 97239,
williamj@ohsu.edu

Acknowledgements: The authors would like to thank Dr. C.P. Ford and members of the Williams laboratory for providing critical feedback on this manuscript. This work was supported by NIH grants, DA08163, DA04523 (JTW) and DK0798749 (STH).

[This manuscript is submitted in Journal of Neuroscience]

Abstract

Opioids increase the activity of dopamine neurons by inhibiting GABA input. This disinhibition was originally proposed to result from an inhibition of interneurons in the ventral tegmental area (VTA), however multiple opioid-sensitive GABA inputs are now known to exist. To examine the relative opioid sensitivity of these different GABA terminals, channelrhodopsin2 (ChR2) was expressed in the VTA, nucleus accumbens (NAc), and rostromedial tegmental nucleus (RMTg) in rats. Activation of ChR2 in neurons from these areas evoked GABA-A IPSCs in dopamine neurons. The sensitivity of GABA-A IPSCs to μ-opioid receptor (MOR) agonists from these pathways varied considerably with IPSCs from VTA interneurons being the least sensitive while inputs from the RMTg were the most sensitive. Repetitive activation of ChR2 from each GABA input evoked GABA-B IPSCs in dopamine neurons that had a similar sensitivity to opioids as the GABA-A IPSCs. In addition to innervating dopamine cells, GABA neurons in the VTA projected to cholinergic interneurons in the NAc. The opioid sensitivity of this projection was similar to that on dopamine cells in the VTA, suggesting that GABA neurons in the VTA may be both interneurons and projection cells. Lastly, two separate GABA projections were identified from the striatum to the VTA and SN reticulata based on the sensitivity to opioids and dopamine. The results indicate that opioid regulation of GABA transmission in the mesolimbic circuit involves multiple pathways and suggest that opioid inhibition of GABA inputs from the RMTg is particularly important for the disinhibition of VTA dopamine neurons.

Introduction

Dopamine neurons in VTA and substantia nigra pars compacta (SNc) respond by burst firing following salient stimuli, motivation or impulsive movement (Schultz, 2007; Bromberg-Martin et al., 2010). Bursts of action potentials in dopamine neurons result in the release of dopamine and long-term modifications of neuronal circuits in projection areas involved in processes of reward learning. The activity of dopamine neurons is tightly controlled by the balance of intrinsic activity and excitatory and inhibitory inputs. At least 70% of synaptic inputs to dopamine neurons are GABAergic arising from multiple areas including the substantia nigra pars reticulata (SNr), nucleus accumbens (NAc), globus pallidus, ventral pallidum, and diagonal band of Broca (Bolam and Smith, 1990; Tepper et al., 1995; Tepper and Lee, 2007; Watabe-Uchida et al., 2012). Tonic GABA input is sufficient to suppress burst firing even with excitatory inputs intact (Lobb et al., 2010; Jalabert et al., 2011). Thus, it is important to understand the mechanisms that modulate the release of GABA onto dopamine neurons.

Activation of GABA input from the NAc and dorsal striatum to the ventral midbrain have been shown to result in IPSCs in GABA but not dopamine neurons (Chuhma et al., 2011; Xia et al., 2011). However, a recent trans-synaptic retrograde study indicated that dopamine neurons in VTA and SNc also receive direct inputs from NAc and dorsal striatum (Watabe-Uchida et al., 2012). Based on pharmacological results, it was suggested that the striatal input to dopamine neurons selectively activate GABA-B receptors to result in a G-protein coupled inwardly rectifying potassium (GIRK) channel dependent IPSP (Sugita et al.,

1992b);(Johnson and North, 1992a; Shoji et al., 1999). The functional r0le of the GABA input from the NAc and dorsal striatum to dopamine neurons therefore remains to be determined.

GABA input to dopamine neurons is reduced by the activation of μ-opioid receptors (MORs), resulting in an increase in firing rate of dopamine neurons through disinhibition originally thought to be mediated by local interneurons (Gysling and Wang, 1983; Johnson and North, 1992a). Recently, the rostromedial tegmental nucleus (RMTg) was found to send a dense GABA input to dopamine neurons (Kaufling et al., 2009; Jhou et al., 2009a; 2009b). As GABA-A-mediated IPSCs from the RMTg to dopamine neurons were almost completely abolished by opioids, the possibility exists that the local interneurons may not be the major site of action of opioids (Jalabert et al., 2011; Matsui and Williams, 2011). It therefore remains to be determined which GABA inputs are responsible for the disinhibition of dopamine neurons.

This study focuses on the major opioid-sensitive GABA inputs including interneurons in the VTA and projection neurons from the NAc and the RMTg. In addition, the opioid sensitivity of the reciprocal GABA connection from the VTA to the NAc was examined. The results indicate that GABA neurons in the VTA synapse locally on dopamine neurons and project to cholinergic interneurons (CINs) in NAc. Activation of GABA projections from the NAc and dorsal striatum resulted in IPSCs in both dopamine and GABA neurons of the VTA/SNr. IPSCs evoked from interneurons in the VTA and projections from the NAc were less

sensitive to opioids than the IPSCs evoked from the RMTg. In addition, repetitive stimulation of each GABA input induced GABA-B-dependent IPSCs in dopamine neurons that were also inhibited by opioids. In summary, dopamine neurons receive multiple opioid sensitive GABA inputs and opioids most strongly inhibited the RMTg projection.

Materials & Methods

All procedures were performed in accordance with the guidelines of Oregon Health & Science University and the Animal Care and Use Committees approved all of the experimental procedures.

Intracerebral microinjections

Male and female Sprague-Dawley rats (p20-22, Charles River Laboratories) were used for intracerebral microinjections. Rats were anesthetized with isoflurane and immobilized in a Stereotaxic Alignment System (Kopf Instruments). Channelrhodopsin-2 (ChR2) was expressed using adeno-associated virus (AAV) constructs prepared by the Vollum Institute Viral Core (Portland, OR). The vector AAV-CAG-ChR2-Venus (serotype 9 or DJ, 100 nl; 5 x 10^{12} genomes/ml) was injected bilaterally using a nanoject II (Drummond Scientific Company) into VTA [from bregma (in mm); -4.35 anteroposterior, ±0.8 lateral, -7.5 ventral], NAc [from bregma (in mm); 0.9 anteroposterior, ±1.8 lateral, -5.5 ventral], or RMTg [from bregma (in mm); -5.7 anteroposterior, ±0.8 lateral, -7.25 ventral]. Experiments were performed in 36 of 40 rats where injections were successfully placed in VTA, 24 of 34 rats in the NAc injections, and 17 of 20 rats in RMTg injections. Acute brain slices were prepared 14-21 days after the VTA injection, 21-28 days after NAc injection, and 7-10 days after RMTg injections. ChR2 expressions at the injection sites were conformed before experiments, and animals were excluded from the study when ChR2 expression spread outside of the target.

Slice preparation and recording

Adult rats (150-300 g) were anesthetized with isoflurane and killed. Brains were quickly removed and placed in a vibratome (Leica). Sagittal slices (220-230 μm) were prepared in ice-cold physiological solution containing the following (in mM): 126 NaCl, 2.5 KCl, 1.2 $MgCl_2$, 2.4 $CaCl_2$, 1.4 NaH_2PO_4, 25 $NaHCO_3$, 11 D-glucose, and 0.005 MK-801. Slices were incubated in warm (35 °C) 95%O_2/5%CO_2 oxygenated saline containing MK-801 (10 μM) for at least 30 min. Slices containing midbrain or NAc were then transferred to the recording chamber that was constantly perfused with 35°C 95%O_2/5%CO_2 oxygenated saline solution at the rate of 1.5-2 ml/min.

Midbrain and NAc neurons were visualized with a 40x water-immersion objective on an upright fluorescent microscope (BX51WI, Olympus USA) equipped with gradient contrast infrared optics. Wide field activation of ChR2 was achieved with collimated light from an LED (470 nm; Thorlabs). A 20-100 μm diameter focal laser spot (473 nm laser, IkeCool) was used to activate a ChR2 within VTA using a 40x objective. Physiological identification of dopamine neurons was based on the presence of D2-autoreceptor-mediated GIRK currents and the rate of spontaneous action potential activity (1-5 Hz) with spike widths ≥1.2 ms (Ungless et al., 2004; Ford et al., 2006; Chieng et al., 2011; Li et al., 2012). The identification of MSN and CIN were based on the size/membrane capacitance, the resting membrane potential and opioid sensitivity (Britt and McGehee, 2008).

Whole-cell voltage clamp recordings were made using an Axopatch-1D amplifier (Molecular Devices). All recordings were digitized at 10 kHz and filtered at 5 kHz. GABA-A IPSCs were recorded with patch pipettes (2-2.5 MΩ) filled with an internal solution containing the following (in mM): 57.5 KCl, 57.5 K-methylsulfate, 20 NaCl, 1.5 $MgCl_2$, 5 HEPES (K), 10 BAPTA, 2 ATP, 0.2 GTP, and 10 phosphocreatine, pH 7.35, 280 mOsM. All neurons were voltage clamped at -60 mV. Series resistance was monitored throughout the experiment (range; 3-15 MΩ), and compensated by 80%. GABA-A IPSCs were evoked by the activation of ChR2 (2 stimuli at 20 Hz; every 20 or 30 s). All recordings were performed in the presence of 6,7-dinitroquinoxaline-2,3 (1*H*,4*H*)-dione (DNQX; 10 μM) to isolate GABA-A IPSCs.

Data Analysis

Data were collected on a Macintosh computer using AxoGraphX (Axograph Scientific), and stored for offline analysis. Statistical significance was assessed with Student's *t* tests or one-way ANOVA (Bonferonni's *post hoc* analysis); $*p<0.05$ and $**p<0.001$. Data are presented as mean ± SEM.

In situ hybridization

Seventeen days after virus containing the ChR2-Venus construct was injected, rats were anesthetized with an overdose of pentobarbital (400 mg/kg, i.p. injection) and transcardially perfused with 10% sucrose followed by 4% formaldehyde in PBS. Brains were removed and postfixed overnight in 4% formaldehyde at 4°C. The *in situ* hybridizations were performed as previously described (Jarvie and Hentges, 2012)

with the exception that glutamate decarboxylase (*Gad*) *65* and *67 mRNAs* were simultaneously detected to reveal all *Gad* positive cells with one fluorophore. In brief, sagittal slices (50 μm) containing the VTA were prepared on a vibratome and placed in diethylpyrocarbonate (DEPC) treated PBS. The tissue was exposed to proteinase K (10 μg/mL) diluted in PBS containing 0.1% Tween-20 (PBST) for 15 minutes at room temperature. Tissue was then rinsed in PBST containing glycine (2 mg/mL) to inactivate the proteinase K and then subjected to two 5-minute washes in PBST. Slices were then postfixed with 4% paraformaldehyde/0.2% gluteraldehyde in PBST for 20 minutes at room temperature and then rinsed in PBST. Sections were dehydrated in ethanol of increasing concentrations (50, 70, 95, and 100%) and then rinsed briefly with PBST before being placed into hybridization buffer containing the following: 66% formamide, 13% dextran, 260 mM NaCl, 13 mM Tris, 1.3 mM EDTA, 0.5 mg/mL yeast tRNA, 10 mM DTT, and 1X Denhardt's Solution (pH 8.0). After 1 h in hybridization buffer probes were added.

Digoxigenin (DIG)-labeled antisense RNA probes for the 65 and 67 kDa isoforms of GAD were made as previously descrived (Jarvie and Hentges, 2012). The *Gad67* probe corresponded to base pairs 1196-2001 of accession number NM_017007.1, which has 94% homology with the cDNA for rat *Gad67*. *Gad65* was labeled using two probes simultaneously corresponding to base pairs 312-945 and 940-1770 of accession number NM_012563.1, both of which have 100% homology with rat cDNA. Each probe was used at a concentration of 150 pg/μl. The *Gad67* probe was hybridized first for 18-20 h at 70ºC, then the tissue was moved into hybridization

buffer containing the *Gad65* probes and incubated for 20 h at 52ºC. Sense probes were used to establish specificity of antisense probes.

Following hybridization, sections were subjected to three 30-minute washes with 50% formamide in 5XSSC (pH 4.5) and three 30-minute washes with 50% formamide in 2xSSC at 60ºC. Tissue was then digested for 30 min at 37ºC with RNAse A (20 μg/mL) in Tris buffer plus 0.5 M NaCl, pH 8.0 then washed 3 times in TNT (0.1 M Tris-HCl pH 7.5, 0.15M NaCl, 0.05% Tween-20), and blocked for one hour at room temperature in TNB (TN plus 0.5% Blocking Reagent provided in the TSA kit, Perkin Elmer). Venus fluorescence was quenched by the *in situ* hybridization procedure, however antigenicity remained allowing immunohistochemical detection of the ChR2-Venus. For detection of Venus and DIG, sections were incubated overnight at 4ºC with sheep anti-DIG conjugated to horseradish peroxidase (Roche Applied Sciences, 1:1000) and chicken anti-GFP (abcam ab13970, 1:2000) in TNB. After 3 washes in TNT, sections were subjected to a 30-minute biotin amplification using a TSA Plus Biotin Kit (Perkin Elmer) following manufacturer's instructions. After biotin amplification, sections were incubated for 30 minutes in streptavidin conjugated to Alexa Fluor 488 (Invitrogen, 1:1000), then washed 3 times in TNT. Finally, sections were incubated for 2 hours in donkey anti-chicken conjugated to Alexa Fluor 647 secondary antibody (Jackson ImmunoResearch), washed 3 times in TNT. Sections were then placed on glass slides and cover-slipped using Aqua Poly/Mount (Polysciences, Inc., Warrington, PA).

Image and Analysis

Images were collected with a Zeiss laser scanning confocal LSM780 microscope. Z-stack tile images were taken from all of the tissue containing VTA and SNc. The percentage of co-localized neurons was calculated by counting the total number of colabeled neurons divided by the total ChR2 positive neurons. In order to count the neurons co-labeling ChR-2 and GAD, ChR2 positive neurons were identified first and observed the co-localization with GAD65/67. The images were analyzed in ImageJ software (National Institute of Health, Bethesda, MD) for cell count.

Materials

Drugs were applied by bath pefusion. The solution containing [Met^5]enkephalin (ME) included the peptidase inhibitors, bestatin hydrochloride (10 μM) and thiorphan (1 μM). ME, [D-Ala^2, N-Me-Phe^4, Gly^5-ol]enkephalin (DAMGO), (+)-(5α,7α,8β)-N-Methyl-N-[7-(1-pyrrolidinyl)-1-oxaspiro[4.5]dec-8-yl]-benzeneacetamide (U69593), naloxone, picrotoxin, SR 95531, dopamine, sulpiride, 4-Amunopyridine, DNQX, and tetrodotoxin (TTX) were obtained from Sigma-Aldrich (St. Louis, MO). MK-801 was purchased from Ascent Scientific (Weston-Super-Mare, UK). CGP55845 and quinpirole were obtained from Tocris Bioscience (Ellisville, MO).

Results

ChR2 expression in VTA dopamine and GABA neurons

Injection of AAV-DJ (100 nl, AAV-CAG-ChR2-Venus) resulted in the expression of ChR2 that was limited to small regions of VTA and substantia nigra (SN, Figure 3.1). Fluorescent *in situ* hybridization was used to detect mRNA for GAD65 and GAD67 (Jarvie and Hentges, 2012), the enzymes responsible for GABA synthesis. *Gad65/67* expression was found in areas known to contain GABA neurons, including the VTA and SN. The number of the neurons that expressed ChR2 was counted from 6 injection sites from 3 animals. Of the ChR2-positive neurons in both the VTA and SN, 21.7% expressed *Gad65*/*Gad67* mRNA (Figure 3.1; 418/1924 neurons, n=6 injections). Previous reports indicated that approximately 30-35% of VTA and 20% of SNc neurons are GABAergic (Van Bockstaele and Pickel, 1995; Nair-Roberts et al., 2008; Dobi et al., 2010). Thus ChR2 was non-selectively expressed in both GABA and dopamine neurons in the VTA and SN.

VTA GABA neurons innervate both VTA dopamine and cholinergic interneurons in NAc

Whole-cell voltage clamp recordings were made from dopamine neurons and brief focal laser stimulation (3 ms paired stimuli; 50 ms interval; every 30 seconds; 20-100 μm diameter) was applied to evoke GABA release from ChR2-expressing GABA interneurons in the VTA (Figure 3.2A). High chloride internal

solution was used for all experiments to evoke large amplitude inward GABA-A IPSCs (E_{Cl}=-14 mV). In some cases, the GABA-A IPSCs followed a direct ChR2 mediated current. In those cases, ChR2 mediated currents were subtracted from GABA-A IPSCs post-hoc following the application of the GABA-A receptor antagonists (picrotoxin, 100 μM or SR 95531, 3 μM). In all cases, the ChR2-evoked GABA-A IPSCs were blocked with the sodium channel blocker TTX (300 nM), thus GABA-A IPSCs were mediated by presynaptic action potentials. Application of a saturating concentration of the MOR-specific agonist DAMGO (1 μM) significantly decreased the amplitude of IPSCs (66.0±5.3% of control, n=10, p<0.001, Student's t test single group comparison to 100% control). The κ-opioid receptor (KOR) agonist U69653 (1 μM) caused a very small inhibition of the GABA-A IPSC (92.7±3.1% of control, n=23, p=0.028). Dopamine (3-10 μM) or the D2-like receptor agonist quinpirole (3 μM) did not change the IPSC amplitude significantly (101.5±3.5% of control, n=5, p=0.69; and 99.0±1.9% of control, n=12, p=0.62 respectively; Figure 3.2C). MORs have recently been found to produce a near complete inhibition of GABA release from RMTg inputs (Matsui and Williams, 2011), such that the present results suggest that MORs may less effectively inhibit GABA release arising from local VTA interneurons.

Previous reports indicate that the GABA neurons in VTA project to the NAc (Van Bockstaele and Pickel, 1995; van Zessen et al., 2012). Here, the opioid-sensitivity of this projection was examined. When ChR2 was expressed in the VTA, light-evoked GABA-A IPSCs in the NAc were frequently found in CINs (average amplitude 463±132 pA, n=34; Figure 3.2B). The IPSCs in CINs were significantly

inhibited by the MOR agonist DAMGO (1 μM; 61.4±2.0% of control, n=16, $p<0.001$), but were insensitive to the KOR agonist U69593 (1 μM; 100.4±2.6% of control, n=11, $p=0.85$; Figure 3.3C). Application of dopamine (3 μM) did not inhibit GABA-A IPSCs (109.2±5.1% of control, n=6, $p=0.14$), suggesting that GABA was not being released from projecting dopamine neurons. The inhibition of GABA-A IPSCs induced by DAMGO (1 μM) in CINs was similar in magnitude to the inhibition measured in dopamine neurons (61.4±2.0% in CINs vs 66.0±5.3% in dopamine neurons). Occasionally small amplitude of GABA-A IPSCs were also observed in medium spiny neurons (MSNs; data not shown). The infrequent and small amplitude GABA-A IPSCs in MSNs were not characterized further.

As previously described (Britt and McGehee, 2008), MOR agonists induced an outward current in the CINs (DAMGO 1 μM; 109.8±24.68 pA, n=11). To examine whether the opioid inhibition of GABA-A IPSCs in CINs was mediated by a presynaptic mechanism, the paired-pulse ratio (PPR = IPSC2/IPSC1) was measured. The PPR was significantly increased from 0.51±0.03 to 0.69±0.05 after application of DAMGO (1 μM, n=34, $p<0.0001$, Student's *t* test paired comparison; data not shown). However, the PPR was not changed after application of KOR agonist, U69593 (1 μM, 0.50±0.05 to 0.51±0.05, n=11, $p=0.43$). The increase in the PPR suggests that the probability of GABA release decreased following the activation of MORs. Thus, in addition to the local VTA GABA inputs, MOR agonists inhibited the GABA projection to CINs by a presynaptic mechanism.

Identification of a direct D2-receptor containing, MOR-sensitive GABA input to DA neurons from the NAc

Recent studies have demonstrated that dopamine neurons receive GABA input from a specific subset of striatal neurons (Watabe-Uchida et al., 2012); however, the strength of these synaptic connections and presynaptic receptors at those terminals remains controversial (Chuhma et al., 2011; Xia et al., 2011; Watabe-Uchida et al., 2012). ChR2 was expressed in NAc using a ubiquitous promoter (CAG) in an AAV-9 serotype (Figure 3.3A). Additional retrograde expression of ChR2 in dopamine neurons was observed in the midbrain 4 weeks after viral injection (data not shown). To avoid the activation of retrogradely labeled cells, experiments were performed within 3 weeks after injection. Activation of ChR2 in terminals from the NAc induced GABA-A IPSCs in VTA dopamine neurons indicating that there is a functional connection between NAc and VTA dopamine neurons (Figure 3.3B). The amplitude of GABA-A IPSCs in dopamine neurons was significantly decreased by the MOR agonist DAMGO (1 μM, 49.3±4.2% of control, n=9, $p<0.001$, Student's *t* test single group comparison to 100% control); however, the KOR agonist U69593 (1 μM) did not alter the GABA-A IPSC amplitude (96.4±4.7% of control, n=6, $p=0.47$; Figure 3.3C). In addition, dopamine (3 μM) also significantly decreased GABA-A IPSC amplitude (55.7±5.3% of control, n=9, $p<0.001$). This inhibition was mimicked with an application of D2-like receptor agonist quinpirole (3 μM). These results suggest that in the rat, a direct GABAergic input from the NAc to the VTA exists that is sensitive to both MOR- and D2-receptor agonists.

GABA neurons in the VTA and substantia nigra pars reticulata receive two types of GABA input from striatum

Traditionally, the striatal medium spiny output neurons are divided into two classes that make up the direct and indirect pathways. The direct pathway expresses KOR and D1-like receptors, and projects to GABA neurons in SNr. The indirect pathway expresses MOR and D2-like receptors, and projects directly to the external globus pallidus (Alexander and Crutcher, 1990). To further understand how opioids modulate the activity of midbrain neurons, expression of ChR2 in NAc and dorsal striatum was used to identify GABA inputs to GABA neurons in the VTA and substantia nigra pars reticulata (SNr). ChR2 activation of striatal terminals elicited GABA-A IPSCs in GABA neurons in SNr and some VTA GABA neurons. GABA-A IPSCs were most often observed in SNr when ChR2 was expressed in the dorsal striatum. In this study, the general opioid agonist [Met^5]enkephalin (ME,1 μM) was used to test MOR sensitivity because ME washes out of the brain slice preparations so that the action of a subsequent application of the KOR agonist (U69593) could be observed. Based on the sensitivity to MOR (ME, DAMGO) and KOR (U69593) agonists, GABA-A IPSCs fell into one of two groups. In one group (6 of 17 neurons), the GABA-A IPSCs from striatum were inhibited by the KOR agonist U69593 (1 μM; 35.2±9.6% of control, p=0.0011, Student's t test single group comparison to 100% control) and were insensitive to ME (1 μM; 110±5.2% of control, p=0.12; Figure 3.4A,C). In the second group (7 of 17 neurons) the GABA IPSCs were inhibited by ME (1 μM; 26.8±4.0% of control, p<0.001) and were insensitive to U69593 (1 μM;

94.5±6.2% of control, p=0.41; Figure 3.4B,D). The MOR specific agonist DAMGO (1 μM) also caused the inhibition of GABA-A IPSC in the second group (28.7±5.3% of control, p<0.001). In addition, there were a few cells that were inhibited by both ME and U69593 (n=3) or neither (n=1; Figure 3.4D). Thus, with a few exceptions, there was a clear distribution of GABA inputs that were inhibited by either MOR or KOR agonists (Figure 3.4D). In cells where the GABA-A IPSCs were inhibited by U69593, the application of dopamine (3 μM) tended to facilitate GABA-A IPSC amplitude (Figure 3.4E blue; 122±12.5% of control; n=6, p=0.14). In contrast, the ME-sensitive GABA inputs were significantly decreased by dopamine (3 μM, Figure 3.4E red; 77.8±4.1% of control, n=7, p=0.0017). The results suggest that KOR agonist-sensitive GABA terminals express D1-like receptors, whereas MOR agonist-sensitive GABA terminals express D2-like receptors. The decay time constants of the GABA-A IPSCs were different in the two groups of cells. The IPSCs that were sensitive to MOR agonists decayed more rapidly than the KOR agonist-sensitive IPSCs (MOR sensitive 4.32±0.52 ms, n=7; and KOR sensitive 7.98±0.75 ms, n=6; p=0.0028, Student's t test; Figure 3.4C). There was no difference in input resistance between cells in the two groups (MOR sensitive 228±30.5 MΩ, and KOR sensitive 375±115.6 MΩ; p=0.26). Thus, the majority of GABA neurons in the VTA and SNr received GABA input from two different striatal sources that were distinguished based on the kinetics of the IPSCs and expression of MOR or KORs.

RMTg is the major opioid sensitive GABA input to DA neurons

The dense GABA input from RMTg to dopamine neurons has been previously shown to be potently inhibited by opioids (Matsui and Williams, 2011). To determine the relative amount of inhibition from each GABA afferent, a sub-saturating concentration of ME (1 μM) was applied. The GABA-A IPSCs from the RMTg were decreased by 74.5±4.7% (n=25), whereas the input from NAc and local VTA interneurons were inhibited only by 45.0±5.1% (n=8) and 17.4±4.2% (n=36), respectively (Figure 3.5A,B). Thus, RMTg input was significantly inhibited by opioid compared to NAc and VTA inputs (p<0.01, one-way ANOVA bonferroni). To further characterize the sensitivity of the different inputs, concentration-response curves for DAMGO in each of the GABA inputs were constructed (Figure 3.5C). The concentration-response curve for the RMTg input was adapted from a previous study (Matsui and Williams, 2011). The maximum effect of DAMGO on the GABA-A IPSCs from the RMTg was 81.5±10.2% whereas the inhibition of the IPSCs evoked from the NAc and VTA interneurons was 52.8±6.8% and 35.2±8.7%, respectively. The EC50 was similar for each of the GABA pathways (65 nM, 95% confidence interval (CI)=32-136 nM for RMTg; 163 nM, CI=90-293 nM for NAc; and 79 nM CI=21-297 nM for VTA). Thus, the potency of MOR-dependent inhibition of each GABA input did not differ, however, the maximum effect of DAMGO was very different. Thus the biggest component of the opioid inhibition of GABA IPSCs measured on dopamine neurons results from terminals arising from the RMTg.

Opioid sensitivity of GABA-B IPSCs were similar to GABA-A IPSCs in DA neurons

The activation of GABA-B receptors leads to an increase in the conductance of a G-protein coupled inwardly rectifying potassium (GIRK/Kir 3.2) channels. A train of stimuli (2 ms LED flash, 5 stimuli at 40 Hz) was used to activate ChR2 expressed in the RMTg or striatum while recording from dopamine neurons. This stimulation protocol induced GABA-B IPSCs in dopamine neurons. The average peak amplitude and total charge (area under the curve) of GABA-B IPSCs from each projection were similar. The amplitude from RMTg input was 39.9±10 pA (charge 15.3±4.2 pA.s n=11), and from the striatum was 45.1±7.7 pA (21.7±6.0 pA.s n=22; Figure 3.6A,B). The GABA-B IPSC evoked from the NAc input was observed in some case without a GABA-A IPSC (n=6). In order to observe a GABA-B IPSC in dopamine neurons evoked from the activation of VTA interneurons, a train of 10 stimuli was required and IPSCs were not often observed. The average peak amplitude and total charge of GABA-B IPSCs were smaller (18.2±2.2 pA, and 3.72±1.04 pA.s, respectively; Figure 3.6B). Thus, GABA-B IPSCs were more often evoked from neurons in the RMTg and striatum than interneurons in the VTA.

In order to measure an inhibition of the GABA-B IPSCs, the amplitude of the IPSC was increased with the addition of the potassium channel blocker 4AP (3-100 μM). GABA-B IPSCs evoked from RMTg inputs were significantly inhibited by DAMGO (1 μM; 50.8±4.2% of control, n=7, $p<0.0001$, Student's *t* test single

group comparison to 100% control) whereas U69593 (1 μM) had no effect (105.2±6.3% of control, n=6, p=0.44; Figure 3.6E). The IPSCs evoked from the striatal input, were sensitive to DAMGO (1 μM) and U69593 (1 μM) (DAMGO 73.2±5.6% of control, n=11, p=0.0007; U69593 73.0±4.4% of control, n=14, p<0.0001). Simultaneous application of DAMGO (1 μM) and U69593 (1 μM) further inhibited the GABA-B IPSC (54.7±5.6% of control, n=6, p=0.0005; Figure 3.6D). The additive inhibitory effects observed with saturating concentrations of both agonists suggest that two separate GABA afferents produced the GABA-B IPSC from striatum. It was difficult to evoke a GABA-B IPSC from interneurons in the VTA even in the presence of 4AP. In cases where IPSCs were evoked however, DAMGO (1 μM) did not inhibit the amplitude of GABA-B IPSCs (89.8±4.5% of control, n=5, p=0.08). U69593 had no effect in the two cells where it was applied (91.2±5.6% of control). Altogether, the GABA-B results provide further evidence that opioid inhibition of GABA release is more robust for GABA inputs originating outside of the VTA.

Discussion

Opioids increase dopamine neuron activity through inhibition of GABA input resulting in an increase in dopamine release in the brain (Di Chiara and Imperato, 1988). The mechanism of this disinhibition was thought to result from an inhibition of interneurons in the VTA (Johnson and North, 1992a). It is clear however that there are additional opioid-sensitive GABA inputs to dopamine neurons originating from the RMTg and NAc. The present results demonstrate that sensitivity to opioids was the highest for the RMTg input, slightly less for the NAc input and surprisingly the IPSCs evoked by the activation of interneurons in the VTA was the least sensitive to opioids (Figure 3.5D). Thus, the most likely GABA input to dopamine neurons that underlies the opioid-dependent disinhibition arises from the RMTg.

MOR agonist regulation of VTA GABA neurons

It is established that opioids hyperpolarize VTA GABA neurons by activating a GIRK conductance that reduces or completely blocks spontaneous firing (Johnson and North, 1992a; Chieng et al., 2011; Jalabert et al., 2011). Likewise, opioids activate a potassium conductance in neurons of the RMTg (Matsui and Williams, 2011). There is however, a marked difference in the amount of presynaptic inhibition induced by opioids in the two groups of neurons. The maximal opioid inhibition of IPSCs arising from the RMTg is almost complete (81.8%) whereas the inhibition of local GABA neurons in the VTA is only 35.4%.

The increased extent of inhibition observed from the RMTg may result from a higher expression of MORs, a secondary mechanism, such as inhibition of calcium current, or VTA interneurons may be heterogeneous population of opioid sensitive and insensitive neurons.

The activity of dopamine neurons is strongly influenced by the GABA input from RMTg (Hong et al., 2011; Jalabert et al., 2011; Lecca et al., 2011; Matsui and Williams, 2011; Bourdy and Barrot, 2012; Lecca et al., 2012). A steady GABA input to dopamine cells is generated from the RMTg. In vivo studies have found that the average spontaneous firing rate of RMTg neurons was 15-20 Hz (Jhou et al., 2009a; Hong et al., 2011; Jalabert et al., 2011; Lecca et al., 2011). In addition, the RMTg neurons were suggested to synapse onto proximal dendrites of dopamine neurons whereas other GABA synapses were more distal (Omelchenko and Sesack, 2009; Balcita-Pedicino et al., 2011). Thus, the inhibition of a steady GABA input from RMTg may effectively suppress the activity of dopamine neurons. This possibility is supported by the fact that morphine infused into the RMTg increases the firing rate of dopamine neurons (Jalabert et al., 2011). When interneurons were selectively inhibited by morphine there was no change in the firing of dopamine neurons (Jalabert et al., 2011). Therefore, although GABA neurons in the VTA fire at a rate of 10-30 Hz (Steffensen et al., 1998; Li et al., 2012) it appears that opioid inhibition of VTA interneurons does not strongly interfere with dopamine neuron firing.

Previous studies have shown that when GABA neurons in the VTA were specifically stimulated using ChR2, aversive behavior and a reduction of free-reward consumption was observed (Tan et al., 2012; van Zessen et al., 2012). The behavioral consequences of GABA neuron activation in the VTA were thought to result from the GABA-dependent inhibition of dopamine neurons. The present study supports this possibility since activation of GABA neurons in the VTA evoked IPSCs in local dopamine neurons. However, the surprising result was that the amount of inhibition mediated by opioids was lower for GABA terminals originating from the VTA compared to GABA inputs originating from outside of the VTA. In addition, GABA neurons in the VTA also projected to cholinergic interneurons (CINs) in the NAc. The IPSCs recorded in these cells had similar opioid sensitivity (35.4% of control on dopamine neuron, and 39.8% on CINs; Figure 3.5C). It remains unclear whether the same VTA GABA neurons project to both VTA dopamine neurons and CINs (Omelchenko and Sesack, 2009).

Striatum inputs to midbrain

A direct connection from the striatal medium spiny projection neurons to dopamine neurons was identified in the present study. This observation is unlike previous work which did not observe direct NAc-dopamine neuron connection (Chuhma et al., 2011; Xia et al., 2011). The reasons for the different observations could be due to the amount and location of ChR2 expression. In the present study, GABA input onto dopamine neurons from NAc was observed infrequently

compared to the frequency of GABA inputs onto GABA neurons in the VTA and SNc. Thus, if ChR2 expression level was low it would be difficult to evoke GABA-A IPSCs on dopamine neurons. The striatal subregions consisting of patch and matrix compartments differentially send projections to dopamine and GABA neurons, respectively (Watabe-Uchida et al., 2012). Thus, the specific sites of ChR2 expression may also result in different outcomes. All GABA-A IPSCs from NAc on to dopamine neurons were inhibited by MOR agonists and dopamine, indicating that NAc afferents express MORs and D2-like receptors. Whether this NAc input originated from so-called "indirect pathway" or an unidentified subset of neurons was not certain. In addition there was a strong GABA projection from ventral and dorsal striatum to GABA neurons in the midbrain. Consistent with a previous ChR2 study, some striatum inputs to GABA neurons were inhibited with MOR agonists (Xia et al., 2011). However, other GABA inputs were inhibited with KOR agonist, which would have been predicted based on the presence of KORs on neurons in the direct pathway (Chuhma et al., 2011). The kinetics of MOR- and KOR-agonist sensitive GABA-A IPSCs were different in the midbrain GABA neurons. The decay of IPSCs can be strongly influenced by the expression of different α subunits of GABA-A receptor (Barberis et al., 2007; Picton and Fisher, 2007). In VTA and SN, GABA receptors mainly expresses the α1 subunit (Fritschy and Mohler, 1995) and α3 subunit immunoreactivity has also been found (Pirker et al., 2000; Schwarzer et al., 2001). It is also possible that extrasynaptic or distal dendritic GABA input could result in the slow kinetics of GABA-A IPSCs in one group of neurons. Likewise IPSCs resulting from extrasynaptic receptors may

cause a tonic GABA current that could shunt currents induced by other inputs (Liang et al., 2008). The identity of the neurons receiving the differential input has not been determined but it is clear that the opioid modulation of striatal inputs is more complex than described by the classical model of direct and indirect pathways.

GABA-B IPSCs in dopamine neurons

Previous *in vivo* studies suggest that striatal GABA input to dopamine neurons in rats were completely inhibited by GABA-A receptor antagonists, but not GABA-B receptor antagonists (Paladini et al., 1999a). In addition, ChR2 activation of NAc terminals did not evoke GABA-B IPSCs in dopamine neurons (Xia et al., 2011). However, a train of ChR2 stimulation was used in this study to reveal GABA-B IPSCs originated mainly from ventral and dorsal striatum and RMTg inputs. The differential sensitivity to 5-HT between GABA-A and GABA-B IPSCs suggested that GABA-B IPSCs arise selectively from the striatum (Sugita et al., 1992a). It is possible that repetitive stimulation and high levels of ChR2 expression level result in spill over to produce GABA-B IPSCs. Whether GABA-B IPSCs from each of the GABA inputs occur naturally still remains to be determined.

Conclusion

The present results challenge the previous conclusion that opioid disinhibition of dopamine neurons is solely mediated by inhibition of the local VTA interneurons. Although there are multiple opioid sensitive GABA afferents to dopamine neurons, the projection from RMTg plays a dominant role in the opioid receptor dependent regulation of dopamine neurons. The opioid sensitive afferents that dominate the regulation of dopamine neurons *in vivo* will be dependent on the initial activity of the various GABA inputs. This study suggests that the opioid regulation of dopamine neurons is more integrated than previously proposed. Identifying the key structures that control the dopamine system will help identify therapeutic targets for opioid actions in the reward pathway.

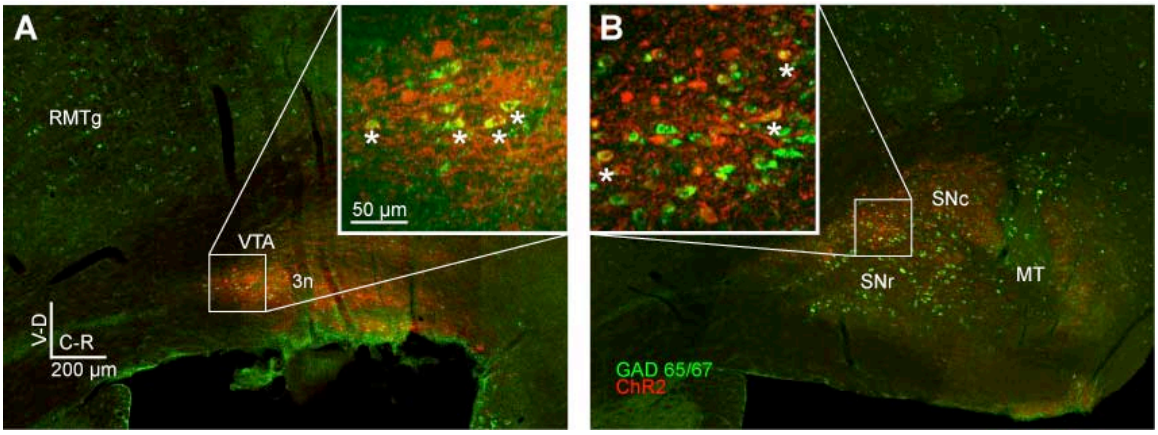

Figure 3.1: Dopamine and GABA neurons express ChR2 following viral injection into the VTA/SN of rats

Images of brain sections with GAD65/67 (Green) labeled by fluorescent *in situ* hybridization and ChR2 (Red) immunolabeled against Venus show GABA neurons within VTA/SN that express ChR2. A. Medial sagittal slice of midbrain containing VTA. ChR2 expression was restricted within VTA. Inset shows enlarged view of the boxed area. Some cells showing colocalization of GAD65/67 and ChR2 are indicated with asterisks. B. Lateral sagittal slice containing substantia nigra pars compacta (SNc) and reticulata (SNr). ChR2 expression was observed in SNc and SNr. RMTg, rostromedial tegmental nucleus; VTA, ventral tegmental area; 3n, oculomotor nerve; MT, medial terminal nucleus of accessory optic tract.

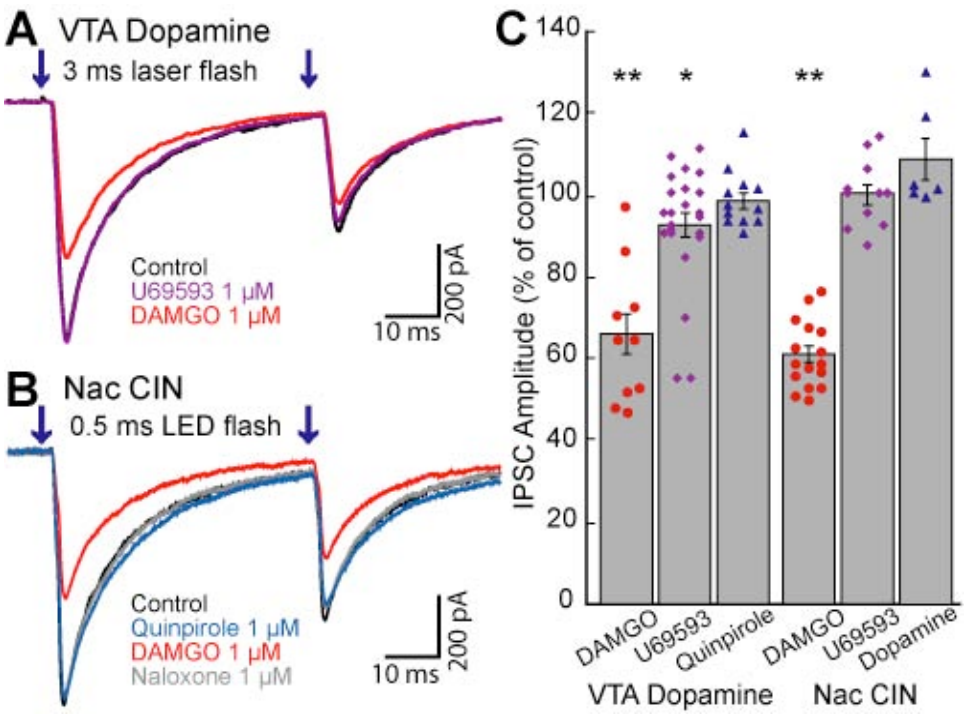

Figure 3.2: Opioids cause only a small inhibition of GABA IPSCs originating from VTA/SN

ChR2 was expressed in VTA/SN neurons and GABA-A IPSCs were recorded from VTA dopamine neurons and cholinergic interneurons (CINs) in NAc. ChR2 was activated by paired focal laser flashes or paired LED flashes (3 ms or 0.5 ms, respectively; 50 ms interval; 473 nm). A. Superimposed traces of IPSCs in dopamine neuron. GABA-A IPSCs were inward because of the high chloride internal solution. B. Superimposed traces of IPSCs in CIN. C. Summary graph of the inhibition of IPSCs in dopamine and CINs. DAMGO (1 µM) significantly decreased IPSC amplitude to a similar extent in both neuronal population. U69593 (1 µM) significantly decreased IPSC amplitude in dopamine neurons, but not in CIN. Quinpirole or dopamine did not change the IPSC amplitude. Results from individual experiments are shown in dots. Traces shown are averages of 5 sweeps. Error bars indicate SEM. *p< 0.05 and **p<0.001 by one-sample Student's t test.

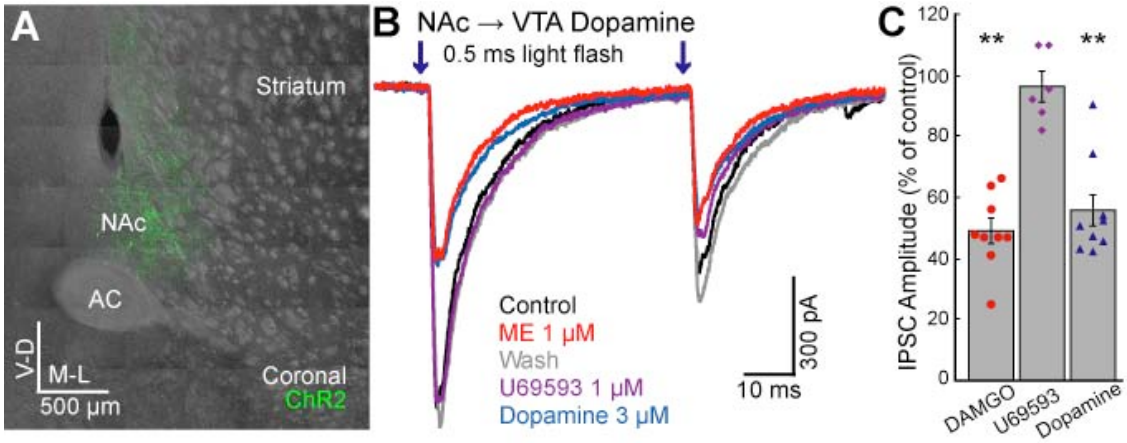

Figure 3.3: GABA projections from NAc to dopamine neurons are inhibited by MORs

ChR2 was expressed in the NAc and GABA-A IPSCs were recorded from dopamine neurons in the VTA. ChR2 was activated by a paired LED flashes (0.5 ms; 50 ms interval; 473 nm). A. Coronal image of a brain section expressing ChR2 in NAc (green). B. Representative traces showing the ME (1 µM) and dopamine (3 µM) induced inhibition of IPSCs in dopamine neurons. ME was used to test MOR sensitivity so that the sensitivity to subsequent application of U69593 could be observed. C. DAMGO (1 µM), and dopamine (3 µM) significantly inhibited IPSCs. U69593 (1 µM) had no effect. AC, anterior commissure; NAc, nucleus accumbens. Traces shown are averages of 5 sweeps. Error bars indicated SEM. $^{**}p<0.001$ by one-sample Student's *t* test.

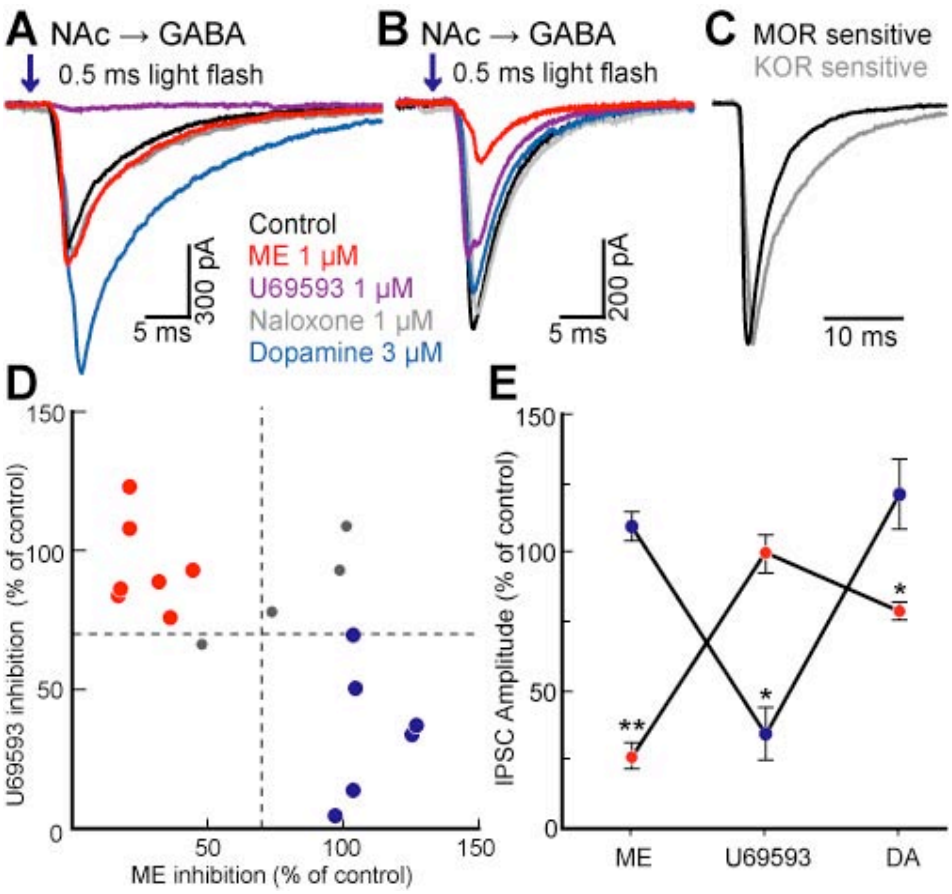

Figure 3.4: Two pharmacologically distinct inputs from striatum terminated on midbrain GABA neurons

ChR2 was expressed in the ventral and dorsal striatum and GABA-A IPSCs were recorded from GABA neurons in VTA and SNr. ChR2 was activated by paired LED flashes (0.5 ms; 50 ms interval; 473 nm). A. A cell in which the IPSCs were almost completely abolished by U69593, unchanged by ME, and increased by dopamine. B. A cell in which the IPSC was not sensitive to U69593 but was inhibited by ME. C. Superimposed GABA-A IPSCs traces from MOR- and KOR-sensitive inputs revealed the decay kinetics were different in two inputs. D. Scatter plots represent the IPSC inhibition with ME (1 µM) or U69593 (1 µM) from single neurons. The dashed line is an arbitrary cutoff (at 70%) that was used to distinguish the two different groups of cells. Red dots indicate cells where the IPSCs were inhibited by ME but not U69593. Blue dots indicate cells where the IPSCs were inhibited by U69593 but not ME. E. The average of agonist-selective inhibition in the two groups of cells is plotted along with the sensitivity to dopamine. Traces shown are averages of 5 sweeps. Error bars indicated SEM. *p< 0.05 and **p<0.001 by one-sample Student's t test.

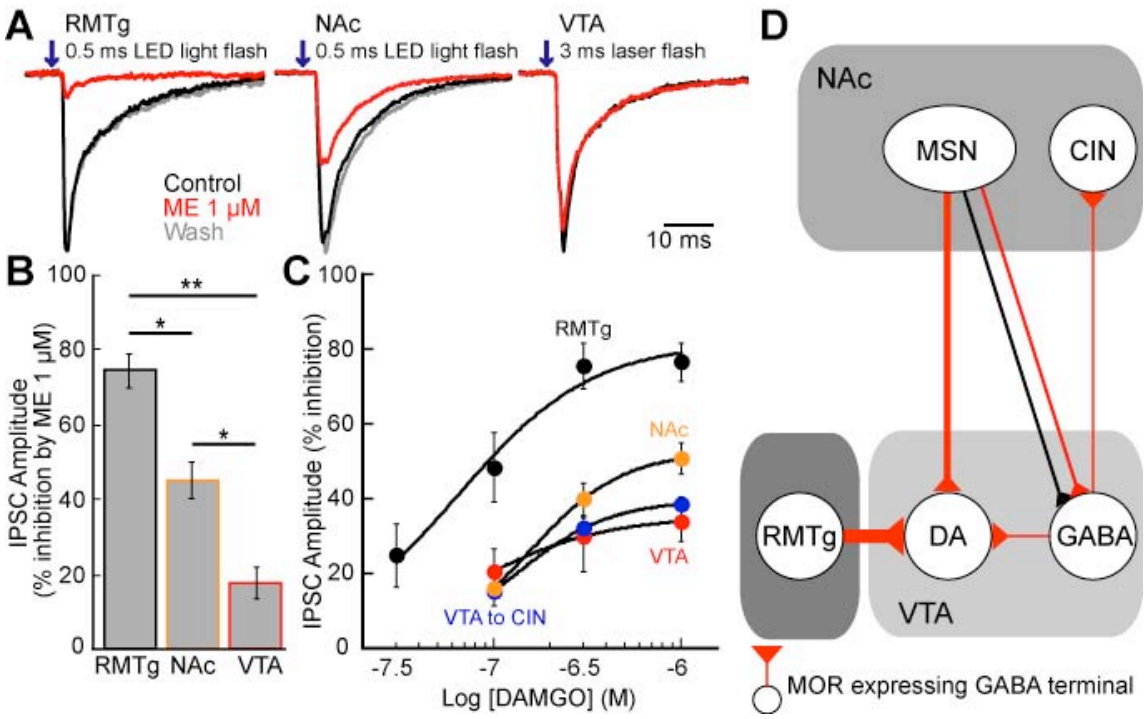

Figure 3.5: RMTg is the major opioid sensitive GABA input to DA neurons

ChR2 was expressed in RMTg, NAc, VTA neurons and GABA-A IPSCs were recorded from dopamine neurons. ChR2 was activated by paired LED flashes (0.5 ms; 50 ms interval; 473 nm) or a paired focal laser flash (3 ms; 50 ms interval; 473 nm). A. Representative traces of IPSCs from RMTg, NAc, or VTA inputs. ME (1 μM) sensitivity of those inputs were distinguishable. B. Summary graph shows % inhibition of the IPSC by ME (1 μM) for each input. C. Concentration response curves of the inhibition of IPSCs by DAMGO. Concentration response curve from RMTg were adapted from previous paper (Matsui and Williams, 2011). RMTg (black), NAc (orange), and VTA (red) inputs were constructed by recording from dopamine neurons. VTA GABA projection to CIN (blue) is also shown. D. Schematic image showing the MOR sensitive GABA inputs that was examined in the present study (red lines). Width of the red line represents the strength of MOR inhibition. Traces are shown in average of 5. Error bars indicated SEM. *p< 0.05 and **p<0.001 by one-way ANOVA with bonferroni's post-test.

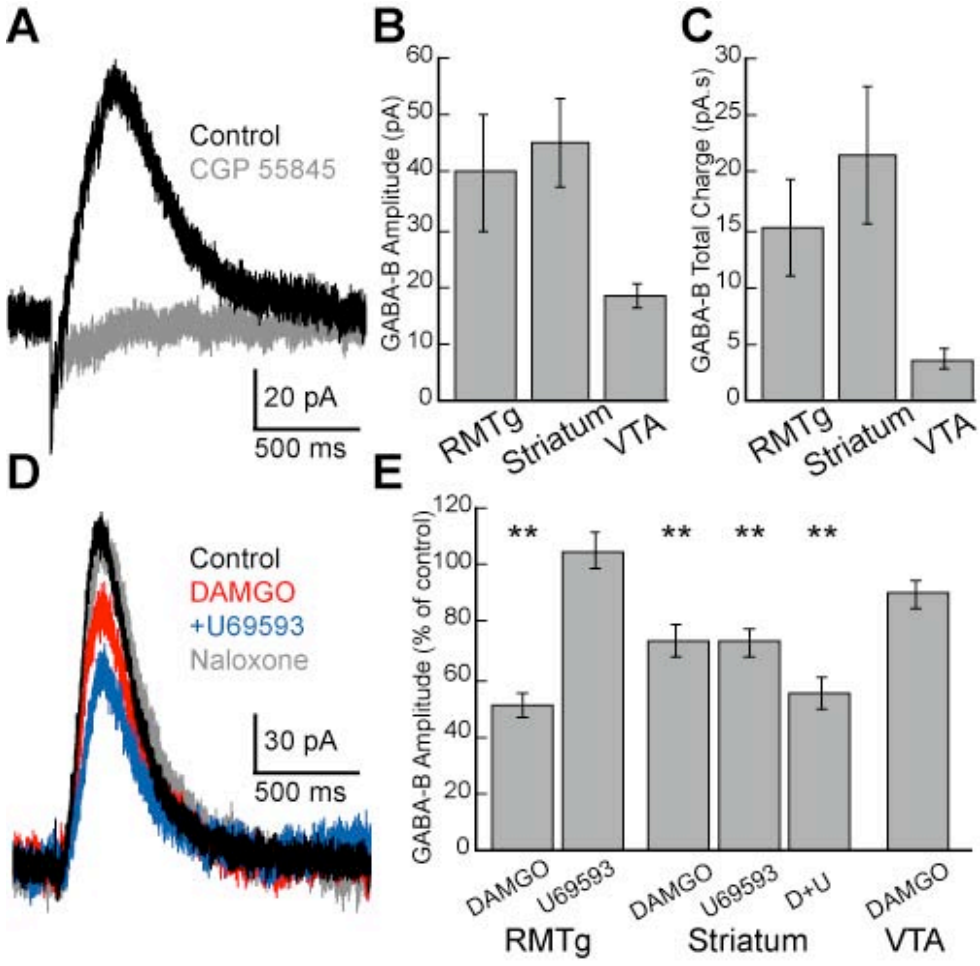

Figure 3.6: GABA-B-mediated IPSCs from each of the GABA inputs were found in dopamine neurons

ChR2 was expressed in RMTg, striatum and VTA. GABA-B IPSCs were recorded from dopamine neurons. ChR2 was activated by 5 LED flashes in RMTg and striatal inputs or 10 flashes in VTA inputs (2 ms; 40 Hz; 473 nm). A. 10 LED flashes evoked GABA-B IPSCs by activating striatal input. CGP 55848 (100 nM) completely blocked GABA-B IPSCs. B and C. Summary graphs of the peak amplitude and area under the curve of GABA-B IPSCs from each of the inputs. D. Superimposed traces of GABA-B IPSCs from striatal inputs. 4AP was applied to easily observe the opioid sensitivity. E. Summary graph of opioid inhibition of GABA-B IPSCs from the each of the GABA inputs. Traces are shown as an average of 3. Error bars indicate SEM. $**p<0.001$ by one-sample Student's *t* test.

Appendix: Additional results accompany with the manuscript

Dopamine inputs to MSNs in the NAc

A recent finding suggested that GABA transmitter is also released by activation of dopamine neurons (Tritsch et al., 2012). Dopamine neurons do not express the vesicular GABA transporter, which is present in most GABA neurons. However, dopamine neurons have the vesicular monoamine transporter VMAT2 known to package dopamine into the vesicle. GABA release from dopamine neurons was mediated by the VMAT2 that can also transport GABA into the vesicle (Tritsch et al., 2012). To test whether GABA was released from dopamine neurons, ChR2 was expressed in the VTA and light evoked GABA-A IPSCs were observed in both cholinergic interneurons (CINs) and medium spiny neurons (MSNs) in NAc. A small portion of MSNs exhibits small amplitude GABA-A IPSCs (Figure 3.7A). GABA-A IPSCs in MSNs were infrequently observed and when present were small in amplitude (average amplitude 47.4±17.1 pA, n=13; Figure 3.7A). GABA-A IPSCs in MSNs were significantly inhibited by D2-like receptor agonist quinpirole (3 μM; 36.7±9.1% of control, n=5, p=0.002), and not significantly inhibited by ME application (1 μM; 99.5±3.8% of control, n=5, p=0.13; Figure 3.7B). Thus, the MSNs received GABA input from GABA-releasing dopamine neurons as recently discovered (Tritsch et al., 2012).

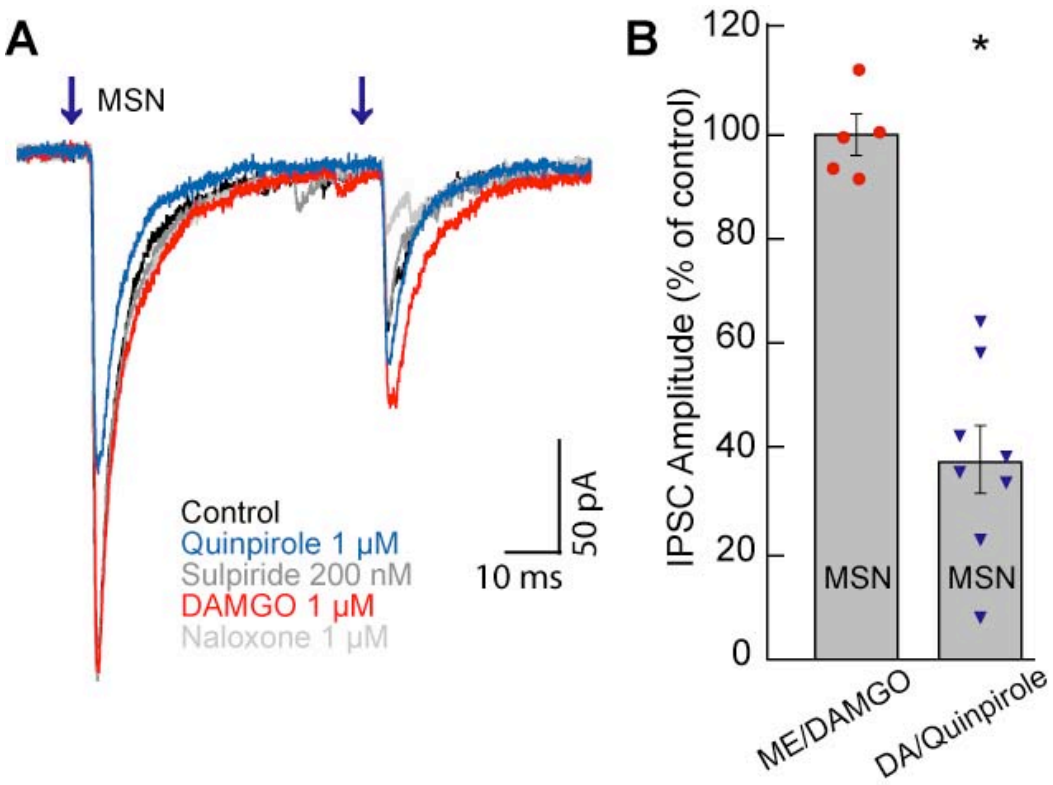

Figure 3.7: GABA input from dopamine neurons to MSNs are inhibited by D2 receptor agonists

ChR2 was expressed in the VTA/SN and GABA-A IPSCs were recorded from medium spiny neurons (MSNs). ChR2 was activated by a paired LED flashes (0.5 ms; 50 ms interval; 473 nm). A. Superimposed traces of IPSCs in MSNs. B. Summary graph of IPSC inhibition % of control. D2 receptor agonist quinpirole inhibited IPSCs but DAMGO did not have effect on IPSC amplitude in MSNs. Traces are shown in average of 5. Error bars indicated SEM. *p< 0.05 and **p<0.001.

Chapter 4: Summary and Discussion

This work elucidated the mechanisms of MOR agonist disinhibition of dopamine neurons. ChR2 expression in several GABAergic pathways including the RMTg, VTA interneurons, and NAc successfully evoked GABA-A IPSCs in dopamine neurons. The opioid inhibition of GABA-A IPSCs was noticeably different from each afferent. Unlike the previous hypothesis, MOR agonists only weakly inhibited ChR2 evoked GABA-A IPSCs originating from VTA interneurons. On the contrary, MOR agonists robustly inhibited GABA-A IPSCs from the RMTg. Given the dense GABA innervation of dopamine neurons as well as high intrinsic activity of RMTg neurons, this input creates a strong GABA tone to diminish burst firing of dopamine neurons. MOR activation of RMTg neurons removes the GABA tone such that dopamine neurons can generate burst firing. Additionally, neurons from NAc synapse on dopamine neurons. MOR and D2-receptor agonists inhibited the GABA-A IPSCs from NAc and the sensitivity to opioids was less than the RMTg input, but more than interneurons. Another surprising finding was that GABA neurons in VTA specifically terminated onto cholinergic interneurons (CINs) in NAc. GABA input from the VTA interneurons to CINs had a similar opioid sensitivity to the projection from VTA interneurons to dopamine neurons. Thus GABA inputs to CINs could originate from the same neurons with axon collaterals. Reciprocal GABA connections from NAc/Striatum to VTA and SNr were also observed. The sensitivity to opioids was a mixture of either MOR or KOR sensitive inputs. Altogether, there is a strong GABA input

from RMTg nucleus that was robustly inhibited by MOR. Thus, the RMTg may play a key role in disinhibiting dopamine neurons.

The μ-opioid action in dopamine system

This thesis and previous studies suggested that RMTg neurons expressed MORs and that the activity of dopamine neurons are strongly influenced by GABA inputs from RMTg (Hong et al., 2011; Jalabert et al., 2011; Lecca et al., 2011; Matsui and Williams, 2011; Bourdy and Barrot, 2012; Lecca et al., 2012). GABA inputs from VTA interneurons and NAc were less sensitive to opioids. The EC50 concentrations of GABA-A IPSC inhibition from those GABA afferents were comparable. Thus the difference in opioid sensitivity between the GABA afferents may be due to the expression level of MORs. The reasons for the difference in opioid sensitivity could be either some of the synapses lacked MORs expression or axon terminals expressed generally fewer MORs. However, MOR, like many other GPCRs, can couple to several effectors to inhibit transmitter release. Thus the interpretation of this result is not conclusive in the thesis study.

There is steady GABA tone generated from the RMTg and VTA inputs. Previous *in vivo* studies showed that average spontaneous firing rate of RMTg neurons is 15-20 Hz (Jhou et al., 2009a; Hong et al., 2011; Jalabert et al., 2011; Lecca et al., 2011), and 10-30 Hz in VTA interneurons (Steffensen et al., 1998; Li et al., 2012; Schiemann et al., 2012). The firing pattern of NAc neurons was episodic and relatively low rate. The membrane voltage of NAc neurons

fluctuated between up and down states where the membrane potential shifted from -60 mV to -80 mV (Wilson and Groves, 1981; Mahon et al., 2006). The primary source of GABA tone *in vivo* appears to be from the RMTg. When RMTg neurons were inhibited by morphine infusion in RMTg, the firing rate of dopamine neurons increased. However when RMTg neurons were silenced, morphine infusion into the VTA failed to increase the activity of dopamine neurons (Jalabert et al., 2011). Thus, the pacemaker firing of dopamine neurons may be strongly controlled by steady GABA input from RMTg neurons. Since NMDA receptor activation is required for burst firing, the inhibition of GABA inputs could act as coincident detection for the regulation of dopamine neuron activity.

VTA interneurons are capable of inhibiting dopamine neuron activity, yet the degree of disinhibition of dopamine neurons, and extent of opioid inhibition might not be as prominent as previously believed. Strong ChR2 activation of interneurons in VTA failed to evoke GABA-B IPSCs in dopamine neurons compared to RMTg and NAc inputs suggesting that GABA release from interneurons in VTA is small. However, it is also possible that the availability of GABA-B receptors at the release sites could be less. Nevertheless, repetitive activation of interneurons in VTA failed to induce spill over of GABA to evoke GABA-B IPSCs. Moreover, only a small inhibition of GABA-A IPSCs was observed with a subsaturating concentration of ME. Although the actual concentration of endogenous opioids at the synapse is unknown, it may be below the concentration that results in an acute desensitization. Thus, GABA inputs from

interneurons in VTA may not be responsible for the opioid modulation of dopamine neuron activity.

CIN modulation of dopamine release

VTA GABA neurons specifically project to CINs and the release of GABA is inhibited by opioids. Activation of CINs increase dopamine levels in the NAc by an action potential independent mechanism (Threlfell et al., 2012). Presynaptic terminals of dopamine neurons were activated by acetylcholine released from CINs, which evoked dopamine release in NAc. Although opioids decrease GABA-A IPSCs on CINs, the CINs were also directly sensitive to opioids and hyperpolarized by an increase in GIRK conductance (Britt and McGehee, 2008). Thus, the action of opioid on CINs to alter dopamine release is difficult to predict. Microinjection of μ-opioid agonists within NAc increased dopamine levels in NAc (Spanagel et al., 1990), suggesting that there is not a direct opioid action on CINs that induce dopamine release. Even so, the increase in dopamine release by systemic opioid administration was probably mediated by disinhibition of dopamine neurons in VTA (Klitenick et al., 1992; Devine et al., 1993). Thus, GABA input from VTA to CINs plays a less important role in controlling dopamine release.

Additional GABA inputs that can modulate dopamine neurons

GABA inputs from RMTg, VTA interneurons, and NAc were used to activate GABA-A IPSCs in dopamine neurons. However, there are more GABA inputs that might contribute to opioid modulation of dopamine neuron activity. One candidate is the ventral pallidum. The ventral pallidum receives input from NAc and projects to the midbrain. Some ventral pallidum neurons express MORs, thus the input from ventral pallidum can be another opioid sensitive GABA input to dopamine neurons. Another input arises from the globus pallidus. The globus pallidus input to midbrain was thought to project to GABA neurons in SNr. Further research is required to elucidate whether those GABA inputs terminate on dopamine neurons and to examine the strength of opioid inhibition.

Future directions: Chronic opioid treatment

With repeated administration of opioids, tolerance, physical and psychological dependence to opioids develop. One of the mechanisms leading to adaptive changes is an alteration in the synaptic strength of inputs to dopamine neurons. After chronic morphine treatment, the probability of GABA release is enhanced during withdrawal in the slice (Bonci and Williams, 1996; 1997). The increase in GABA release is associated with sensitization of adenylyl cyclase and cAMP-dependent pathway at the presynaptic terminals after morphine withdrawal. In control animals, dopamine facilitates GABA release and increases activation of GABA-B receptors by activating presynaptic D1 receptors (Cameron

and Williams, 1993; Radnikow and Misgeld, 1998). However, a week after opioid withdrawal, application of dopamine failed to facilitate GABA-B IPSC amplitudes (Bonci and Williams, 1996). The mechanism underlying dopamine inhibition of GABA-B IPSCs was associated with elevated concentration of adenosine. After chronic morphine treatment, adenylyl cyclase is upregulated such that dopamine activation of D1 receptors elevates the extracellular adenosine concentration. Therefore, elevated level of adenosine activates presynaptic Gi/Go-protein coupled A1 receptors, and masked the facilitation of GABA release. The A1 receptor antagonist, DPCPX, completely reversed dopamine inhibition of GABA release (Bonci and Williams, 1996).

Increase in the probability of GABA release was also observed in GABA-A IPSCs. During morphine withdrawal, the mIPSCs frequency of GABA-A IPSCs was increased without having any effect in mIPSCs amplitude. Thus, the facilitation of GABA release was also observed in GABA-A IPSCs. Unlike GABA-B IPSCs, GABA-A IPSCs were not affected by blocking A1 receptors (Bonci and Williams, 1997). The reason for this discrepancy may be due to where the GABA inputs originate. GABA-A and GABA-B IPSCs are thought to arise from the separate terminals (Sugita et al., 1992a). Dopamine facilitation of GABA-B IPSCs suggested that the D1 expressing striatal inputs evoke GABA-B IPSCs. Whereas GABA-A IPSCs originate from interneurons in VTA (Johnson and North, 1992a). The separate terminals similarly enhanced transmitter release, yet they had different pharmacological effects. Therefore, the individual GABA terminals observed in the thesis study may be modulated differently after chronic morphine

treatment. A preliminary study suggests that after chronic morphine treatment, cFOS activity induced by naloxone increased in the RMTg and was robustly activated in interneurons of the VTA (Figure 4.1). Thus, it will be interesting to discover the effects of chronic morphine treatment in GABA terminals independently.

In order to observe the change in the probability of GABA release from individual GABA terminals, the expression of Designer Receptors Exclusively Activated by Designer Drugs (DREADDs) in target nucleus can be used. DREADDs are engineered GPCR which coupled to Gs-, Gi/o-, and Gq-proteins, and activated by the designer agonist, clozapine-N-oxide (CNO). GABA release from the terminals that express inhibitory DREADDs will reduced after CNO application. Using expression of inhibitory DREADDs in specific GABA terminal, the difference in mIPSCs frequency and amplitude can be observed after chronic morphine treatment. Thus, DREADDs can be used to identify which GABA input is facilitated after chronic morphine treatment.

The consequence of global activation of MORs was observed in chronic morphine treatment; however, it is still unknown which nucleus is responsible for series of effects after the long-term MORs activation. Using expression of DREADDs in target nucleus, chronic opioid effects can be mimicked by continuous activation of inhibitory DREADDs with CNO. The characteristics of electrophysiological and behavioral outcomes after chronic opioid treatment can be compared with the phenotype after a long-term activation of inhibitory

DREADDs. If stimulatory DREADDs counteracts Gi/o-protein signaling to some degree, continuous activation of stimulatory DREADDs might ameliorate long-term effects of chronic opioid treatments. If stimulatory DREADDs reversed the consequences after chronic morphine treatment, the therapeutic strategy for activating target nucleus can be developed to treat opioid addiction.

During the chronic opioid treatment, RMTg neurons might be inactivated, however, it remains unknown whether RMTg neurons are involved in opioid addiction. In order to test this hypothesis, prolonged inactivation of RMTg neurons can be achieved by using cFOS-lacZ-GFP transgenic rats (Koya et al., 2009). In the cFOS-lacZ-GFP transgenic animals, the cFOS promoter control expression of the β-galactosidase protein (Kasof et al., 1995). Thus all cFOS positive neurons express β-galactosidase. Upon the infusion of Daun02 compound, β-galactosidase converts Daun02 to daunorubicin which is known to inactivate neurons (Koya et al., 2009). Therefore, in order to increase cFOS and β-galactosidase level in RMTg neurons, psychostimulant will be injected in this transgenic animal. Two hours after psychostimulant injection, Daun02 will be microinjected into the RMTg to inactivate neurons that express cFOS and β-galactosidase. If daunorubicin successfully inactivates RMTg neurons, the activity of dopamine neuron would increase to imitate long-term opioid treatment. This cell specific inactivation might elucidate the adaptive neuronal circuit mediated exclusively by RMTg.

NMDA receptor activation is required for burst firing of dopamine neurons, however, the source of glutamate inputs that are responsible for the burst firing has not been defined. Like this thesis work, expression of ChR2 in each of the glutamate afferents will be useful to explore whether the stimulation of a particular pathway can trigger burst firing. Additionally, the dynamic clamp technique or pharmacology can be applied to examine other obligate synaptic inputs, such as acetylcholine. Glutamate synaptic transmission is inhibited by opioids in dopamine neurons (Manzoni and Williams, 1999). After animals are treated with opioids, glutamate transmission is also enhanced (Saal et al., 2003). In addition to GABA inputs, specific glutamate inputs that are sensitive to opioids can be explored by the optogenetic approach. Considering the importance of glutamate inputs for dopamine neuron activity, it will be important to know the underlying mechanism that facilitates glutamate release after chronic opioid treatment.

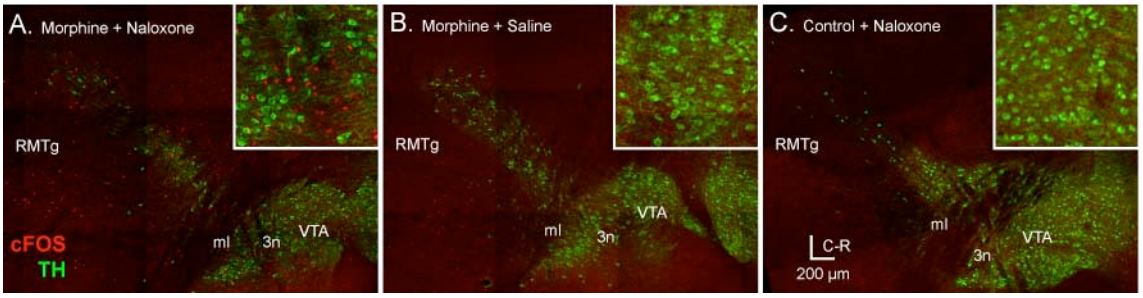

Figure 4.1: Augmentation of cFOS activity in withdrawn animal after chronic morphine treatment

Rats received morphine sulfate continuously by implanting osmotic pump in treatment animals (50 mg/kg/day). Rats received either naloxone or saline 7 days after implantation. A. Sagittal brain image from naloxone-precipitated withdrawn rat indicating cFOS immunoactivity (red) and dopamine neurons with TH staining (green). cFOS activity was upregulated in the RMTg and interneurons in VTA. B. Sagittal brain image from chronic morphine treated animals receiving saline. cFOS activity was only observed in some neurons in RMTg. C. Sagittal brain image from control animals that received naloxone without chronic morphine treatment. There is little cFOS activity was observed. VTA, ventral tegmental area; RMTg, rostromedial tegmental nucleus; ml, medial lemniscus; 3n, oculomotor nerve.

References

Alexander GE, Crutcher MD (1990) Functional architecture of basal ganglia circuits: neural substrates of parallel processing. Trends Neurosci 13:266–271.

Balcita-Pedicino JJ, Omelchenko N, Bell R, Sesack SR (2011) The inhibitory influence of the lateral habenula on midbrain dopamine cells: ultrastructural evidence for indirect mediation via the rostromedial mesopontine tegmental nucleus. J Comp Neurol 519:1143–1164.

Bals-Kubik R, Ableitner A, Herz A, Shippenberg TS (1993) Neuroanatomical sites mediating the motivational effects of opioids as mapped by the conditioned place preference paradigm in rats. J Pharmacol Exp Ther 264:489–495.

Barberis A, Mozrzymas JW, Ortinski PI, Vicini S (2007) Desensitization and binding properties determine distinct $\alpha1\beta2\gamma2$ and $\alpha3\beta2\gamma2$ GABAA receptor-channel kinetic behavior. European Journal of Neuroscience 25:2726–2740.

Beckstead MJ, Grandy DK, Wickman K, Williams JT (2004) Vesicular dopamine release elicits an inhibitory postsynaptic current in midbrain dopamine neurons. Neuron 42:939–946.

Bertran-Gonzalez J, Bosch C, Maroteaux M, Matamales M, Hervé D, Valjent E, Girault J-A (2008) Opposing patterns of signaling activation in dopamine D1 and D2 receptor-expressing striatal neurons in response to cocaine and haloperidol. J Neurosci 28:5671–5685.

Blackmer T, Larsen EC, Bartleson C, Kowalchyk JA, Yoon E-J, Preininger AM, Alford S, Hamm HE, Martin TFJ (2005) G protein betagamma directly regulates SNARE protein fusion machinery for secretory granule exocytosis. Nat Neurosci 8:421–425.

Bolam JP, Smith Y (1990) The GABA and substance P input to dopaminergic neurones in the substantia nigra of the rat. Brain Res 529:57–78.

Bonci A, Williams JT (1996) A common mechanism mediates long-term changes in synaptic transmission after chronic cocaine and morphine. Neuron 16:631–639.

Bonci A, Williams JT (1997) Increased probability of GABA release during withdrawal from morphine. J Neurosci 17:796–803.

Bourdy R, Barrot M (2012) A new control center for dopaminergic systems: pulling the VTA by the tail. Trends Neurosci. [Epub ahead of print].

Britt JP, McGehee DS (2008) Presynaptic opioid and nicotinic receptor

modulation of dopamine overflow in the nucleus accumbens. J Neurosci 28:1672–1681.

Bromberg-Martin ES, Matsumoto M, Hikosaka O (2010) Dopamine in motivational control: rewarding, aversive, and alerting. Neuron 68:815–834.

Cameron DL, Wessendorf MW, Williams JT (1997) A subset of ventral tegmental area neurons is inhibited by dopamine, 5-hydroxytryptamine and opioids. Neuroscience 77:155–166.

Cameron DL, Williams JT (1993) Dopamine D1 receptors facilitate transmitter release. Nature 366:344–347.

Cameron DL, Williams JT (1994) Cocaine inhibits GABA release in the VTA through endogenous 5-HT. J Neurosci 14:6763–6767.

Chan CS, Guzman JN, Ilijic E, Mercer JN, Rick C, Tkatch T, Meredith GE, Surmeier DJ (2007) 'Rejuvenation' protects neurons in mouse models of Parkinson's disease. Nature 447:1081–1086.

Chieng B, Azriel Y, Mohammadi S, Christie MJ (2011) Distinct cellular properties of identified dopaminergic and GABAergic neurons in the mouse ventral tegmental area. J Physiol (Lond) 589:3775–3787.

Christoffersen CL, Meltzer LT (1995) Evidence for N-methyl-D-aspartate and AMPA subtypes of the glutamate receptor on substantia nigra dopamine neurons: possible preferential role for N-methyl-D-aspartate receptors. Neuroscience 67:373–381.

Chuhma N, Tanaka KF, Hen R, Rayport S (2011) Functional connectome of the striatal medium spiny neuron. J Neurosci 31:1183–1192.

Devine DP, Leone P, Pocock D, Wise RA (1993) Differential involvement of ventral tegmental mu, delta and kappa opioid receptors in modulation of basal mesolimbic dopamine release: in vivo microdialysis studies. J Pharmacol Exp Ther 266:1236–1246.

Di Chiara G, Bassareo V, Fenu S, De Luca MA, Spina L, Cadoni C, Acquas E, Carboni E, Valentini V, Lecca D (2004) Dopamine and drug addiction: the nucleus accumbens shell connection. Neuropharmacology 47 Suppl 1:227–241.

Di Chiara G, Imperato A (1988) Drugs abused by humans preferentially increase synaptic dopamine concentrations in the mesolimbic system of freely moving rats. Proc Natl Acad Sci USA 85:5274–5278.

Dobi A, Margolis EB, Wang H-L, Harvey BK, Morales M (2010) Glutamatergic

and nonglutamatergic neurons of the ventral tegmental area establish local synaptic contacts with dopaminergic and nondopaminergic neurons. J Neurosci 30:218–229.

Dommett E, Coizet V, Blaha CD, Martindale J, Lefebvre V, Walton N, Mayhew JEW, Overton PG, Redgrave P (2005) How visual stimuli activate dopaminergic neurons at short latency. Science 307:1476–1479.

Fiorillo CD, Williams JT (1998) Glutamate mediates an inhibitory postsynaptic potential in dopamine neurons. Nature 394:78–82.

Floresco SB, West AR, Ash B, Moore H, Grace AA (2003) Afferent modulation of dopamine neuron firing differentially regulates tonic and phasic dopamine transmission. Nat Neurosci 6:968–973.

Ford CP, Beckstead MJ, Williams JT (2007) Kappa opioid inhibition of somatodendritic dopamine inhibitory postsynaptic currents. J Neurophysiol 97:883–891.

Ford CP, Mark GP, Williams JT (2006) Properties and opioid inhibition of mesolimbic dopamine neurons vary according to target location. J Neurosci 26:2788–2797.

Fritschy JM, Mohler H (1995) GABAA-receptor heterogeneity in the adult rat brain: Differential regional and cellular distribution of seven major subunits. J Comp Neurol 359:154–194.

Geisler S, Derst C, Veh RW, Zahm DS (2007) Glutamatergic afferents of the ventral tegmental area in the rat. J Neurosci 27:5730–5743.

Geisler S, Marinelli M, Degarmo B, Becker ML, Freiman AJ, Beales M, Meredith GE, Zahm DS (2008) Prominent activation of brainstem and pallidal afferents of the ventral tegmental area by cocaine. Neuropsychopharmacology 33:2688–2700.

Georges F, Aston-Jones G (2001) Potent regulation of midbrain dopamine neurons by the bed nucleus of the stria terminalis. J Neurosci 21:RC160.

Georges F, Aston-Jones G (2002) Activation of ventral tegmental area cells by the bed nucleus of the stria terminalis: a novel excitatory amino acid input to midbrain dopamine neurons. J Neurosci 22:5173–5187.

Gerachshenko T, Blackmer T, Yoon E-J, Bartleson C, Hamm HE, Alford S (2005) Gbetagamma acts at the C terminus of SNAP-25 to mediate presynaptic inhibition. Nat Neurosci 8:597–605.

Grace AA, Floresco SB, Goto Y, Lodge DJ (2007) Regulation of firing of

dopaminergic neurons and control of goal-directed behaviors. Trends Neurosci 30:220–227.

Greenwell TN, Zangen A, Martin-Schild S, Wise RA, Zadina JE (2002) Endomorphin-1 and -2 immunoreactive cells in the hypothalamus are labeled by fluoro-gold injections to the ventral tegmental area. J Comp Neurol 454:320–328.

Grenhoff J, Nisell M, Ferré S, Aston-Jones G, Svensson TH (1993) Noradrenergic modulation of midbrain dopamine cell firing elicited by stimulation of the locus coeruleus in the rat. J Neural Transm 93:11–25.

Gronier B, Rasmussen K (1998) Activation of midbrain presumed dopaminergic neurones by muscarinic cholinergic receptors: an in vivo electrophysiological study in the rat. Br J Pharmacol 124:455–464.

Gysling K, Wang RY (1983) Morphine-induced activation of A10 dopamine neurons in the rat. Brain Res 277:119–127.

Hong S, Jhou TC, Smith M, Saleem KS, Hikosaka O (2011) Negative reward signals from the lateral habenula to dopamine neurons are mediated by rostromedial tegmental nucleus in primates. J Neurosci 31:11457–11471.

Hope BT, Nye HE, Kelz MB, Self DW, Iadarola MJ, Nakabeppu Y, Duman RS, Nestler EJ (1994) Induction of a long-lasting AP-1 complex composed of altered Fos-like proteins in brain by chronic cocaine and other chronic treatments. Neuron 13:1235–1244.

Jalabert M, Bourdy R, Courtin J, Veinante P, Manzoni OJ, Barrot M, Georges F (2011) Neuronal circuits underlying acute morphine action on dopamine neurons. Proc Natl Acad Sci USA 108:16446–16450.

James MH, Charnley JL, Levi EM, Jones E, Yeoh JW, Smith DW, Dayas CV (2011) Orexin-1 receptor signalling within the ventral tegmental area, but not the paraventricular thalamus, is critical to regulating cue-induced reinstatement of cocaine-seeking. Int J Neuropsychopharmacol 14:684–690.

Jarvie BC, Hentges ST (2012) Expression of GABAergic and glutamatergic phenotypic markers in hypothalamic proopiomelanocortin neurons. J Comp Neurol 520:3863-3876.

Jhou T (2005) Neural mechanisms of freezing and passive aversive behaviors. J Comp Neurol 493:111–114.

Jhou TC, Fields HL, Baxter MG, Saper CB, Holland PC (2009a) The rostromedial tegmental nucleus (RMTg), a GABAergic afferent to midbrain dopamine neurons, encodes aversive stimuli and inhibits motor responses. Neuron

61:786–800.

Jhou TC, Geisler S, Marinelli M, Degarmo BA, Zahm DS (2009b) The mesopontine rostromedial tegmental nucleus: A structure targeted by the lateral habenula that projects to the ventral tegmental area of Tsai and substantia nigra compacta. J Comp Neurol 513:566–596.

Jhou TC, Xu S-P, Lee MR, Gallen CL, Ikemoto S (2012) Mapping of reinforcing and analgesic effects of the mu opioid agonist Endomorphin-1 in the ventral midbrain of the rat. Psychopharmacology [Epub ahead of print]

Ji H, Shepard PD (2007) Lateral habenula stimulation inhibits rat midbrain dopamine neurons through a GABA(A) receptor-mediated mechanism. J Neurosci 27:6923–6930.

Johnson SW, Mercuri NB, North RA (1992) 5-hydroxytryptamine1B receptors block the GABAB synaptic potential in rat dopamine neurons. J Neurosci 12:2000–2006.

Johnson SW, North RA (1992a) Opioids excite dopamine neurons by hyperpolarization of local interneurons. J Neurosci 12:483–488.

Johnson SW, North RA (1992b) Two types of neurone in the rat ventral tegmental area and their synaptic inputs. J Physiol (Lond) 450:455–468.

Johnson SW, Wu Y-N (2004) Multiple mechanisms underlie burst firing in rat midbrain dopamine neurons in vitro. Brain Res 1019:293–296.

Jones S, Kauer JA (1999) Amphetamine depresses excitatory synaptic transmission via serotonin receptors in the ventral tegmental area. J Neurosci 19:9780–9787.

Kalivas PW, Churchill L, Klitenick MA (1993) GABA and enkephalin projection from the nucleus accumbens and ventral pallidum to the ventral tegmental area. Neuroscience 57:1047–1060.

Karreman M, Moghaddam B (1996) The prefrontal cortex regulates the basal release of dopamine in the limbic striatum: an effect mediated by ventral tegmental area. J Neurochem 66:589–598.

Kasof GM, Mandelzys A, Maika SD, Hammer RE, Curran T, Morgan JI (1995) Kainic acid-induced neuronal death is associated with DNA damage and a unique immediate-early gene response in c-fos-lacZ transgenic rats. J Neurosci 15:4238–4249.

Kaufling J, Veinante P, Pawlowski SA, Freund-Mercier M-J, Barrot M (2009) Afferents to the GABAergic tail of the ventral tegmental area in the rat. J

Comp Neurol 513:597–621.

Kaufling J, Veinante P, Pawlowski SA, Freund-Mercier M-J, Barrot M (2010a) gamma-Aminobutyric acid cells with cocaine-induced DeltaFosB in the ventral tegmental area innervate mesolimbic neurons. Biol Psychiatry 67:88–92.

Kaufling J, Waltisperger E, Bourdy R, Valera A, Veinante P, Freund-Mercier M-J, Barrot M (2010b) Pharmacological recruitment of the GABAergic tail of the ventral tegmental area by acute drug exposure. Br J Pharmacol 161:1677–1691.

Khaliq ZM, Bean BP (2008) Dynamic, nonlinear feedback regulation of slow pacemaking by A-type potassium current in ventral tegmental area neurons. J Neurosci 28:10905–10917.

Khaliq ZM, Bean BP (2010) Pacemaking in dopaminergic ventral tegmental area neurons: depolarizing drive from background and voltage-dependent sodium conductances. J Neurosci 30:7401–7413.

Kita H, Kitai ST (1987) Efferent projections of the subthalamic nucleus in the rat: light and electron microscopic analysis with the PHA-L method. J Comp Neurol 260:435–452.

Klitenick MA, DeWitte P, Kalivas PW (1992) Regulation of somatodendritic dopamine release in the ventral tegmental area by opioids and GABA: an in vivo microdialysis study. J Neurosci 12:2623–2632.

Koga E, Momiyama T (2000) Presynaptic dopamine D2-like receptors inhibit excitatory transmission onto rat ventral tegmental dopaminergic neurones. J Physiol (Lond) 523 Pt 1:163–173.

Korotkova TM, Sergeeva OA, Eriksson KS, Haas HL, Brown RE (2003) Excitation of ventral tegmental area dopaminergic and nondopaminergic neurons by orexins/hypocretins. J Neurosci 23:7–11.

Koya E, Golden SA, Harvey BK, Guez-Barber DH, Berkow A, Simmons DE, Bossert JM, Nair SG, Uejima JL, Marin MT, Mitchell TB, Farquhar D, Ghosh SC, Mattson BJ, Hope BT (2009) Targeted disruption of cocaine-activated nucleus accumbens neurons prevents context-specific sensitization. Nat Neurosci 12:1069–1073.

Koyama S, Appel SB (2006) A-type K+ current of dopamine and GABA neurons in the ventral tegmental area. J Neurophysiol 96:544–554.

Lacey MG, Calabresi P, North RA (1990) Muscarine depolarizes rat substantia nigra zona compacta and ventral tegmental neurons in vitro through M1-like

receptors. J Pharmacol Exp Ther 253:395–400.

Lammel S, Hetzel A, Häckel O, Jones I, Liss B, Roeper J (2008) Unique properties of mesoprefrontal neurons within a dual mesocorticolimbic dopamine system. Neuron 57:760–773.

Lammel S, Ion DI, Roeper J, Malenka RC (2011) Projection-specific modulation of dopamine neuron synapses by aversive and rewarding stimuli. Neuron 70:855–862.

Lecca S, Melis M, Luchicchi A, Ennas MG, Castelli MP, Muntoni AL, Pistis M (2011) Effects of drugs of abuse on putative rostromedial tegmental neurons, inhibitory afferents to midbrain dopamine cells. Neuropsychopharmacology 36:589–602.

Lecca S, Melis M, Luchicchi A, Muntoni AL, Pistis M (2012) Inhibitory inputs from rostromedial tegmental neurons regulate spontaneous activity of midbrain dopamine cells and their responses to drugs of abuse. Neuropsychopharmacology 37:1164–1176.

Li B, Piriz J, Mirrione M, Chung C, Proulx CD, Schulz D, Henn F, Malinow R (2011) Synaptic potentiation onto habenula neurons in the learned helplessness model of depression. Nature 470:535–539.

Li W, Doyon WM, Dani JA (2012) Quantitative Unit Classification of Ventral Tegmental Area Neurons In Vivo. J Neurophysiol 107:2808-2820.

Liang J, Suryanarayanan A, Chandra D, Homanics GE, Olsen RW, Spigelman I (2008) Functional consequences of GABAA receptor alpha 4 subunit deletion on synaptic and extrasynaptic currents in mouse dentate granule cells. Alcohol Clin Exp Res 32:19–26.

Liss B, Roeper J (2008) Individual dopamine midbrain neurons: functional diversity and flexibility in health and disease. Brain Res Rev 58:314–321.

Lobb CJ, Troyer TW, Wilson CJ, Paladini CA (2011) Disinhibition bursting of dopaminergic neurons. Front Syst Neurosci 5:25.

Lobb CJ, Wilson CJ, Paladini CA (2010) A dynamic role for GABA receptors on the firing pattern of midbrain dopaminergic neurons. J Neurophysiol 104:403–413.

Lodge DJ, Grace AA (2006) The laterodorsal tegmentum is essential for burst firing of ventral tegmental area dopamine neurons. Proc Natl Acad Sci USA 103:5167–5172.

Lokwan SJ, Overton PG, Berry MS, Clark D (1999) Stimulation of the

pedunculopontine tegmental nucleus in the rat produces burst firing in A9 dopaminergic neurons. Neuroscience 92:245–254.

Lüscher C, Malenka RC (2011) Drug-evoked synaptic plasticity in addiction: from molecular changes to circuit remodeling. Neuron 69:650–663.

Madhavan A, Bonci A, Whistler JL (2010) Opioid-Induced GABA potentiation after chronic morphine attenuates the rewarding effects of opioids in the ventral tegmental area. J Neurosci 30:14029–14035.

Mahler SV, Smith RJ, Aston-Jones G (2012) Interactions between VTA orexin and glutamate in cue-induced reinstatement of cocaine seeking in rats. Psychopharmacology. [Epub ahead of print]

Mahon S, Vautrelle N, Pezard L, Slaght SJ, Deniau J-M, Chouvet G, Charpier S (2006) Distinct patterns of striatal medium spiny neuron activity during the natural sleep-wake cycle. J Neurosci 26:12587–12595.

Mameli-Engvall M, Evrard A, Pons S, Maskos U, Svensson TH, Changeux J-P, Faure P (2006) Hierarchical control of dopamine neuron-firing patterns by nicotinic receptors. Neuron 50:911–921.

Manzoni OJ, Williams JT (1999) Presynaptic Regulation of Glutamate Release in the Ventral Tegmental Area During Morphine Withdrawal. J Neurosci 19:6629–6636.

Margolis EB, Hjelmstad GO, Bonci A, Fields HL (2003) Kappa-opioid agonists directly inhibit midbrain dopaminergic neurons. J Neurosci 23:9981–9986.

Margolis EB, Lock H, Hjelmstad GO, Fields HL (2006) The ventral tegmental area revisited: is there an electrophysiological marker for dopaminergic neurons? J Physiol (Lond) 577:907–924.

Maroteaux M, Mameli M (2012) Cocaine evokes projection-specific synaptic plasticity of lateral habenula neurons. J Neurosci 32:12641–12646.

Matsui A, Williams JT (2011) Opioid-sensitive GABA inputs from rostromedial tegmental nucleus synapse onto midbrain dopamine neurons. J Neurosci 31:17729–17735.

Matsumoto M, Hikosaka O (2007) Lateral habenula as a source of negative reward signals in dopamine neurons. Nature 447:1111–1115.

Mejías-Aponte CA, Drouin C, Aston-Jones G (2009) Adrenergic and noradrenergic innervation of the midbrain ventral tegmental area and retrorubral field: prominent inputs from medullary homeostatic centers. J Neurosci 29:3613–3626.

Moorman DE, Aston-Jones G (2010) Orexin/hypocretin modulates response of ventral tegmental dopamine neurons to prefrontal activation: diurnal influences. J Neurosci 30:15585–15599.

Murase S, Grenhoff J, Chouvet G, Gonon FG, Svensson TH (1993) Prefrontal cortex regulates burst firing and transmitter release in rat mesolimbic dopamine neurons studied in vivo. Neurosci Lett 157:53–56 .

Nair-Roberts R, Chatelain-Badie S, Benson E (2008) Stereological estimates of dopaminergic, GABAergic and glutamatergic neurons in the ventral tegmental area, substantia nigra and retrorubral field in the rat. Neuroscience 152:1024–1031.

Neuhoff H, Neu A, Liss B, Roeper J (2002) I(h) channels contribute to the different functional properties of identified dopaminergic subpopulations in the midbrain. J Neurosci 22:1290–1302.

Nicola SM, Malenka RC (1997) Dopamine depresses excitatory and inhibitory synaptic transmission by distinct mechanisms in the nucleus accumbens. J Neurosci 17:5697–5710.

Nicoll RA, Alger BE, Jahr CE (1980) Enkephalin blocks inhibitory pathways in the vertebrate CNS. Nature 287:22–25.

Omelchenko N, Sesack SR (2009) Ultrastructural analysis of local collaterals of rat ventral tegmental area neurons: GABA phenotype and synapses onto dopamine and GABA cells. Synapse 63:895–906.

Overton P, Clark D (1992) Iontophoretically administered drugs acting at the N-methyl-D-aspartate receptor modulate burst firing in A9 dopamine neurons in the rat. Synapse 10:131–140.

Paladini CA, Celada P, Tepper JM (1999a) Striatal, pallidal, and pars reticulata evoked inhibition of nigrostriatal dopaminergic neurons is mediated by GABA(A) receptors in vivo. Neuroscience 89:799–812.

Paladini CA, Fiorillo CD, Morikawa H, Williams JT (2001) Amphetamine selectively blocks inhibitory glutamate transmission in dopamine neurons. Nat Neurosci 4:275–281.

Paladini CA, Iribe Y, Tepper JM (1999b) GABAA receptor stimulation blocks NMDA-induced bursting of dopaminergic neurons in vitro by decreasing input resistance. Brain Res 832:145–151.

Paladini CA, Williams JT (2004) Noradrenergic inhibition of midbrain dopamine neurons. J Neurosci 24:4568–4575.

Perrotti LI, Bolaños CA, Choi K-H, Russo SJ, Edwards S, Ulery PG, Wallace DL, Self DW, Nestler EJ, Barrot M (2005) DeltaFosB accumulates in a GABAergic cell population in the posterior tail of the ventral tegmental area after psychostimulant treatment. Eur J Neurosci 21:2817–2824.

Phillips AG, Vacca G, Ahn S (2008) A top-down perspective on dopamine, motivation and memory. Pharmacol Biochem Behav 90:236–249.

Picton AJ, Fisher JL (2007) Effect of the α subunit subtype on the macroscopic kinetic properties of recombinant GABAA receptors. Brain Res 1165:40–49.

Pirker S, Schwarzer C, Wieselthaler A, Sieghart W (2000) GABAA receptors: immunocytochemical distribution of 13 subunits in the adult rat brain. Neuroscience 101:815–850.

Puopolo M, Raviola E, Bean BP (2007) Roles of subthreshold calcium current and sodium current in spontaneous firing of mouse midbrain dopamine neurons. J Neurosci 27:645–656.

Putzier I, Kullmann PHM, Horn JP, Levitan ES (2009) Cav1.3 Channel Voltage Dependence, Not Ca2+ Selectivity, Drives Pacemaker Activity and Amplifies Bursts in Nigral Dopamine Neurons. J Neurosci 29:15415-15419.

Radnikow G, Misgeld U (1998) Dopamine D1 receptors facilitate GABAA synaptic currents in the rat substantia nigra pars reticulata. J Neurosci 18:2009–2016.

Saal D, Dong Y, Bonci A, Malenka RC (2003) Drugs of abuse and stress trigger a common synaptic adaptation in dopamine neurons. Neuron 37:577–582.

Scammell TE, Estabrooke IV, McCarthy MT, Chemelli RM, Yanagisawa M, Miller MS, Saper CB (2000) Hypothalamic arousal regions are activated during modafinil-induced wakefulness. J Neurosci 20:8620–8628.

Schiemann J, Schlaudraff F, Klose V, Bingmer M, Seino S, Magill PJ, Zaghloul KA, Schneider G, Liss B, Roeper J (2012) K-ATP channels in dopamine substantia nigra neurons control bursting and novelty-induced exploration. Nat Neurosci 15:1272–1280.

Schultz W (2007) Behavioral dopamine signals. Trends Neurosci 30:203–210.

Schwarzer C, Berresheim U, Pirker S, Wieselthaler A, Fuchs K, Sieghart W, Sperk GN (2001) Distribution of the major gamma-aminobutyric $acid_a$ receptor subunits in the basal ganglia and associated limbic brain areas of the adult rat. J Comp Neurol 433:526–549.

Seutin V, Johnson SW, North RA (1993) Apamin increases NMDA-induced burst-firing of rat mesencephalic dopamine neurons. Brain Res 630:341–344.

Shepard PD, Bunney BS (1988) Effects of apamin on the discharge properties of putative dopamine-containing neurons in vitro. Brain Res 463:380–384.

Shepard PD, Bunney BS (1991) Repetitive firing properties of putative dopamine-containing neurons in vitro: regulation by an apamin-sensitive Ca(2+)-activated K+ conductance. Exp Brain Res 86:141–150.

Shoji Y, Delfs J, Williams JT (1999) Presynaptic inhibition of GABA(B)-mediated synaptic potentials in the ventral tegmental area during morphine withdrawal. J Neurosci 19:2347–2355.

Smith ID, Grace AA (1992) Role of the subthalamic nucleus in the regulation of nigral dopamine neuron activity. Synapse 12:287–303.

Smith Y, Bolam JP (1990) The output neurones and the dopaminergic neurones of the substantia nigra receive a GABA-containing input from the globus pallidus in the rat. J Comp Neurol 296:47–64.

Spanagel R, Herz A, Shippenberg TS (1990) The effects of opioid peptides on dopamine release in the nucleus accumbens: an in vivo microdialysis study. J Neurochem 55:1734–1740.

Steffensen SC, Svingos AL, Pickel VM, Henriksen SJ (1998) Electrophysiological characterization of GABAergic neurons in the ventral tegmental area. J Neurosci 18:8003–8015.

Sugita S, Johnson SW, North RA (1992a) Synaptic inputs to GABAA and GABAB receptors originate from discrete afferent neurons. Neurosci Lett 134:207–211.

Sugita S, Johnson SW, North RA (1992b) Synaptic inputs to GABAA and GABAB receptors originate from discrete afferent neurons. Neurosci Lett 134:207–211.

Tan KR, Yvon C, Turiault M, Mirzabekov JJ, Doehner J, Labouèbe G, Deisseroth K, Tye KM, Lüscher C (2012) GABA Neurons of the VTA Drive Conditioned Place Aversion. Neuron 73:1173–1183.

Tepper JM, Lee CR (2007) GABAergic control of substantia nigra dopaminergic neurons. Prog Brain Res 160:189–208.

Tepper JM, Martin LP, Anderson DR (1995) GABAA receptor-mediated inhibition of rat substantia nigra dopaminergic neurons by pars reticulata projection neurons. J Neurosci 15:3092–3103.

Thomas MJ, Beurrier C, Bonci A, Malenka RC (2001) Long-term depression in the nucleus accumbens: a neural correlate of behavioral sensitization to

cocaine. Nat Neurosci 4:1217–1223.

Threlfell S, Lalic T, Platt NJ, Jennings KA, Deisseroth K, Cragg SJ (2012) Striatal dopamine release is triggered by synchronized activity in cholinergic interneurons. Neuron 75:58–64.

Tong ZY, Overton PG, Clark D (1996a) Stimulation of the prefrontal cortex in the rat induces patterns of activity in midbrain dopaminergic neurons which resemble natural burst events. Synapse 22:195–208.

Tong ZY, Overton PG, Clark D (1996b) Antagonism of NMDA receptors but not AMPA/kainate receptors blocks bursting in dopaminergic neurons induced by electrical stimulation of the prefrontal cortex. J Neural Transmission 103:889–904.

Tritsch NX, Ding JB, Sabatini BL (2012) Dopaminergic neurons inhibit striatal output through on-canonical release of GABA. Nature 490: 262-266.

Tsai H-C, Zhang F, Adamantidis A, Stuber GD, Bonci A, de Lecea L, Deisseroth K (2009) Phasic firing in dopaminergic neurons is sufficient for behavioral conditioning. Science 324:1080–1084.

Ungless MA, Magill PJ, Bolam JP (2004) Uniform inhibition of dopamine neurons in the ventral tegmental area by aversive stimuli. Science 303:2040–2042.

Valjent E, Bertran-Gonzalez J, Hervé D, Fisone G, Girault J-A (2009) Looking BAC at striatal signaling: cell-specific analysis in new transgenic mice. Trends Neurosci 32:538–547.

Van Bockstaele EJ, Pickel VM (1995) GABA-containing neurons in the ventral tegmental area project to the nucleus accumbens in rat brain. Brain Res 682:215–221.

van Zessen R, Phillips JL, Budygin EA, Stuber GD (2012) Activation of VTA GABA neurons disrupts reward consumption. Neuron 73:1184–1194.

Watabe-Uchida M, Zhu L, Ogawa SK, Vamanrao A, Uchida N (2012) Whole-Brain Mapping of Direct Inputs to Midbrain Dopamine Neurons. Neuron 74:858–873.

Wilson CJ, Callaway JC (2000) Coupled Oscillator Model of the Dopaminergic Neuron of the Substantia Nigra. J Neurophysiol 83:3084-3100.

Wilson CJ, Groves PM (1981) Spontaneous firing patterns of identified spiny neurons in the rat neostriatum. Brain Res 220:67–80.

Wise RA (1996) Neurobiology of addiction. Curr Opin Neurobiol 6:243–251.

Wolfart J, Neuhoff H, Franz O, Roeper J (2001) Differential expression of the small-conductance, calcium-activated potassium channel SK3 is critical for pacemaker control in dopaminergic midbrain neurons. J Neurosci 21:3443–3456.

Wolfart J, Roeper J (2002) Selective coupling of T-type calcium channels to SK potassium channels prevents intrinsic bursting in dopaminergic midbrain neurons. J Neurosci 22:3404–3413.

Xia Y, Driscoll JR, Wilbrecht L, Margolis EB, Fields HL, Hjelmstad GO (2011) Nucleus accumbens medium spiny neurons target non-dopaminergic neurons in the ventral tegmental area. J Neurosci 31:7811–7816.

Yawata S, Yamaguchi T, Danjo T, Hikida T, Nakanishi S (2012) Pathway-specific control of reward learning and its flexibility via selective dopamine receptors in the nucleus accumbens. Proc Natl Acad Sci USA 109:12764–12769.

Zahm DS (1989) Evidence for a morphologically distinct subpopulation of striatipetal axons following injections of WGA-HRP into the ventral tegmental area in the rat. Brain Res 482:145–154.

Zweifel LS, Argilli E, Bonci A, Palmiter RD (2008) Role of NMDA receptors in dopamine neurons for plasticity and addictive behaviors. Neuron 59:486–496.

Zweifel LS, Parker JG, Lobb CJ, Rainwater A, Wall VZ, Fadok JP, Darvas M, Kim MJ, Mizumori SJY, Paladini CA, Phillips PEM, Palmiter RD (2009) Disruption of NMDAR-dependent burst firing by dopamine neurons provides selective assessment of phasic dopamine-dependent behavior. Proc Natl Acad Sci USA 106:7281–7288.

Appendix/Additional Manuscript

Activation of μ-Opioid Receptors and Block of GIRK and NMDA Conductance by *l*- and *d*-methadone in Rat Locus Coeruleus

Aya Matsui and John T. Williams
Vollum Institute, Oregon Health and Science University, Portland, OR, USA

Corresponding author:
John T. Williams
Vollum Institute,
Oregon Health & Science University,
Portland, Oregon 97239,
williamj@ohsu.edu

Acknowledgements: This work was supported by NIH grants, DA08163 (JTW)

[This manuscript is presented as published in British Journal of Pharmacology, Nov 30, 2010, 161(6):1403-13.]

Summary

Background and purpose. Methadone activates opioid receptors to increase a potassium conductance mediated by g-protein coupled inwardly rectifying potassium ($K_{IR}3$) channels. In addition, methadone blocks $K_{IR}3$ channels and NMDA receptors. However, the concentration dependence and stereospecificity of receptor activation and channel blockade by methadone on single neurons has not been characterized.

Experimental approach. Intracellular and whole cell recording were made from locus coeruleus neurons in brain slices and the activation of μ-opioid receptors and blockade of $K_{IR}3$ and NMDA channels with *l*- and *d*-methadone was examined.

Key results. The potency of *l*-methadone measured by the amplitude of hyperpolarization was 16.5-fold higher than *d*-methadone. A maximum hyperpolarization was caused by both enantiomers (~30 mV), however, the maximum outward current measured with whole cell voltage-clamp recording was smaller than the current induced by [Met]^{5}enkephalin (ME). The $K_{IR}3$ conductance induced by α2-adrenoceptors was decreased with high concentrations of *l*- and *d*-methadone (10-30 μM). In addition, methadone blocked the resting inward rectifying conductance (K_{IR}). Both *l*- and *d*-methadone blocked the NMDA receptor dependent current. The block of NMDA dependent current was voltage dependent suggesting that methadone acted as a channel blocker.

Conclusions and Implications. Methadone activates μ-opioid receptors at low concentrations in a stereospecific manner. $K_{IR}3$ and NMDA receptor channel block was not stereospecific and required substantially higher concentrations. The separation in the concentration range suggests that the activation of μ-opioid receptors rather than the channel blocking properties mediate both the therapeutic and toxic actions of methadone.

Keywords. *l*- and *d*-methadone, MOR, GIRK, NMDA, Stereospecificity

Introduction

Methadone is used commonly for the treatment of opiate dependence (Dole and Nyswander, 1965). The initiation of treatment even in tolerant individuals begins with low doses that are escalated over time until a high degree of tolerance to opioids is attained. With the increase in dose, non-opioid receptor dependent actions of methadone may account for some of the therapeutic and/or toxic consequences (Kreek, 2000). In addition to the activation of opioid receptors, methadone blocks ion channels, such as G-protein coupled inwardly rectifying potassium ($K_{IR}3$) and N-methyl-D-aspartic acid (NMDA) receptors (Ebert et al., 1998; Gorman et al., 1997; Rodriguez-Martin et al., 2008). The block of NMDA receptors by methadone has been identified as a potentially important therapeutic action because the NMDA receptor antagonist, MK801, reduced hyperalgesia (Mao et al., 1992), enhanced opiate analgesia (Ebert et al., 1998) and attenuated morphine tolerance and dependence (Bilsky et al., 1996; Elliott et al., 1995; Trujillo and Akil, 1991). It is possible that in individuals receiving the highest doses of methadone, the channel blocking actions may contribute to the therapeutic outcome. It is therefore necessary to determine the concentrations of methadone that are required to activate opioid receptors relative to the concentrations that result in channel block.

Stereoselective binding of ligands to opioid receptors was one of the properties used to define receptor specific binding (Pert and Snyder, 1973a; Pert and Snyder, 1973b). The enantiomers of methadone differentially activate mu-opioid receptors. Depending on the assay, *l*-methadone was 4-50 times more

potent than *d*-methadone (Scott et al., 1948; Wallisch et al., 2007). Thus, like enantiomers of morphine, naloxone and many other natural opiates, the *l*-methadone binds to μ-opioid receptors selectively over the *d*-enantiomer (Pert and Snyder, 1973a; Pert and Snyder, 1973b). The present study examines the potency and efficacy of the two enantiomers and racemic (*l*/*d*) methadone to activate μ-opioid receptors and block ion channels ($K_{IR}3$ and NMDA receptor dependent currents). Recordings were made from locus coeruleus (LC) neurons in brain slices and the concentration dependence and stereoselectivity of the activation of μ-opioid receptors was compared with the blockade $K_{IR}3$ and NMDA receptor dependent currents.

The results show that *l*-methadone was 16.5-fold more potent than *d*-methadone in the activation of $K_{IR}3$ conductance. At higher concentrations both enantiomers of methadone reduced the α2-adrenoceptor activated $K_{IR}3$ conductance as well as the NMDA receptor dependent current. The results suggest that therapeutic concentrations of methadone do not reach a concentration that is sufficient to block $K_{IR}3$ and NMDA receptors. Thus the actions of methadone are primarily dependent on the activation of μ-opioid receptors.

Methods

Slice and solutions

Male Sprague-Dawley rats (150-300 g) were obtained from Charles River. The details of the methods for slice preparation and recording have been reported elsewhere (Williams et al., 1984). Briefly, the rats were anesthetized with isoflurane and killed. The brain was removed and placed in vibratome (Leica) containing cold (4°C) oxygenated (95% O_2, 5% CO_2) artificial cerebrospinal fluid (ACSF) containing (in mM) 126 NaCl, 2.5 KCl, 1.2 $MgCl_2$, 2.4 $CaCl_2$, 1.2 NaH_2PO_4, 25 $NaHCO_3$, and 11 D-glucose. In experiments where the NMDA receptor dependent current was examined, slices were cut and incubated in kynurinate (1.5 mM) until being placed in the recording chamber, otherwise the cutting and incubation solution contained MK801 (3 μM). Horizontal slices (220-230, and 280-300 μm for whole-cell, and intercellular recording, respectively) containing the locus coeruleus (LC) were obtained from the rostral pons. Slices were incubated for at least 30 min before recording in warm (35°C) oxygenated ACSF that contained MK801 (10 μM), or kynurinate (1.5 mM) in experiments where the current induced by NMDA receptor activation was examined. All experiments were approved by the Institutional Animal Care and Use Committee at Oregon Health and Science University and conducted in accordance with the National Institutes of Health guidelines.

Recordings

Slices were placed in a chamber and superfused with ACSF in physiological temperature (35°C) at the rate of 1.5 ml/min. In experiments that used intracellular recording, the area of the LC was visualized using a dissecting microscope located just lateral to the fourth ventricle and recordings were made blind. Intracellular electrodes (50–100 MΩ) were filled with 2 M KCl. LC neurons were identified by their intrinsic electric properties including, spontaneous firing at a rate of 1-5 Hz, an action potential that was 80 mV, with a threshold of -55 mV, a duration of 1.2-1.4 ms and a large after-hyperpolarization. Hyperpolarizing current (5~15 pA) was applied to maintain the membrane potential just below the threshold for action potential generation (≈ -60 mV). Data were collected using Power Lab (Chart software; ADInstruments, Colorado Springs, CO) and acquired at 200 Hz.

Whole-cell voltage clamp recordings were made with a 40× water-immersion objective on an upright microscope (Zeiss Axioscop 1) equipped with gradient contrast infrared optics. Glass pipettes contained (in mM): 126 KMethylsulfate (or 115 CsCl), 20 NaCl, 10 HEPES, 10 BAPTA, 2 Mg-ATP, 0.2 Na_2-GTP, and 10 Na_2phosphocreatine, at pH 7.3, and 275 mOsm. Pipette resistance was 1.5–3 MΩ. Acceptable access resistance was <15 MΩ. Series resistance compensation was not applied. Slices were placed in the recording chamber and superfused with oxygenated (95% O_2, 5% CO_2) ACSF at 35°C. An

Axopatch 1D amplifier (Molecular Devices) was filtered at 5 KHz, digitized at 10 KHz using AxoGraph X (AxoGraphX) and stored on a Macintosh computer.

Iontophoretic pipettes were pulled with the resistance of ≈100 MΩ, and filled with L-aspartate (1 M) or noradrenaline (500 mM). The iontophoretic pipette was placed adjacent to the soma within 5-20 μm. A backing current (≈1 nA) was applied. L-aspartate was ejected with negative current (≈50 nA) for 20 ms once every 20 sec using an Axoclamp 2A amplifier (Molecular Devices). Noradrenaline was applied with positive current (50 nA) once every 30 sec. The current evoked by N-methyl-D-aspartate (NMDA) receptors was pharmacologically isolated using AMPA receptor antagonist, 2,3-dihydroxy-6-nitro-7-sulfamoyl-benzo[f]quinoxaline-2,3-dione (NBQX; 5 μM).

Drugs

Drugs were applied by bath perfusion. The solution containing [Met]^{5}enkephalin (ME) also included the peptidase inhibitors, bestatin hydrochloride (10 μM) and thiorphan (1 μM). Racemic methadone, *l*- and *d*-methadone, morphine sulfate, and cocaine were obtained from NIDA (National Institute on Drug Abuse, Bethesda, MD). UK14304, kynuric acid, and β-chlornaltrexamine (β-CNA) were from (Tocris Cookson, Ellisville, MO). All other drugs were from Sigma (St Louis, MO, USA). MK-801, noradrenaline, UK14304, thiorphan, β-CNA, and NBQX were dissolved in dimethyl sulfoxide (DMSO). The final concentration of DMSO

did not exceed 0.01%. All other drugs were dissolved in water. All nomenclature conforms to BJP's Guide to Receptors and Channels (Alexander, Mathei and Peters, 2009).

Data analysis and statistical procedure

Concentration-response curves were constructed by normalizing the amplitude of the hyperpolarization induced by *l*- or *d*-methadone to the hyperpolarization induced by a saturating concentration of UK14304 (3 μM). A single recording was made in each slice and only one concentration of methadone was applied. The duration of the application varied with concentration so that a steady state hyperpolarization was obtained (up to 60 min). Once a steady state hyperpolarization was obtained, naloxone (1 μM) was applied to reverse the hyperpolarization. Then, the α2-adrenoceptor agonist, UK14304 (3 μM), was applied to activate the same population of $K_{IR}3$ conductance and reverse its effect with antagonist, yohimbine (2 μM). The hyperpolarization induced by methadone was then normalized to that induced by UK14304, to eliminate cell to cell variability. This protocol was necessary because the time course of the hyperpolarization induced by methadone, particularly *d*-methadone was very slow and the most accurate measure of the amplitude of the hyperpolarization was the difference in membrane potential before and after the addition of naloxone. In experiments where the block NMDA receptors were examined methadone was added cumulatively. The maximal hyperpolarization (E-max),

EC-50, and IC-50 values were determined using KaleidaGraph software (Synergy Software) calculated using a logistic function.

Data were expressed as mean ± SEM. Statistical significance was determined with unpaired Student's t test or one-way ANOVA followed by the post-hoc Student Newman-Keuls test. p=<0.05 was considered significance and expressed as $*p < 0.05$, $**p < 0.01$, and $***p < 0.001$.

Results

l-, and *d*-methadone hyperpolarize LC neurons

The activation of μ-opioid receptors by *l*- and *d*-methadone was first examined by application of a single concentration of each enantiomer (1 μM). Both *l*- and *d*-methadone caused a hyperpolarization that was reversed by naloxone (1 μM, Fig 1). The amplitude of the hyperpolarization induced by *l*-methadone was 26.0±2.3 mV (n=5), whereas *d*-methadone resulted in a hyperpolarization of 17.7±1.7 mV (n=8; Figure 1A, p=0.01). The onset of the hyperpolarization induced by *l*- and *d*-methadone (1 μM) also differed. The time it took to reach the half amplitude of the steady hyperpolarization was 5.4±0.9 min (n=5) for *l*-methadone and 22.9±2.7 min (n=7) for *d*-methadone (p=0.002). Thus, *l*-methadone (1 μM) was more potent than *d*-methadone (1 μM). As a control for the long duration application of methadone, a saturating concentration of UK14304 (3 μM) was applied at the end of each experiment. The amplitude of the hyperpolarization induced by UK14304 following *l*-methadone (1 μM) was 28.6±1.6 mV (n=5), and after *d*-methadone (1 μM) was 30.5±1.2 mV (n=8, p>0.05). The amplitude of the hyperpolarization was not changed following the prolonged application of methadone (1 μM, 30-60 min).

Concentration-response curves to *l*-, *d*-, and racemic (*l*/*d*)-methadone were constructed by normalizing the hyperpolarization induced by methadone to the hyperpolarization induced by UK14304 (3 μM, Figure 1B). The half maximal effective concentration (EC-50) of *l*- and *d*-methadone was 37±3.8 nM and

609±73.4 nM, respectively (Figure 1B). When *l*- and *d*-methadone were compared at equally effective concentrations (EC-50) there was no difference in the half time it took to reach a steady-state hyperpolarization (*l*-methadone 23±0.8 min, *d*-methadone 23±0.9 min; n=3 each). Thus, *l*-methadone was 16.5-fold more potent than *d*-methadone, and the time course of activation at equally effective concentrations was the same for both enantiomers. The concentration response to *l*/*d*-methadone was not different from *l*-methadone (Figure 1B). The hyperpolarization induced by a maximal concentration of *l*-methadone (3 μM) was 25.4±2.1 mV (n=7) which was not different from that induced by *d*-methadone (10 and 30 μM; 23.7±1.1 mV; n=8; $p>0.05$). With this assay both l- and d-methadone caused a maximal hyperpolarization and by this measure would be considered full opioid agonists.

A second assay was used to address the efficacy of *l*- and *d*-methadone. The outward current induced by a maximal concentration of each isomer was examined using whole cell voltage-clamp recordings. The use of voltage-clamp is more accurate at estimating the maximal action of opioid agonists because it removes the change in driving force for potassium that results when experiments are carried out under current-clamp conditions. Saturating concentrations of [Met]^{5}enkephalin (30 μM), morphine (15 μM), *l*-methadone (10 μM) and *d*-methadone (10 μM) were applied, the peak outward currents were measured and normalized to the current induced by UK14304 (3 μM; Figure 2A). The ME (30 μM) induced current was 123±4.7% of the UK14304 current, whereas morphine

(15 μM) caused a current that was only 47.4±7.3% of the UK14304 current. The currents induced by *l*- and *d*-methadone (10 μM) were 56.5±4.6%, and 36.3±2.7% of the UK14304 current, respectively (Figure 2B). These observations suggest that both *l*- and *d*-methadone are partial agonists, however this interpretation must be cautioned because the peak current induced by methadone may be blunted by two mechanisms. First, the slow rise in current may result in the combination of the activation of the $K_{IR}3$ conductance and the simultaneous development of acute receptor desensitization. Second, methadone is known to block $K_{IR}3$ mediated potassium conductance such that at the high concentrations used to reach the peak the potassium conductance may be reduced.

$K_{IR}3$ blockade by *l*-, and *d*-Methadone

The activation of μ-opioid receptors and α2-adrenoceptors results in an increase in the same $K_{IR}3$ conductance (North and Williams, 1985). The hyperpolarization induced by noradrenaline (NA) acting on α2-adrenoceptors was used to examine the blockade of $K_{IR}3$ conductance by methadone. Prior to the experiment, brain slices were incubated with the irreversible opioid receptor antagonist, β-chlornaltrexamine (β-CNA 1 μM, 30 min) to block μ-opioid receptors so that methadone did not cause a hyperpolarization. NA (10 μM + cocaine 10 μM) was applied for 2.5 min at 10 min intervals over a period of 1 hr. The amplitude of the hyperpolarization caused by NA was 20.9±0.4 mV (n=21) in control and was stable for 1-2 hours. Application of high concentrations of *l*/*d*-

methadone (10-30 μM) resulted in a gradual decline in the NA induced hyperpolarization over 50 min from 20.9 mV to 12.9±1.1 mV (n=4, Figure 3A). A similar reduction in the hyperpolarization induced by NA was observed with both *l*- and *d*-methadone (10 μM, *l*-methadone 69±2.1% of control, n=7; *d*-methadone 71±3.3% of control, n=8). The decrease was larger with the application of a higher concentration of methadone (*l*-methadone 30 μM, 54±6.8% of control, n=5; *d*-methadone 47±2.0% of control, n=6, Figure 3C).

The slow time course over which even high concentrations of methadone blocked $K_{IR}3$ limited experiments aimed at characterizing the concentration dependence of this action. Therefore slices were incubated in *d*/*l*-methadone (1-30 μM, naloxone 1 μM, prazosin 100 nM) for 4-8 hours prior to making recordings. Following the incubation period and in the continued presence of the appropriate concentration of methadone, whole cell recordings were made and the current induced by a saturating concentration of NA (90 μM, cocaine 10 μM, prazosin 100 nM) was applied. In order to reduce cell-to-cell variability, the current induced by NA was normalized to the capacitance of each cell (Figure 3B). The results indicate that there was a significant decrease in $K_{IR}3$ after an incubation period of 4-8 hours methadone (10 μM, $p=0.02$; 30 μM, $p<0.001$). Incubation in methadone (3 μM) did not result in a significant reduction in the NA current density ($p=0.2$). Thus, methadone partially blocked $K_{IR}3$ conductance in dose dependent manner that was not stereoselective.

When current/voltage plots were constructed in slices that were incubated in methadone (10 μM, and naloxone, 1 μM, >1 hour), there was a dramatic decrease in the conductance mediated by the inward rectifying potassium conductance (K_{IR}, Figure 4C). The voltage dependence of the block of $K_{IR}3$ by *d/l*-methadone was examined in experiments where I/V curves were constructed with a ramp protocol (-55 to -135 mV, 0.5 s) before and after NA was applied by iontophoresis (Figure 4A). This protocol was repeated at 30 s intervals in the continued presence of d/l-methadone (1 and 10 μM, naloxone 1 μM). There was no change in the NA I/V plots induced by methadone (1 μM, 15 min) whereas methadone (10 μM, 10 min) reduced the NA current over the entire voltage range (Figure 4B,D).

Methadone blocks NMDA current

Previous studies have shown that methadone inhibits NMDA receptor current by binding at the same site as MK-801 (Ebert et al., 1998; Gorman et al., 1997). Whole cell voltage-clamp recordings were used to examine the actions of methadone on the current induced by the activation of NMDA receptors. Slices were treated with ß-CNA (1 μM, 30 min) prior to recording in order to block μ-opioid receptors. Extracellular magnesium was removed in order to measure NMDA receptor dependent currents induced while holding the cell at -60 mV. Iontophoretic application of L-aspartate (50 nA, 20 ms) was used to activate NMDA receptors every 20 seconds in the presence of AMPA receptor antagonist

NBQX (5 μM). The current induced by L-aspartate was completely blocked by the non-selective glutamate antagonist, kynurenic acid (1.5 mM; data not shown). After steady NMDA currents were obtained for at least 5 minutes, *d*-, *l*-, or *l*/*d*-methadone were superfused. The amplitude of the NMDA current progressively declined following the addition of methadone and reached a steady state within 15-20 min. The extent of the inhibition was dependent on the concentration of *l*/*d*-methadone applied (Figure 5C). The inhibition curve indicated that the half maximal concentration (IC-50) of *l*/*d*-methadone was 3.5±0.3 μM (Figure 5C). At 3 and 30 μM both enantiomers of methadone decreased the NMDA current equally (*l*-methadone 3 μM 52±6% of control, n=7, 30 μM 16±2% of control, n=6; *d*-methadone 3 μM 59±6% of control, n=8, 30 μM 21±2% of control, n=7, Figure 5B). Therefore, the block of NMDA dependent current was not stereoselective.

The voltage dependence of the block of NMDA current by *l*/*d*-methadone was examined to determine if the inhibition resulted from a channel block. The amplitude of the current induced by NMDA receptors was examined over a range of -100 to +40 mV in 20 mV increments. In each experiment the amplitude of NMDA current was normalized to the current measured at -60 mV in control and I/V plots were constructed (Figure 5D). When LC neurons were held at -60 mV, *l*/*d*-methadone (30 μM) decreased the NMDA current to 33±6.4% (n=4, $p<0.0001$) of control. At +40 mV however, the amplitude of the NMDA current was not significantly different from control (63±14% of the control current at -60 mV) and methadone (61±19% of the control current at -60 mV). Thus, methadone

blocked the inward current induced by the activation of NMDA receptors but had no effect on outward current measured at positive membrane potentials. This result is consistent with methadone acting as a pore blocker of the NMDA receptor.

Discussion and Conclusions

A racemic mixture of methadone is used clinically for opiate maintenance therapy primarily because of the prolonged pharmacokinetics (Dole and Nyswander, 1965). In addition to the action on opioid receptors, the blockade of NMDA receptors is thought to facilitate the treatment of opiate addiction (Ebert et al., 1998). This study demonstrated that *l*-methadone was more potent and efficacious than *d*-methadone on μ-opioid receptors measured by activation of potassium conductance. The results indicate that the concentration of methadone required to activate μ-opioid receptors was significantly lower than that required to block $K_{IR}3$ and NMDA conductance and the channel blocking action was not stereoselective. Thus the action of methadone when used at therapeutic levels is primarily mediated by opioid receptors and channel blocking actions may only be observed after reaching very high levels.

Potency and efficacy of *l*-, and *d*-methadone

A distinct difference in potency between *l*- and *d*-methadone was demonstrated in this study. *l*-methadone was 16.5-fold more potent than *d*-methadone at inducing hyperpolarization of LC neurons. Similar results have been reported in the binding affinity to μ-opioid receptors and GTPγS binding assay (Codd et al. 1995; and Wallisch et al. 2007). The binding affinity of *l*-methadone was 21-30 fold higher than *d*-methadone (Codd et al., 1995; Wallisch et al., 2007). In a GTPγS binding assay *l*-methadone had a 23 fold greater potency

than *d*-methadone (Wallisch et al., 2007). The difference in potency was slightly lower in our study (16.5 fold) perhaps because of the difference in the time it took to reach a steady state hyperpolarization for the two isomers. It required about 1 hour to reach a steady state hyperpolarization with *d*-methadone (1 μM) while a steady state was reached within 15-20 min with *l*-methadone (1 μM). The long duration required for *d*-methadone to reach steady state may have resulted in an accumulation of this lipophilic agonist in slice preparation and thus been an underestimation of the true concentration.

The efficacy of *l*- and *d*-methadone was examined using both current- and voltage-clamp recording. Intracellular recording of membrane potential indicated that both *l*- and *d*-methadone induced a maximal hyperpolarization suggesting that under these conditions both enantiomers of methadone were full agonists. The advantage of using intracellular recording is that long lasting stable measurement of membrane potential is routine without the potential for rundown that often occurs with whole cell recording. The maximum hyperpolarization is, however, limited by the approach of the membrane potential toward the potassium equilibrium potential. The maximum hyperpolarization will therefore overestimate agonist efficacy. Another consideration is the observation that the resting inward rectification (K_{IR}) was dramatically reduced by methadone, such that the amplitude of the hyperpolarization would be increased, in spite of a decrease in the opioid receptor dependent current. Voltage-clamp recording using whole cell recordings indicated that the maximum current induced by methadone was substantially

less than that induced by ME. The current induced by *d*-methadone was less than *l*-methadone and both were less than that induced by ME. Different assays have concluded that methadone is a full (Rodriguez-Martin et al., 2008; Selley et al., 1998; Wallisch et al., 2007) or a partial (Saidak et al., 2006; Virk and Williams, 2008) agonist at μ-opioid receptors. The maximal efficacy of methadone ranged from 85% to 100% of the activation by DAMGO. The present results demonstrate that receptor reserve is assay dependent. That is the maximum hyperpolarization was attained with methadone even though the outward current was less than the peak outward current induced by ME.

In the continued presence of a saturating concentration of methadone, the hyperpolarization peaked and declined to a greater extent than that observed with a saturating concentration of morphine or ME (Arttamangkul et al., 2008). The decline in the amplitude of the hyperpolarization induced by a prolonged high concentration of methadone may result from (1) the induction of desensitization or (2) block of the potassium conductance. The mechanism(s) that account for acute opioid receptor dependent desensitization have not been definitively identified. A component of the methadone-induced decline may result from a block of the $K_{IR}3$ conductance. The block of the $K_{IR}3$ conductance has a slow onset so the peak activation of $K_{IR}3$ may precede the onset of channel block. It is unlikely, however, that channel block accounts entirely for the decrease in the peak current because the time course of block of the current induced by activation of adrenoceptors was slower than the onset of opioid receptor dependent desensitization.

Methadone/alkaloid blockade of ion channels

Ligands such as morphine, fentanyl, codeine, and naloxone, have been shown to block NMDA receptors at high concentrations (Ki>100 μM; Yamakura et al., 1999). The morphine induced block of NMDA receptors has been reported to be stereospecific, where *l*-morphine has a lower Ki value (160 μM) than *d*-morphine (4.7 μM; Stringer et al., 2000). Morphine has also been reported to block GIRK conductance when applied at high concentrations, but the stereoselectivity of this action has not been examined (Blanchet et al., 2003). The present results indicate however, that the block of NMDA receptors by *l*- and *d*-methadone was similar, confirming the lack of a stereoselective action (Choi and Viseskul, 1988; Ebert et al., 1998; Gorman et al., 1997). The greater conformational flexibility of methadone compared to other opiates was proposed to result in the non-stereospecific channel block (Pert and Snyder, 1973a). Previous studies have found that methadone blocked voltage-gated potassium channels by acting at an intracellular site, similar to the blockade induced by tetraethylamonium binding in the inner vestibule of voltage gated potassium channels (Horrigan and Gilly, 1996). The block of $K_{IR}3$ channels may result from a similar mechanism. The slow time course of the block of $K_{IR}3$s may result from the slow penetration of methadone into cytoplasm.

Clinical relevance and Significance

Racemic methadone is prescribed for the treatment of opiate addiction and analgesia. The half-life of methadone is long enough to maintain the basal level of methadone so that it can be used on an outpatient basis (Dole and Kreek, 1973; Dole and Nyswander, 1965). The danger of methadone is the rapid partitioning into the brain resulting in high levels. The initiation of methadone maintenance therefore begins with low doses even in morphine tolerant individuals (Dole and Nyswander, 1965). Studies in patients who are on methadone maintenance have an average plasma concentration of 700-800 nM (Kreek, 2000). When the distribution of methadone between plasma and CSF were compared, CSF levels were only a small fraction (2-73%) of the plasma levels (Rubenstein et al., 1978). Chronic treatment of rats with methadone also required initiation of treatment with low doses of methadone over a 2 day period before escalating the dose using osmotic minipumps (Virk et al., unpublished). Rats that received (*l*/*d*) methadone (60 mg/kg/day) for 7-days had a plasma concentration that was in the same range (*l*-methadone - 309 nM, and *d*-methadone - 452 nM, Virk et al unpublished) as measurement in humans (Kreek, 2000). Lethal plasma levels of methadone in patients on maintenance therapy averaged 3 μM (Perret et al., 2000). The results of this study suggest that the concentrations of methadone measured in human studies do not reach values where there is a large decrease in $K_{IR}3$ or NMDA dependent conductance. Levels that approach the channel blocking concentrations are only described in overdose cases (Perret et al., 2000). Studies in rodent models have shown that methadone

is capable of decreasing NMDA induced firing in the spinal cord and NMDA receptor dependent measures of pain (Davis and Inturrisi, 1999; Sotgiu, Valente, Storchi, Caramenti and Biella, 2009). While there is no question that methadone is capable of these actions, the concentrations that are achieved in the experiments done in vivo are difficult to relate to the present work. The conclusion is therefore that the most of the clinical actions of methadone are mediated by opioid receptors.

References

Alexander SPH, Mathie A and Peters JA (2009) Guide to receptors and Channels (GRAC). Brit J Pharmacol 158(suppl 1):S1-254.

Arttamangkul S, Quillinan N, Low MJ, von Zastrow M, Pintar J and Williams JT (2008) Differential activation and trafficking of micro-opioid receptors in brain slices. Mol Pharmacol 74(4):972-979.

Bilsky EJ, Inturrisi CE, Sadee W, Hruby VJ and Porreca F (1996) Competitive and non-competitive NMDA antagonists block the development of antinociceptive tolerance to morphine, but not to selective mu or delta opioid agonists in mice. Pain 68(2-3):229-237.

Blanchet C, Sollini M and Luscher C (2003) Two distinct forms of desensitization of G-protein coupled inwardly rectifying potassium currents evoked by alkaloid and peptide mu-opioid receptor agonists. Mol Cell Neurosci 24(2):517-523.

Choi DW and Viseskul V (1988) Opioids and non-opioid enantiomers selectively attenuate N-methyl-D-aspartate neurotoxicity on cortical neurons. Eur J Pharmacol 155(1-2):27-35.

Codd EE, Shank RP, Schupsky JJ and Raffa RB (1995) Serotonin and norepinephrine uptake inhibiting activity of centrally acting analgesics: structural determinants and role in antinociception. J Pharmacol Exp Ther 274(3):1263-1270.

Davis AM and Inturrisi CE (1999) d-methdone blocks morphine tolerance and N-methyl-D-aspartate-induced hyperalgesia J Pharmacol Exp Ther 289:1048-1053.

Dole VP and Kreek MJ (1973) Methadone plasma level: sustained by a reservoir of drug in tissue. Proc Natl Acad Sci U S A 70(1):10.

Dole VP and Nyswander M (1965) A Medical Treatment for Diacetylmorphine (Heroin) Addiction. A Clinical Trial with Methadone Hydrochloride. JAMA 193:646-650.

Ebert B, Thorkildsen C, Andersen S, Christrup LL and Hjeds H (1998) Opioid analgesics as noncompetitive N-methyl-D-aspartate (NMDA) antagonists. Biochem Pharmacol 56(5):553-559.

Elliott K, Kest B, Man A, Kao B and Inturrisi CE (1995) N-methyl-D-aspartate (NMDA) receptors, mu and kappa opioid tolerance, and perspectives on new analgesic drug development. Neuropsychopharmacology 13(4):347-356.

Gorman AL, Elliott KJ and Inturrisi CE (1997) The d- and l-isomers of methadone bind to the non-competitive site on the N-methyl-D-aspartate (NMDA) receptor in rat forebrain and spinal cord. Neurosci Lett 223(1):5-8.

Horrigan FT and Gilly WF (1996) Methadone block of K+ current in squid giant fiber lobe neurons. J Gen Physiol 107(2):243-260.

Katchman AN, McGroary KA, Kilborn MJ, Kornick CA, Manfredi PL, Woosley RL and Ebert SN (2002) Influence of opioid agonists on cardiac human ether-a-go-go-related gene K(+) currents. J Pharmacol Exp Ther 303(2):688-694.

Kornick CA, Kilborn MJ, Santiago-Palma J, Schulman G, Thaler HT, Keefe DL, Katchman AN, Pezzullo JC, Ebert SN, Woosley RL, Payne R and Manfredi PL (2003) QTc interval prolongation associated with intravenous methadone. Pain 105(3):499-506.

Kreek MJ (2000) Methadone-related opioid agonist pharmacotherapy for heroin addiction. History, recent molecular and neurochemical research and future in mainstream medicine. Ann N Y Acad Sci 909:186-216.

North RA and Williams JT (1985) On the potassium conductance increased by opioids in rat locus coeruleus neurones. J Physiol 364:265-280.

Perret G, Deglon JJ, Kreek MJ, Ho A and La Harpe R (2000) Lethal methadone intoxications in Geneva, Switzerland, from 1994 to 1998. Addiction 95(11):1647-1653.

Pert CB and Snyder SH (1973a) Opiate receptor: demonstration in nervous tissue. Science 179(77):1011-1014.

Pert CB and Snyder SH (1973b) Properties of opiate-receptor binding in rat brain. Proc Natl Acad Sci U S A 70(8):2243-2247.

Rodriguez-Martin I, Braksator E, Bailey CP, Goodchild S, Marrion NV, Kelly E and Henderson G (2008) Methadone: does it really have low efficacy at micro-opioid receptors? Neuroreport 19(5):589-593.

Rubenstein RB, Kreek MJ, Mbawa N, Wolff WI, Korn R, Gutjahr CL (1978) Human spinal fluid methadone levels. Drug Alcohol Depend 3:103-106.

Saidak Z, Blake-Palmer K, Hay DL, Northup JK and Glass M (2006) Differential activation of G-proteins by mu-opioid receptor agonists. Br J Pharmacol 147(6):671-680.

Scott CC, Robbins EB and Chen KK (1948) Pharmacologic comparison of the optical isomers of methadone. J Pharmacol Exp Ther 93(3):282-286.

Selley DE, Liu Q and Childers SR (1998) Signal transduction correlates of mu opioid agonist intrinsic efficacy: receptor-stimulated [35S]GTP gamma S binding in mMOR-CHO cells and rat thalamus. J Pharmacol Exp Ther 285(2):496-505.

Sotgiu ML, Valente M, Storchi R, Caramenti G and Biella GEM (2009) Cooperative N-methyl-D-aspartate (NMDA) recetor antagonist and μ-opioid receptor agonism mediated the methadone inhibition of the spinal neuron pain-related hyperactivity in a rat model of neuropathic pain. Pharmacol Res 60:284-290.

Stringer M, Makin MK, Miles J and Morley JS (2000) d-morphine, but not l-morphine, has low micromolar affinity for the non-competitive N-methyl-D-aspartate site in rat forebrain. Possible clinical implications for the management of neuropathic pain. Neurosci Lett 295(1-2):21-24.

Trujillo KA and Akil H (1991) Inhibition of morphine tolerance and dependence by the NMDA receptor antagonist MK-801. Science 251(4989):85-87.

Virk MS and Williams JT (2008) Agonist-specific regulation of mu-opioid receptor desensitization and recovery from desensitization. Mol Pharmacol 73(4):1301-1308.

Wallisch M, Nelson CS, Mulvaney JM, Hernandez HS, Smith SA and Olsen GD (2007) Effects of chronic opioid exposure on guinea pig mu opioid receptor in Chinese hamster ovary cells: comparison with human and rat receptor. Biochem Pharmacol 73(11):1818-1828.

Williams JT, Egan TM and North RA (1982) Enkephalin opens potassium channels on mammalian central neurones. Nature 299(5878):74-77.

Williams JT and North RA (1984) Opiate-receptor interactions on single locus coeruleus neurones. Mol Pharmacol 26(3):489-497.

Williams JT, North RA, Shefner SA, Nishi S and Egan TM (1984) Membrane properties of rat locus coeruleus neurones. Neuroscience 13(1):137-156.

Yamakura T, Sakimura K and Shimoji K (1999) Direct inhibition of the N-methyl-D-aspartate receptor channel by high concentrations of opioids. Anesthesiology 91(4):1053-1063.

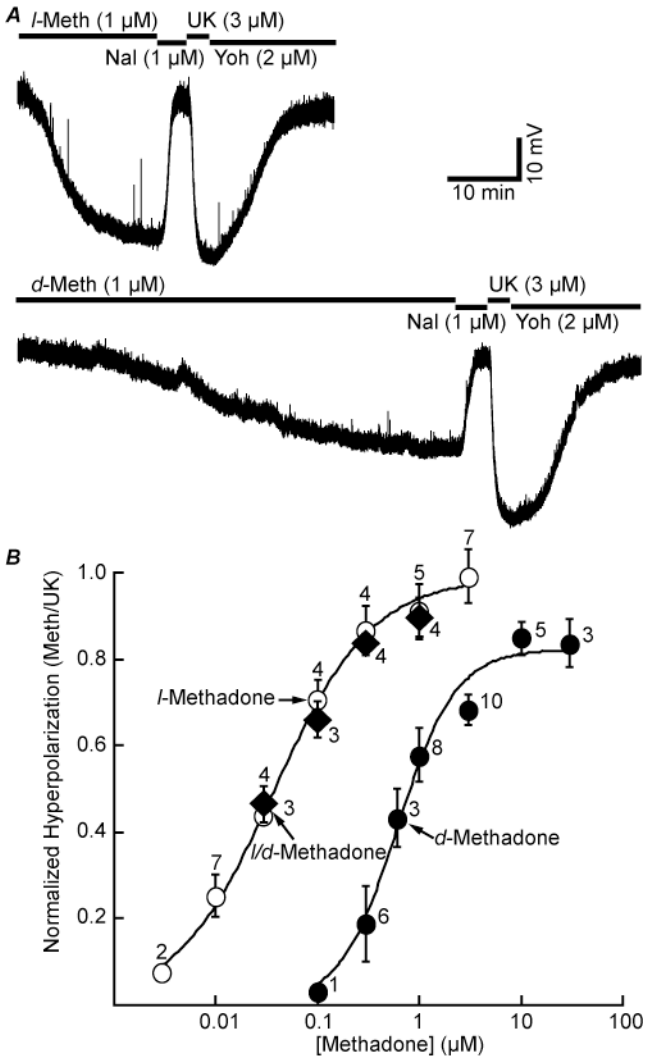

Figure 5.1: The concentration response of *l*- and *d*-methadone are significantly different

A. Representative traces of the hyperpolarization induced by *l*-methadone (*l*-Meth 1 μM; top) and *d*-methadone (*d*-Meth 1 μM; bottom). In each case the hyperpolarization was reversed with naloxone (Nal 1μM). The hyperpolarization induced by UK14304 (UK 3 μM) was reversed by yohimbine (Yoh 2 μM). Note the difference in amplitude and the time course of the hyperpolarization induced by *l*- and *d*-methadone (1 μM). B. Concentration response curves to *l*-methadone (open circle), *d*-methadone (closed circle) and *l*/*d*-methadone (diamonds). The amplitude of the hyperpolarization were normalized to hyperpolarization induced byUK14304 (3 μM). Error bars indicate ± S.E.M.

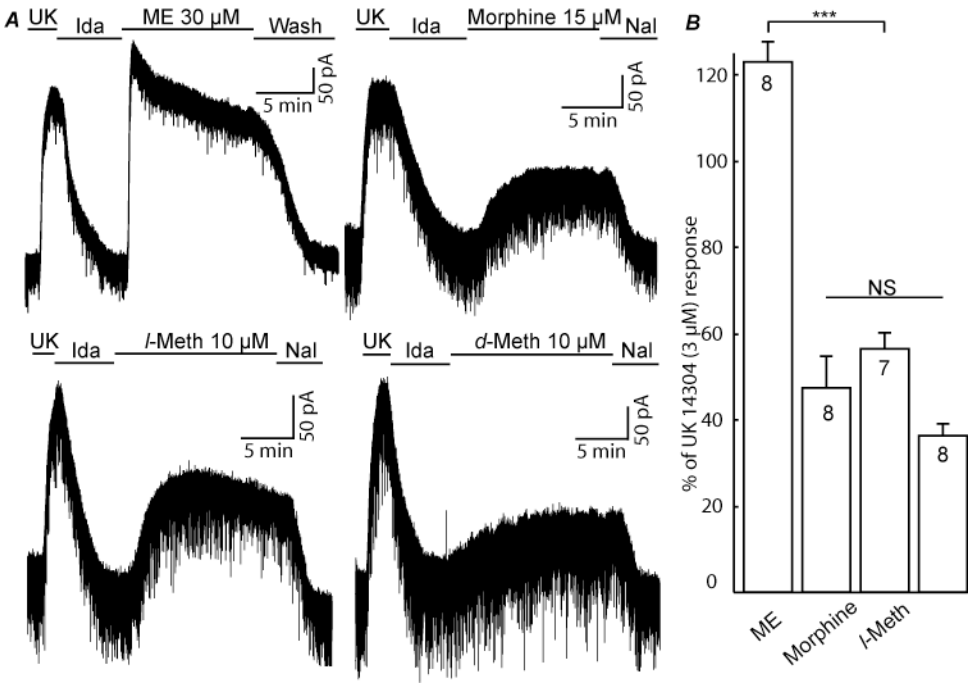

Figure 5.2: Morphine, *l*- and *d*-methadone are partial agonists

A. Raw current traces from whole-cell voltage-clamp recordings. Saturating concentrations of *l*- and *d*-methadone (10 μM) and morphine (15 μM) produced outward currents that were less than the current induced by UK14304 (3 μM). The current induced by ME (30 μM) was larger than the current induced by UK14304. B. Summarized result showing the current activated by ME (30 μM), morphine (15 μM) *l*- and *d*-methadone (10 μM) normalized to the current induced by UK 14304 (3 μM). The ME current was 123±4.6% of UK14304 current, whereas, current evoked by morphine was 47±7.3% and *l*- and *d*-methadone was 56.5±3.62% and 36.3±2.70%.

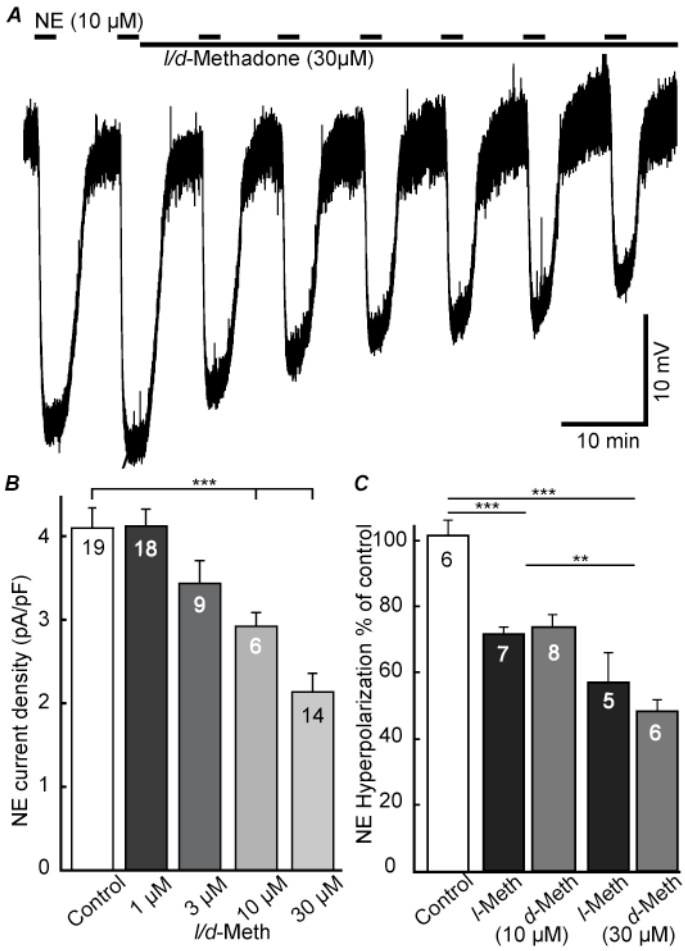

Figure 5.3: Both *l*- and *d*-methadone decreased the hyperpolarization induced by NA

A. Representative intracellular recording showing the protocol used. The hyperpolarization induced by noradrenaline (NA 10 μM+cocaine 10 μM) was reduced from 20.9 mV to 12.0 mV by both *l*/*d*-methadone (30 μM) over a period of one hour. Slices were treated with β-CNA prior to the experiments, so that methadone did not induce a hyperpolarization. B. Summary of the concentration dependent inhibition of the current density (pA/pF) induced by NA (90 μM + cocaine 10 μM). Slices were incubated for 4-8 hours in the indicated concentration of methadone prior to the experiment. There was a significant decrease in NA current density in slices treated with 10 and 30 μM methadone. C. Summary of concentration dependent block of NE induced hyperpolarization measured after 40-50 min. There was no difference in the reduction of hyperpolarization between *l*- and *d*-methadone. Error bars indicate ± S.E.M. and $^{**}p < 0.01$, and $^{***}p < 0.001$ to control.

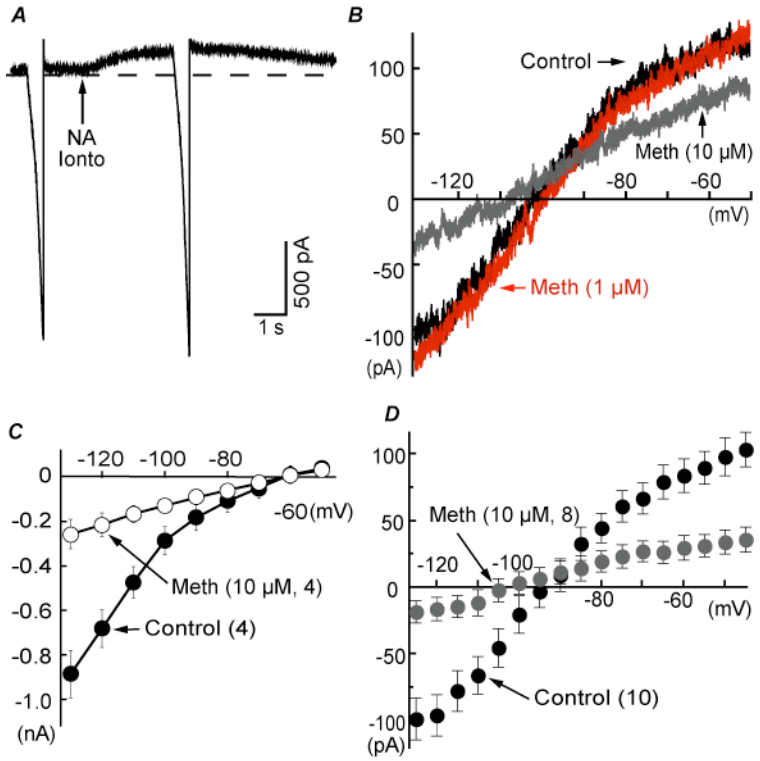

Figure 5.4: Voltage dependence of GIRK block by methadone

A. Raw current trace illustrating the protocol used to characterize the voltage dependence of the current induced by the iontophoretic application of NA (arrow). B. Recording from a single neuron showing the current/voltage plot in control (control, black), after superfusion of 1 µM methadone (Meth 1 µM, red) and 10 µM (Meth 10 µM, gray). C. Methadone decreased resting conductance. Whole cell current/voltage plot in the absence (solid circles) and presence of methadone (10 µM, open circles, n=4 each). D. Summarized current/voltage illustrating the current induced by NA in control (solid circles) and after methadone (10 µM gray circles). Opioid receptors were blocked in all experiments with either ßCNA or naloxone.

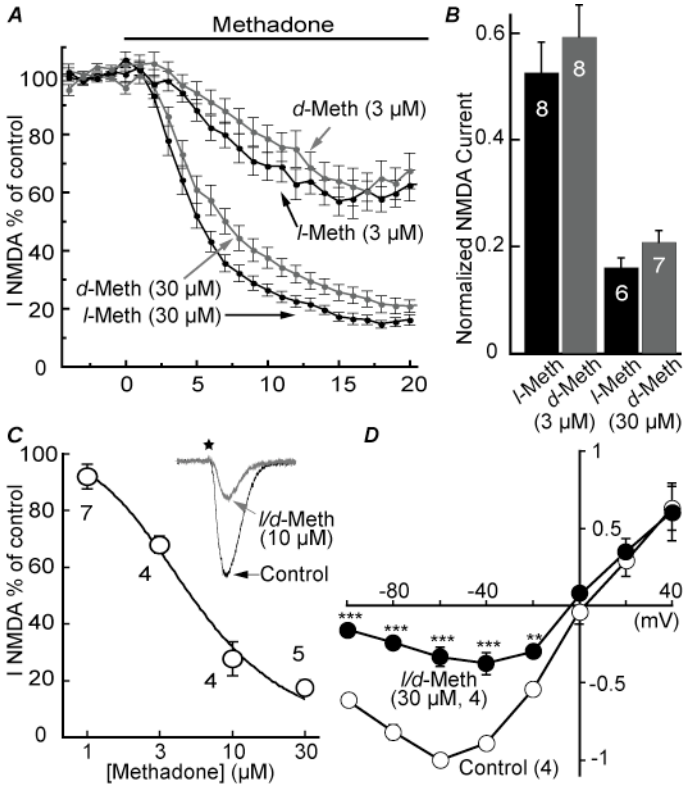

Figure 5.5: Methadone block of NMDA receptors

A. Summary of the time course of inhibition by *l*- and *d*-methadone (3 and 30 μM). B. Summary of inhibition of NMDA current after application of *l*- and *d*-methadone (3 and 30 μM). C. Plot of the concentration-response curve of the *l*/*d*-methadone block of NMDA currents. Inset are superimposed traces of the inward current induced by iontophoretic application of aspartate in control and after superfusion with methadone (10 μM). D. The current-voltage relationship of NMDA receptor dependent current in control (open circle) and after application of *l*/*d*-methadone (30 μM; closed circle). The amplitude of NMDA current was normalized to the current measured at -60 mV in control. At negative potentials, NMDA currents were significantly decreased but were not affected at positive potentials. Error bars indicate ± S.E.M. and $^{**}p < 0.01$, and $^{***}p < 0.001$ to control. Opioid receptors were blocked in all experiments with either ßCNA or naloxone.